Combustor Exhaust Temperature Nonuniformity Sensing Using Diode Laser Absorption

A Dissertation
Presented to
The Academic Faculty

By

Tudor Ioan Palaghiță

In Partial Fulfillment
Of the Requirements for the Degree
Doctor of Philosophy in Aerospace Engineering

Daniel Guggenheim School of Aerospace Engineering
Georgia Institute of Technology
May 2007

Combustor Exhaust Temperature Nonuniformity Sensing Using Diode Laser Absorption

Approved by:

Dr. Jerry M. Seitzman, Advisor
School of Aerospace Engineering
Georgia Institute of Technology.

Dr. Ben T. Zinn
School of Aerospace Engineering
Georgia Institute of Technology.

Dr. Jechiel I. Jagoda
School of Aerospace Engineering
Georgia Institute of Technology.

Dr. Richard Gaeta
Advanced Transportation and Advanced
Systems (ATAS) Laboratory
Georgia Institute of Technology.

Dr. Boris Mizaikoff
School of Chemistry
Georgia Institute of Technology.

Date Approved: December 19, 2006

ACKNOWLEDGEMENTS

This thesis is the culmination of many years of learning and research at The Georgia Institute of Technology. None of this would have been possible without the help and support of my advisor, Dr. Jerry Seitzman, whom I would like to extend my deepest thanks. He provided me with guidance and mentoring as I developed my academic, research, and communication skills, as well as help me grow my confidence and sense of fulfillment.

In addition, I would like to thank my reading committee for taking the time to familiarize themselves with my research and provide useful comments and questions.

I would also like to thank the research engineers, especially David Scarborough and John Holthaus, and the many students in the Combustion Lab for helping me find my way around, setting up my experiments and studying for the qualifiers. Thanks also to my many friends who made my stay in Atlanta so enjoyable and memorable.

And finally, my thoughts and thanks go to my wonderful wife, Nicol, who gives me the strength and the love that nourishes me, supports me, and makes me be a better person. And to my loving family who has been my model in life and without whom this PhD would have not been possible.

TABLE OF CONTENTS

LIST OF TABLES

LIST OF FIGURES

SUMMARY

This thesis describes the development of a sensing technique for temperature nonuniformity along the line of sight through combustion exhaust, geared for gas turbine applications. Tunable diode laser absorption spectroscopy is used to measure three absorption lines and compute a variable to characterize the level of temperature nonuniformity along the laser path.

Nonuniformity information is obtained from one line of sight sensor because the absorption has a nonlinear dependence on temperature. This dependence is analyzed to determine the behaviour, shape, and response of absorption lines measured through mediums with nonuniform temperature profiles. Based on this analysis a new line selection process for nonuniformity sensing is developed.

A sensor for temperature nonuniformity is proposed and demonstrated through computer simulations and experiments in the exhaust of a laboratory-scale combustor. The nonuniformity variable, U, is shown to monotonically track the level of temperature nonuniformity along the laser path. The capabilities of this sensing technique are determined based on a comprehensive analysis of errors and their effect on sensor performance. Methods to mitigate these errors are described, and the overall sensor capability is determined based on the characteristics of state of the art diode laser and absorption sensor technology. Such a sensor is capable of measuring minimum temperature deviations of 17% or more, which is well within the needed capabilities for industrial applications. Furthermore, the results and knowledge presented in this thesis apply to other absorption based sensing techniques.

CHAPTER 1: INTRODUCTION

1.1 Introductory Remarks

Fire gave humanity power over its surroundings and enabled the development of modern humans. Fire also provided the means to power the industrial revolution and the continued technological progress since. Combustion is used extensively by people everywhere and everyday, when lighting a candle, driving a car or every time we use electricity – 85% of our energy is provided by combustion. As our need for power increases and the natural resources used in its production diminish, it becomes more important than ever to better understand and control the combustion process, to increase its efficiency, and to decrease the amount of harmful pollutants and greenhouse gasses that are a result of combustion.[1] Combustion and temperature are intricately related. From the broad field of combustion sensing and control, this thesis focuses on the development of a method for sensing the temperature of combustion gases, in particular information about the spatial distribution of the gas temperature using optical techniques. The author hopes that this research will be a welcome addition to the field of combustion sensing and will facilitate the development of new sensors and control systems based on this technique.

1.2 Overview of the Field and Motivation

All combustion systems require some degree of control, from residential boilers and stoves, to industrial process heaters and power generation equipment, to automobile

and aircraft engines. Combustion control, both passive and active, plays a crucial role in ensuring safety, increasing efficiency, reducing costs, and especially reducing harmful emissions.[1,2] Government agencies such as NASA, DoD, DoE, and companies in such diverse fields as automotive, ore processing, petrochemical, and appliance manufacturing are actively researching technologies for improving combustion control; active control in particular holds the most promise for significant pay-offs. For example, increasing automobile fuel efficiency by only 1% would save nearly 100 million barrels of oil each year.[3] A wide variety of applications would benefit from an improved understanding of combustion and a better ability to control it and tune it to satisfy our requirements.

Control systems rely on sensors for the different gas properties and actuators to drive the combustion system towards a more desirable state. Sensors for measuring such properties as temperature, pressure, velocity, and chemical species are essential in the continuing study of combustion and in the design of new combustion systems. However, the harsh environments typical of combustion – high temperature, reacting flow, soot, difficult access – make it hard to measure some of these properties. Moreover, although combustion has been studied for a long time, we are still unable to completely model and predict turbulent reacting flows characteristic of industrial combustion, thus experimental study and testing of combustion systems remains very important. Consequently, development of new sensors is very important for the study of combustion and the design of new systems.

Temperature is one of the most important variables in combustion; it is related to the chemical reactions occurring in combustion, to the energy released during the process, and to the usefulness of a combustion system in terms of its heat or power

output. Measuring the spatial distribution of temperature would be especially useful for the study of flames and for engine development, yet such measurements are very difficult to obtain. Although there are solutions to measure point-wise temperatures or its spatial distribution under many conditions, there are still many engineering applications where satisfactory temperature measurements are difficult to make. For example, in many combustion applications, gas temperatures can not be measured with enough temporal or spatial resolution, with enough accuracy, or in certain areas of the flows, such as quasi-instantaneous spatial temperature distributions in a gas-turbine combustor.

Gas turbine engines represent an area of particular interest for temperature measurement. Gas-turbines are used for aero propulsion as well as power generation, with the latter recently having experienced a rapid growth. Modern gas turbine engines require continuous improvements in performance, reduction in emission levels, and improved fuel flexibility and safety.[4] Furthermore, engines need to become more intelligent and be able to adapt to changes during their operating life, such as aging, component upgrades, and new environmental restrictions. Improved control systems employed at all operating levels can provide solutions to many of these requirements. The ability to measure the gas temperature through different gas-turbine engine components can impact engine design, performance, lifetime, and cost. In particular, the development of temperature sensors, especially for the hot gas and reacting flow regions, can be a key enabler for many intelligent engine control systems.[2,4,5] Sensing becomes especially important at off-design operation and as engines age.

1.2.1 Temperature and Pattern Factor Sensing Overview

The research presented in this document seeks to address a need that is often mentioned when gas-turbine engine technologies are discussed: pattern factor (PF) sensing and control.[4-8] The pattern factor is a simple measure of the temperature profile at the exit of a combustor and is usually defined as the maximum fractional temperature deviation from the combustor average exit temperature. Thus it is a way to characterize important temperature variations in the combustor exit plane. It is used to refer to either the radial or the circumferential profile in a gas-turbine combustor or annulus. Efforts to measure and control the pattern factor are not new – aircraft engine manufacturers in particular have been trying to design low pattern factor engines and passive control systems for some time,[9-14] but testing and active control strategies have been hampered by the lack of adequate sensors for the gas temperature profile – a problem that this thesis addresses.[5,7,8] The ability to measure the temperature distribution in the combustor exit plane, especially peak temperature fluctuations would enable important advances in engine performance.[7]

For example, temperature fluctuations in the combustor can result in increased emissions of NO_x, which is formed in pockets of hot gas, and CO and unburned hydrocarbons, which can result from cold gas quenching and incomplete combustion. Fluctuations of the combustor exhaust gas temperature in space and time also expose turbine blades and vanes to fluctuations in thermal stress, reducing safety and operability.[5-7] Furthermore, the ability to sense and limit the peak temperatures impinging on the turbine blades would permit less air to be diverted to cooling, thus increasing engine efficiency. The ability to sense and control the temperature profile at the

combustor exit also allows increased average burning temperatures, which leads to better engine performance and efficiency. As seen in Figure 1, a decrease in the amount of nonuniformity for a given maximum temperature constraint, allows an engine designer to use higher average burning temperatures. For gas turbines (Brayton cycle engines), higher turbine inlet temperatures lead directly to higher specific power capability, and with a corresponding increase in the maximum operating pressure can produce higher cycle efficiencies. Real-time monitoring of temperature uniformity also enables health monitoring of engine components, which is useful for lifetime predictions.
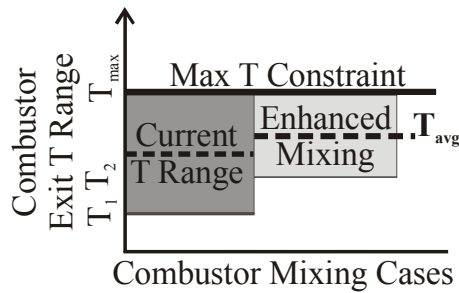
Figure 1. Reduced pattern factor enables higher average exit temperatures

Measurements of combustor exit temperature profile (or PF) provide information about the temperature fluctuations and the quality of mixing in the combustor. Reductions in PF through design and testing allow for better engine performance and increased component lifetime.[5-8] Poor mixing increases emissions and results in hot streaks that impact downstream turbo machinery. Because of the inability to sense and control the combustor exit temperature, turbine blade cooling air requirements have to be increased to accommodate deviations of more than 150 ºC from the design range. Since cooling air can be as much as 30% of the core flow, the ability to measure PF and reduce it by even a small amount would also increase engine efficiency and thrust. The resulting reductions in blade root thermal stress can also result in a doubling of turbine blade life.[5]

Because of the importance of pattern factor in engine design and operation, many companies and government agencies have active programs to develop low pattern factor combustors and PF sensing and control techniques.[6,8,13-17] Kiel[7] and Lord[5] provide an overview of the state of technologies for combustor sensing and control, as well as programs such as the GE Twin Annular Premixing Swirler (TAPS) combustors.[13]

Nevertheless, there are currently no practical temperature nonuniformity sensors that can be used in operational gas-turbine engines. As a result, understanding, measuring, and controlling the temperature in the hot flow regions of gas-turbine engines emerges as a very important need, for both airborne and ground-based systems – a need that the following work addresses.

1.2.2 Temperature Sensing Technologies

There are several technologies for measuring temperature, but few are suitable for use in operational gas turbine engines. One of the simplest ways to measure temperature distributions is with arrays of thermocouples. Thermocouples are relatively inexpensive and provide point-wise measurements, but they are too slow, bulky, and difficult to install in an operational engine.[7] They are best suited for gas turbine testing rigs. Some early work was done at Virginia Tech in developing heat flux sensors deposited on the surface of gas-turbine blades.[18] The experimenters measured time average and unsteady heat flux in a blow-down wind tunnel at relatively low temperatures. Some of the first experimental research on thin film temperature sensors for gas-turbine engines was reported by a team at NASA who has tried to develop thin film thermocouples fabricated into turbine vanes for PF sensing and control.[6,8] Unfortunately, problems with

6

delamination, failure of the wire transitions, and manufacturing difficulty and expense resulted in a failure to obtain a reliable and functioning system. More recently the QinetiQ company has claimed a successful test of a thin film heat sensor for turbine blades,[17] but details of the technology and its capabilities are not available. This seems to be a promising technology that depends on advances in material science and may provide turbine blade surface temperature measurements useful for improving PF and extending component lifetime. Nevertheless, surface sensors can interfere with the flow, blade cooling, or thermal protection coatings. Such sensors also require complex wiring and may add too much weight for aircraft engines.

Optical techniques provide another avenue for temperature measurements in turbines. One of the simpler methods is pyrometry measurements of the turbine surfaces.[15] Although promising for certain applications, uncertainties in the surface emissivity of the vanes and blades, and interference from particulates in the flow and deposits on the blade surfaces make it very difficult to obtain sensitive temperatures. Furthermore, these sensors are commonly used to obtain single-point measurements;[19] temperature profiles or distributions are much more difficult to acquire. In general, little literature exists on temperature distribution sensing for combustion or gas turbine engines.

The methods described above measure the gas temperature indirectly, by measuring the temperature of an engine surface. These methods also contain an inherent drawback for control applications: the blade metal temperature has a slow response to rapid variations in gas temperature and results in a time-averaged response, potentially missing important problems or nonuniformities in the combustor exit gas temperatures. If

7

the location of the gas temperature nonuniformities can not be determined, then it would be more difficult for a control system to adjust the combustor conditions to reduce PF.

The most promising technology for monitoring gas properties for combustion sensing seems to be based on optical, laser-based spectroscopic techniques.[5,7] Lasers are superior to broadband light sources because of the much higher light intensity, narrow spectral features, and tuning abilities.

Diode-lasers, especially those based on technology developed for the telecom industry, have quickly been adopted in a wide range of sensing applications because they are nonintrusive, offer small size, ruggedness derived from their solid-state nature, wide availability, and low cost. In particular, new improvements in power, wider tuning ranges, and access to new spectral regions allow for new sensor applications, keeping diode lasers very much in the arena of active research. (A good reference on diode lasers is the book by Sands.[20])

Temperature measurements can be obtained by a variety of spectroscopic techniques: Rayleigh and Raman scattering, Laser-Induced Fluorescence (LIF) or Phosphorescence (LIP), and absorption spectroscopy.[21] All of these but absorption spectroscopy normally require bulky, complex, and sensitive hardware making them unsuitable for industrial applications. The combination of absorption spectroscopy techniques with diode lasers results in a unique sensing capability that is both powerful and relatively simple.

1.2.2.1 Diode Laser Absorption Spectroscopy

Absorption spectroscopy has been successfully used for many years in the laboratory as well as for industrial applications. The small footprint, relatively low cost,

8

and the possibility of creating integrated sensor packages that can be used by low-skill operators make laser absorption sensors ideal for use outside the laboratory.

Diode-laser sensors based on absorption spectroscopy have been built and demonstrated in the laboratory and have started to be used for industrial applications. Usually the laser is tuned over one or more spectral features and the resulting absorption is used to compute flow properties of interest. To date, these sensors have generally been used to determine species concentrations along the line of sight, and less often to find a path-averaged gas temperature based on the ratio of two absorption features. Sensors for measuring species concentration, average temperature, and even pressure and velocity, have been demonstrated for laboratory and in-situ combustion systems by universities, government labs, and engine manufacturers.[5,7,22-24] Most notably, a group at Stanford University lead by Hanson has published a very large number of papers on diode laser absorption sensors. They have performed measurements in scram-jet combustors,[25-28] shock-tubes,[29-31] pulse-detonation engines,[22,32] and in many other systems.[24,33-39] Measurements included temperature, velocity, and concentrations of a variety of species, such as H_2O, CO_2, NO_2, NO, CO, and O_2.

1.2.2.2 Absorption Spectroscopy for Spatial Temperature Measurements

Building on these techniques, absorption spectroscopy can be extended to spatial measurements of the temperature. For example Liu[28] used several parallel laser beams to measure average temperatures across a rectangular combustor with four injectors, resulting in a 1-D temperature profile. The use of multiple laser beams in a plane crossing the flow path coupled with tomographic methods of reconstruction have been employed to obtain 2-D temperature maps of combustor exit temperature distributions.[40-42] The

drawback of this method for industrial applications is the high computational cost and the hardware complexity and access to the gas flow field.

Another method of inferring the temperature distribution, in this case along the line of sight, can be obtained by interpreting the larger amount of information resulting from measuring multiple absorption lines. Previous work at Georgia Tech[43,44] used numerical simulation of water absorption and a broadband light source to show that with three appropriately chosen absorption lines one can monitor for the presence of hot or cold spikes in the exhaust flow of a high-pressure combustor. A similar approach was later applied to measurements of O_2 profiles in static heated cells of air.[33] Many closely spaced absorption lines were measured and used to compute the mole fraction or column-density of O_2 corresponding to predefined temperature bins over the range of temperatures expected in the gas. This technique was named "temperature binning."[33] Just recently this technique was also demonstrated at relatively low temperatures using a flat flame burner.[45]

1.3 Objectives

For years, the development of measurement and control systems for the temperature profile at the exit of a gas turbine engine (e.g., PF) has been listed as one of the key enablers of next generation engines.[4,5,7] As noted above, many solutions for limited or average temperature measurements exist, but there has been relatively little research in fast and simple sensing of temperature profiles. The research undertaken here addresses the need for temperature profile sensing and extends initial efforts to address temperature nonuniformity.

The ultimate objective of this research is to develop a sensing method for gas temperature nonuniformity along the line of sight through a hot gas region based on diode laser absorption and to understand the factors that would affect its performance in a practical implementation. The intended result is a relatively simple, fast, and economical sensing method that can be used for pattern factor control or for experimental research of new combustion systems.

As part of this research, it was necessary to develop a thorough understanding of the physical principles governing absorption sensors and particularly how they apply to *nonuniformity sensing*. This understanding is used to develop a method for sensing the level of temperature nonuniformity along the line of sight in the exit of a combustor.

A set of software tools based on absorption physics is developed for the design and analysis of performance and operation of absorption sensors. These tools are used to design a nonuniformity sensor and to analyze its operation. Needed hardware for laser absorption sensing of temperature nonuniformity and its effects on performance are also investigated. The sensor concept is tested experimentally and through computer simulations. The final aim of this work is to completely characterize such a sensor system and to asses its feasibility for deployment in practical combustor rigs.

Optical sensing is chosen because gas-turbine engines have stringent requirements. Diode lasers in particular, have proved extremely useful in the development of combustion sensors for the reasons mentioned earlier and their compatibility with fiber-optics, allowing the sensors to be located remotely. Because of the weight restrictions on aero-engines, difficult access to the flow path, and the characteristics of rotating turbomachinery, engines seem best suited for initial application

of such sensors. However, the tighter constraints on operating temperatures and the need to achieve maximum loads for short durations in aeroengines also make the technology appealing for flight applications. Although the sensor concept described in this work is initially aimed at gas-turbine engines, it can also be used for other applications, such as boundary layers, large arrays of industrial burners, and other industrial applications where temperature uniformity is essential for certain chemical processes.

1.4 Thesis Layout

The theoretical basis for temperature sensing based on laser absorption is developed in Chapter 2. The theory of sensing nonuniform temperature profiles is also developed in Chapter 2 and based on it, a sensing concept is introduced. Based on a literature survey and consultation with users and experts, the desired performance of nonuniformity sensors is also defined.

The methodology used to investigate the sensor concept is presented in Chapter 3. This includes the software tools developed for sensor analysis and the experimental setup used for testing the sensor concept, including data processing developments.

Chapter 4 presents the results of the modeling and experimental investigations, a characterization of the senor operation and performance, as well as limitations of this sensing technique. Chapter 5 presents the results of a comprehensive sensor analysis. This includes the analysis or errors affecting absorption sensors, methods of reducing or eliminating these errors, and an assessment of sensor performance based on state of the art hardware. Conclusions and recommendations for future work are presented in Chapter 6.

CHAPTER 2: BACKGROUND AND THEORY

2.1 Absorption Spectroscopy

Absorption spectroscopy is a technique based on measurement of the amount of light that is lost (absorbed) by a medium. The light source can generally be broadband (such as a lamp) or narrowband (e.g., a laser). This research is based solely on the use of narrowband tunable laser sources because of their many advantages, such as wavelength availability, brightness and spectral resolution. The background information given here applies specifically to laser absorption measurements.

Laser absorption measurements relate the attenuation of the laser light signal through a gas region as a function of wavelength to the properties of the gas and its molecular constituents. Part of a laser's incident intensity I_0 is absorbed (or scattered) by the gas molecules in its path resulting in a transmitted signal I. The amount of incoming laser light lost is a function of the physical properties of the gas (such as temperature, pressure, and velocity) and of the spectroscopic properties of the molecules in the gas.

An absorption line is a particular quantum-mechanical transition or change in internal energy of the molecule as a result of absorbing the energy of the laser photon. Absorption occurs when the energy of the incoming photon matches the gap between two energy levels of a molecule in the gas (Figure 2).
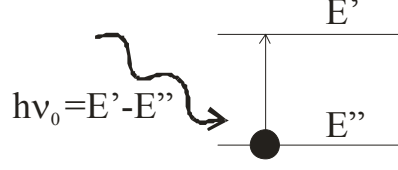
Figure 2. Laser light with photons of energy $h\nu_0$ being absorbed when interacting with molecules in the gas.

The narrowband absorption through a medium of a low power light signal at wavenumber $\nu\,(\text{cm}^{-1})$ with incident intensity I_0 and transmitted intensity I depends on the thickness of the medium, L (cm), the concentration of the absorbers in that medium, and their properties. The relationship that relates these properties is often denoted as the Beer-Lambert Law:[46]

$$\frac{I}{I_0}(\nu) = e^{\int_0^L -k_i(\nu)\,dl} = e^{\int_0^L -pxS_i(T)\phi(\nu-\nu_0,T,x,p)\,dl} \tag{1}$$

where $k_i(\nu)$ (cm^{-1}) is the spectral absorption coefficient, p is the pressure (atm), x is the absorber mole fraction, S_i is the line strength $(\text{cm}^{-2}\,\text{atm}^{-1})$ of the ith transition (centered at ν_0), T is the temperature (K), and ϕ is the line shape function (cm). The Beer-Lambert law holds when the gas is in local thermodynamic equilibrium (LTE), scattering is low (or ignored), and the laser power is low enough not to disturb the LTE assumption.

For a particular transition i centered at $\nu_{0,i}$, its line strength S_i represents the total intensity of the transition per absorbing molecule and is a function of temperature only:

$$S_i(T) \approx S_i(T_0)\frac{Q(T_0)}{Q(T)}\frac{T_0}{T}\exp\left(-\frac{hcE''}{k}\left(\frac{1}{T}-\frac{1}{T_0}\right)\right) \cdot \frac{1-\exp\left(\dfrac{-hc\nu_{0,i}}{kT}\right)}{1-\exp\left(\dfrac{-hc\nu_{0,i}}{kT_0}\right)} \tag{2}$$

where Q is the partition function, E'' is the lower state energy of the transition (cm^{-1}), h is Planck's constant, c is the speed of light, and k is Boltzmann's constant. T_0 is a reference

temperature, taken here to be 296 K, consistent with the HITRAN[47] database. The first exponential is part of the Boltzmann fraction (the fraction of all molecules that are in the energy state E'' at T, or the number of molecules available to absorb a photon of $h\nu_0$), and represents the change in population of the lower state. The last term represents the fraction of molecules in the upper level ($E' = E'' + h\nu_0$) that undergo stimulated emission. This term can sometimes be neglected at wavelengths below 2.5 μm and temperatures below 2500 K. For example, at 1.4μm and 1500K neglecting these terms results in a 0.1% error in $S(T)$, while at 2μm and 2000K it results in a 2.7% error in S). The author recommends that for higher accuracy these terms should be included.

Because of broadening effects, a transition does not occur at a fixed (infinitesimal) frequency or energy, but in a narrow spectral range, giving the absorption line a spectral "bell-curve" appearance described by the line shape function ϕ (Figure 3). The line shape function is defined such that when integrated over a large frequency band it reduces to unity. Broadening occurs when the apparent energy of a particular transition changes from the nominal value. This may be due to small changes in the energy states of the absorbing molecule resulting from interactions with other molecules, called collision or pressure broadening. Collision broadening results in a Lorentzian line shape. Broadening also happens when the molecule is traveling towards or away from the light source, resulting in an apparent Doppler frequency shift of the incoming photon. The molecule will then absorb photons with frequency ν_0 in its frame of reference, or frequency $\nu_0 \pm \delta\nu$ in the observer frame. Doppler broadening results in a Gaussian line shape. Collision and Doppler broadening are the main broadening mechanisms occurring at the temperatures and pressures considered in this work. When both collision and

15

Doppler broadening effects are important, as is the case at high temperatures, the line shape (ϕ) becomes a convolution of Lorentzian and Gaussian profiles called a Voigt profile. A typical absorption line (Voigt profile) is plotted in Figure 3. The absorption line shape is characterized by its center wavelength, v_0 (cm^{-1}), which represents the energy difference between the lower and the upper states, the peak absorption in the center, and the width of the line at half the peak height called the full width at half maximum, FWHM (Figure 3).
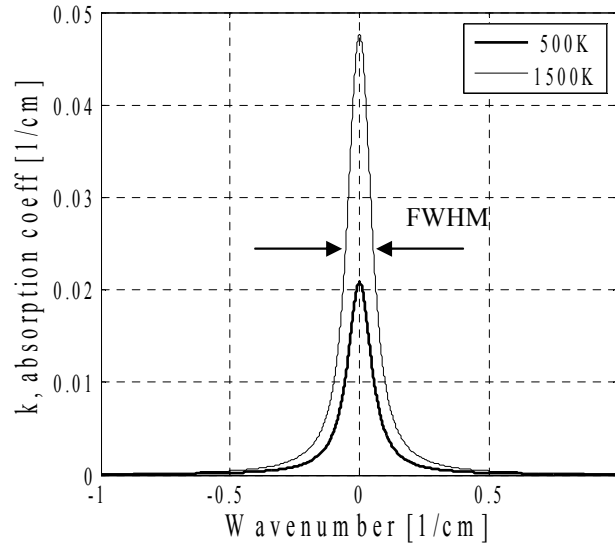
Figure 3. Generic shape of an absorption line (Voigt profile) at two temperatures.

When there are multiple, closely spaced transitions, i.e. lines with closely spaced v_0 representing similar energy differences between the upper and lower levels, then in a first approximation the spectral absorptions of the lines can be added together. This approach neglects line interactions.

2.1.1 Uniform Flow Properties

In a medium with uniform properties (i.e., temperature, pressure and concentration are constant along a path through the medium), the temperature and mole fraction of the species of interest can be determined by probing two of its absorption lines, say i and j. The integrated absorbance, or simply absorbance, is the area under the curve in Figure 3, or the integral of k_ν over a frequency band centered at ν_0 and wide enough to encompass all absorption contributions from the given transition (eq. (3)). The integration process also eliminates the line shape function. Then the ratio of the absorbances, α_i/α_j, of two lines becomes a function of temperature only:

$$\alpha_i = \int_{-\infty}^{\infty} k_\nu d\nu = \int_{-\infty}^{\infty} -\ln\left(\frac{I}{I_0}(\nu)\right) d\nu =$$
$$= \int_{-\infty}^{\infty} \int_0^L p \cdot x \cdot S_i(T)\phi_i(\nu - \nu_{0,i}, T, x, p) dl d\nu = \qquad (3)$$
$$= pxS_i(T)L$$

$$\frac{\alpha_i}{\alpha_j} = \frac{S_i(T)}{S_j(T)} = \frac{S_i(T_0)}{S_j(T_0)}\exp\left(-\frac{hc}{k}(E_i''-E_j'')\left(\frac{1}{T}-\frac{1}{T_0}\right)\right) \qquad (4)$$

$$T_{ij} = \left[\frac{1}{T_0} - \frac{1}{1.44(E_i''-E_j'')}\ln\left(\frac{\alpha_i}{\alpha_j}\frac{S_{0j}}{S_{0i}}\right)\right]^{-1} \qquad (5)$$

Thus for a uniform flow, the temperature of the gas can be determined from eq. (5) and the concentration of the species of interest from eq. (3). In a gas with uniform properties, any two lines would yield the same results (neglecting experimental errors).

There is an alternate method of determining the gas properties without the need of tunable lasers. By simply monitoring the peak absorption values for two lines (or generally the absorption at two different wavelengths, i.e. with two laser beams) one can relate the ratio of peak (or arbitrary) absorption values to gas properties. The drawback

comes from the need to accurately know or determine the broadening characteristics of the lines and to calibrate such a system for good performance. Although this method was investigated earlier by the author, all significant work to accomplish the objectives of this research was done using the integrated absorption measurement method. Details about using peak ratios can be found in Appendix A.

2.1.2 Line Selection and Sensitivity for Two-line Thermometry

In a medium with uniform (or assumed uniform) temperature and concentration profiles, sensors based on measurements of two absorption lines are used to monitor temperature or species. The absorption lines used by such a sensor have a large influence on the sensitivity and signal to noise ratio that can be achieved under a given set of conditions. Usually the available hardware limits the accessible spectral region and consequently the available absorption lines from which to choose. Furthermore, different molecules have absorption features in different regions of the spectrum. There have been several procedures published for choosing absorption lines for temperature sensing.[24,48,49] The process described below is generic and applies to any laser absorption measurements. A database of spectroscopic information has to be used in order to select absorption lines. The largest such database useful for combustion and atmospheric studies is the HITRAN database – which is used throughout this thesis.

Two aspects of the absorbance signal are of primary importance: the strength of the signal in the given temperature range and the relative change in the signal strength with temperature. In order to make a temperature measurement there has to be a measurable amount of absorption at the given frequency – that is to say the signal to

noise ratio has to be, at a minimum, greater than one. This constitutes the first criteria in selecting appropriate absorption lines.

For a given expected temperature range (or average temperature), one should select all lines that have a minimum absorbance greater than some detectable limit. In laboratory measurements of gases or laminar flows, absorption detectivities of better than 10^{-8} cm^{-1} have been reported.[50,51,52] For real, turbulent, unsteady, combustion flows the best measurements seem to be limited to minimum detectable absorbances of roughly 10^{-4} cm^{-1} and uncertainties greater than about 3%.[25,27,39,48]

All measurements are limited by a minimum uncertainty; therefore to resolve small temperature changes it is desirable to have the largest possible relative change in the signal strength with changes in temperature. Two-line thermometry is based on applying eq. (5). For simplicity of notation, R is used for the ratio of the measured absorbances of the two lines, i.e., $R \equiv \alpha_1/\alpha_2$. Then the sensitivity of the measured absorbance ratio $\Delta R/R$ to fractional changes in gas temperature $\Delta T/T$ can be obtained by differentiating equations (4) or (5):

$$\frac{\Delta R}{R} = \frac{\Delta T}{T} \frac{hc/k(E_2^{//} - E_1^{//})}{T} = \frac{\Delta T}{T} \frac{1.44(E_2^{//} - E_1^{//})}{T} \qquad (6)$$

To improve sensitivity and signal to noise ratio, larger fractional changes in $\Delta R/R$ are sought for the same fractional change in $\Delta T/T$. The only variable that can be changed to increase this sensitivity is the difference between the lower state energies of the two lines $\Delta E'' = E_2'' - E_1''$ (by choosing different lines). Consequently, for better sensitivity one should select lines with as high a $\Delta E''$ as possible. Ideally, a $\Delta E'' > T/1.44$ should be used.

Physically, large $\Delta E''$ means that the two lines have different slopes of absorbance to temperature, as expressed by the first derivative of the absorbance, $\partial S/\partial T$.

The higher the slope (1st derivative), the larger is the response to a small change in temperature. At low temperatures, there are more molecules in states with small E'' and relatively few molecules in states with larger E''. As the gas temperature increases, states with lower energies start to get depleted and states with higher energies start to get populated. This change in populations with temperature is measured by the slope of the absorbance.

Absorbance spectra of gases are comprised of many absorption features (Figure 4). Most absorption lines from the same molecule or different molecules overlap to some degree most of the time. If multiple lines overlap than determining the actual absorbance for one transition becomes quite challenging because the convolution of the lines has to be determined, their spectroscopic parameters have to be well known, and a wider scan may be required to capture the baseline. For practical applications, it is desirable to select absorption lines that are relatively isolated such that their baseline can be readily measured and their spectroscopic properties verified experimentally. A few overlapping lines may also be used, but their individual or aggregate properties have to be determined or verified, which is generally more difficult. In this case, isolation is defined as a line that is much stronger that any other line that exists within a certain spectral vicinity. Much stronger is to be defined based on the required accuracy; for example if the line of interest is 100 times stronger than any adjacent line, than the contribution of the adjacent lines to the absorbance of interest is limited to less than a few percent. The spectral vicinity should be defined in terms of the full width at half max (FWHM) of the line of interest. More than about 10 FWHM to either side of the line center are needed for

baseline detection, and thus this region should have limited or no significant interference from other absorption features (see section 5.2.4.2 and Figure 37).

Finding completely isolated lines within the laser tuning range may prove to be impossible. In this case, if just a few known lines overlap, but the overlapping line set is isolated from the rest of the spectrum, than this set can be treated as an absorption feature by measuring the composite absorption and computing its temperature dependence.

The results for uniform mediums presented above are routinely used in the interpretation of laser absorption measurements. However, temperature and gas composition are typically not uniform in practical combustion flows. Therefore, the following section examines absorption measurements with a focus on the influence of nonuniformities.

2.1.3 Nonuniform Flow Properties

The spectral absorption coefficient and the line shape are functions of the local temperature and species concentration at every point along the line light path. When the temperature and concentration of the medium are not uniform, as is generally the case in a combustor, the integral in eq. (3) cannot be solved without prior knowledge of the temperature and concentration values along the path, $T(l)$ and $x(l)$. For arbitrary temperature and concentration profiles along the line of sight, the ratio of the absorbances of two lines i and j becomes:

$$\frac{\alpha_i}{\alpha_j} = \frac{\int_{-\infty}^{\infty}\int_0^L p \cdot x \cdot S_i(T)\phi_i(v - v_{0i}, T, x, p)dldv}{\int_{-\infty}^{\infty}\int_0^L p \cdot x \cdot S_j(T)\phi_j(v - v_{0j}, T, x, p)dldv} = \frac{\int_0^L x(l) \cdot S_i(T(l))dl}{\int_0^L x(l) \cdot S_j(T(l))dl} \neq \frac{S_i(\bar{T})}{S_j(\bar{T})} \qquad (7)$$

Since the absorption is an integral over the path, the actual location of the temperature and concentration values is not important, just their distribution. In other words, the integrated result depends on the path length associated with a given temperature and concentration value, not where it occurs along the laser path. Furthermore, since the path integral acts as an averaging process, the integrated value is different from the absorption of the arithmetic average temperature and concentration because the line strength is a nonlinear function of temperature. As such, information on the temperature and absorber concentration distributions (nonuniformity) is contained in the nonlinear part of the absorbance, through the line strength function S. As an illustration, for a profile of average temperature $\overline{T}$, the absorbance in regions of the profile where T is different than $\overline{T}$ can be expressed using the first terms of a Taylor series expansion around $\overline{T}$:

$$\alpha(\overline{T} + \Delta T) \approx \alpha(\overline{T}) + \frac{\partial \alpha}{\partial T}\bigg|_{\overline{T}} (\Delta T) + \frac{1}{2}\frac{\partial^2 \alpha}{\partial T^2}\bigg|_{\overline{T}} (\Delta T)^2 + ... \tag{8}$$

The first two terms represent the linear part of the absorbance variation with temperature - no distribution information can be had from these terms since the final absorbance would be a function of the arithmetic average temperature only. The third and higher terms represent the nonlinearity of the absorbance to temperature. It is the contribution of these terms that can be used to extract information about the distribution of temperature along the line of sight.

An order of magnitude analysis reveals that the third term is on the order of $\alpha(\overline{T})\Delta T^2 / \overline{T}^2$; thus the leading nonlinear term provides a smaller contribution the larger the average temperature $\overline{T}$ becomes. This observation is important because it means that

more sensitive measurements are needed to resolve the same absolute level of temperature nonuniformities at higher average temperatures.

In practical combustion flows there is always some degree of temperature and concentration nonuniformity along the line of sight. Nevertheless, for simple average temperature sensing, the ratio of two absorption lines can still be used. In this case the ratio is an indicator of the average temperature along the line of sight weighted by the absorber distribution. We can recast equation (7) as follows:

$$R_{ij} = \frac{\alpha_i}{\alpha_j} = \frac{\int_0^L x S_i(T) dl}{\int_0^L x S_j(T) dl} \xrightarrow{define} = \frac{S_i(T_{ij})}{S_j(T_{ij})} \tag{9}$$

where T_{ij} is defined to be the 'average' temperature that would be found by *assuming uniform properties* along the path (obtained using Eq. 5). This method is typically used for determining an "average" gas temperature with absorption spectroscopy.[46] However, because of the nonlinear dependence of the absorbance on temperature and the effects of nonuniform concentration, the two-line ratio does not reflect the arithmetic average. This means that the ratio of the absorbances is a function of the spectroscopic properties of the two chosen lines. Thus for nonuniform profiles, ratios of different lines will yield different temperatures (T_{ij}). The resulting temperature will also depend in great measure on the correlation between concentration and temperature. The more we know about how the mole fraction and temperature are related, the more meaningful T_{ij} becomes. For simplicity in the treatment, throughout most of this thesis it is assumed that the absorber concentration is either constant or a monotonic function of the temperature, which is a reasonable approximation for most combustion applications.

Measurements using eq. (9) can still be used for monitoring a useful "average" temperature, but spatially there can be large temperature deviations from this average number. Sometimes careful selection of lines can reduce some influences, like the effect of boundary layers on the temperature measurement.[53]

2.1.4 Absorption Marker Species

The theory presented above applies to any absorbing species as long as its spectroscopic properties are known or can be measured. Although the results of this research apply to absorption spectroscopy using any species, for the experiments and modeling performed in this research, a choice of species had to me made. In combustion exhaust gasses, water vapor is one of the major species, with concentrations large enough to provide good absorption signal strength. Furthermore, due to its nonlinear nature, the water molecule exhibits a very large number of transitions throughout a wide spectral range; a spectral region for measuring water free from interference from other species can be easily found. Because of this, water was chosen as the marker species for this research. A sample absorption spectrum of water vapor in air is shown in Figure 4; many thousands of lines can be seen forming several bands.
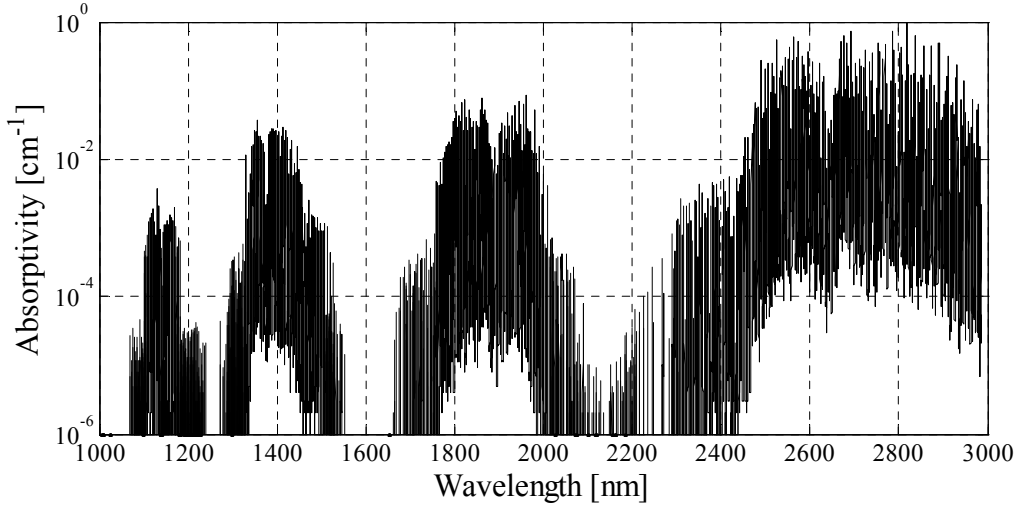
Figure 4. Sample absorption spectrum of water vapor in air.

2.2 Nonuniformity Sensor Concept

As outlined above, measurements of gas absorption features can yield information on physical properties of the gas, such as temperature, pressure, velocity, and concentration of the absorbing species. Because the path-integrated absorption measurements are usually nonlinear functions of the gas properties, measuring more than two lines results in information about more than two average gas properties along the line of sight or more information about one or more property, such as its distribution.

For pattern factor control purposes, it is desirable to have a simple and rapid sensor that gives information on temperature nonuniformity. Good average temperature accuracy is not necessary – a good measure of the degree of nonuniformity is important. While measurements of two absorption lines give path-averaged temperatures, measurements of three lines can yield another piece of information about the temperature distribution along the line of sight. Such supplementary information about the temperature profile can be interpreted as the "spread" of the temperature distribution.

25

While no discrete spatial information can be obtained when using only one line of sight sensor, one can compute various "average" temperatures based on measuring several pairs of absorption lines. As the actual temperature profile becomes uniform, these temperatures (T_{ij}) will converge to the same number. This fact can be used to measure the degree of nonuniformity in the flow. Previous work at Georgia Tech[54,55] used numerical simulation of water absorption using the HITRAN database to show that with three appropriately chosen absorption lines one can monitor for the presence of hot or cold spikes in the exhaust flow of a high-pressure combustor. More recent work by the author introduced a sensing concept based on measuring three water absorption lines that could track the degree of nonuniformity along the line of sight.[43,44]

2.2.1 Nonuniformity Parameter

A sensor that would probe three absorption lines using a tunable diode laser is developed with the aim to create a simple, fast, and rugged sensing system for pattern factor control. Based on the input from three measured absorption values, it is desired to obtain an output parameter that is monotonic with the degree of nonuniformity and can be easily used as an input to a control system. The absorptions of each pair of lines *i and j* from a three line measurement yield a path-averaged temperature, T_{ij}, specific to the chosen pair (eq. (5)). The two resulting 'average' temperatures are combined into a nonuniformity parameter '*U*' defined below:

$$U = \frac{|T_{12} - T_{13}|}{(T_{12} + T_{13})/2} \sim \frac{\Delta T}{\overline{T}} \tag{10}$$

This variable tends to zero when the gas has uniform properties, and increases as the temperature nonuniformity increases or as the degree of mixing decreases. The

operation and performance of this sensor output parameter is analyzed in Chapters 4 and 5.

2.2.2 Other Nonuniformity Sensing Methods

In the case of nonuniform temperature distributions, measuring more than two spectroscopic features gives more information about the temperature distribution along the line of sight. If more absorption lines are measured, more information about the nonuniformity can be extracted. Such data can be used to characterize the statistical distribution of temperature along the line of sight, although the interpretation of absorbance data and what it tells about the nonuniformity is not straight forward. If measurements of two lines yield a measure of the average temperature and measurements of three lines can be thought of providing a measure of the spread of the distribution, or its first moment, then measurements of more than three lines may be interpreted in terms of the higher moments of the temperature distribution. Furthermore, accurate measurements of very many absorption lines can result in a detailed histogram of the temperature distribution

One way to use information from measurements of many lines was devised at Stanford[33] and can yield a limited histogram of the temperature distribution along the line of sight. If lines $i = 1$ to n can be measured accurately, than using eq. (3) a system of equations can be set up as follows:

$$\alpha_i = \sum_{j=1}^{m<n} (xL)_j S_i(T_j) \tag{11}$$

In this case it is assumed that there are $j = 1$ to m regions along the line of sight, each with uniform temperature T_j and uniform mole fraction times length $(xL)_j$, dubbed

27

column density. By choosing a set of predefined temperature bins T_j in the range expected for the application, then the column density $(xL)_j$ corresponding to each predefined temperature bin can be computed resulting in a histogram representative of the temperature distribution. Nevertheless, such a histogram is quite sensitive to the specific temperature bins that were chosen and to the nonuniformity in mole fraction along the line of sight. Interpreting the results of such a measurement is not trivial.

2.3 Characterization of Temperature Profiles for Absorption

In gas turbine engines, the temperature field at the turbine inlet (or combustor exit) is generally not uniform and varies in both time and space. The fluctuations in the temperature field result from a variety of factors, among which is turbulent combustion, uneven mixing and burning, and differences between injectors or combustion cans. The spatial temperature nonuniformity is usually quantified by measuring the maximum temperature deviation above the mean along a radius or the circumference of the annular turbine inlet. Throughout the literature the terms pattern factor (PF) or profile factor have been used interchangeably for these measures. The PF is normally defined as in Eq. (12) below, where $\overline{T_4}$ is the mean combustor exit temperature along the measurement line.

$$PF = \frac{T_{4,\text{max}} - \overline{T_4}}{\overline{T_4}} \tag{12}$$

PF quantifies only the peak temperature in space at the combustor exit, providing very limited information about the actual temperature distribution. Since absorbance is a function of the whole temperature distribution along the line of sight and not only the

peak temperature, for the current research PF is not a good aggregate measure of the temperature distribution along the line of sight.

When talking about nonuniformity sensing, it is useful to define a quantity that quantifies the level of nonuniformity of a given temperature profile. Many such measures may be defined, some of them better suited for certain purposes. For this research it is desired to quantify the level of variation in the temperature profile, or some statistical measure of the temperature distribution. Since it is departures from a uniform (T - T_{avg}) profile that affect the absorbance, the standard deviation of the temperature distribution emerges as a natural measure of the nonuniformity, $\sigma_T = \sqrt{1/N \sum \left(T_i - T_{avg} \right)^2}$. Furthermore, to reduce the dependence on the average temperature, the percent standard deviation (or coefficient of variation) of the temperature profile, defined as $T_{std}/T_{avg} = \sigma_T/T_{avg}$ will be adopted in this research as a measure of the temperature nonuniformity along the line of sight.

As mentioned earlier, since absorption is a path integrated measurement, all temperature values affect the measurement, although the spatial distribution of the temperature profile does not matter. What matters is the percent of the path length for each temperature and concentration value, which is equivalent to the histogram of the temperature profile.

For example, several typical temperature profiles with a temperature spread between 1000 K and 1800 K are shown in Figure 5 left. These are a uniform profile, linear and quadratic, 5th degree polynomial representative of large temperatures in the center and colder boundary layers, and a sinusoidal profile that might represent a gas with a hot and a cold region. For line-of-sight absorption, these profiles are equivalent to their

temperature-sorted versions, shown to the right in Figure 5. For example, a temperature profile with uniform random fluctuations around the mean, when sorted in order of increasing temperature as a function of path length, would look like the linear profile in Figure 5 right. In general, it can be seen (Figure 5 right) that most of these profiles may be approximated by a linear profile or a combination of a linear region over most of the length and a constant maximum temperature region.
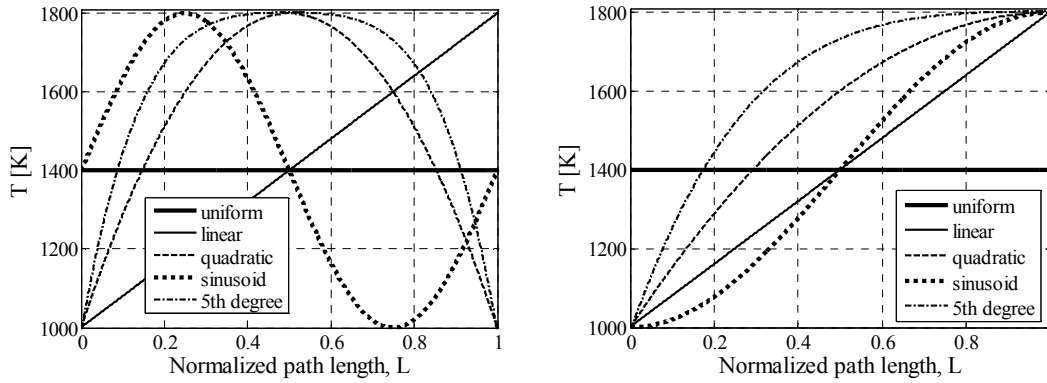
Figure 5. Temperature profiles along the path (left) and sorted by increasing temperature (right).

For the study of absorption, two idealized temperature profiles will be used to approximate these and other real-life temperature profiles: (A) profiles with two temperature regions and (B) profiles with a linear temperature dependence on path length (Figure 6). The profiles of type (A) are characterized by three parameters, T, b, and s: given a uniform temperature T, the profile exhibits a spike of magnitude bT over $s\%$ of the length. The average temperature of this type of profiles is $\overline{T}_A = T(1-s+bs)$. The second set of profiles, (B), is characterized by a mean temperature, T_{avg}, and the maximum temperature above the mean ΔT_{max}. It is assumed that the temperature is a

linear function of length, or in other words the temperatures are uniformly distributed between $T_{avg} - \Delta T_{max}$ and $T_{avg} + \Delta T_{max}$.
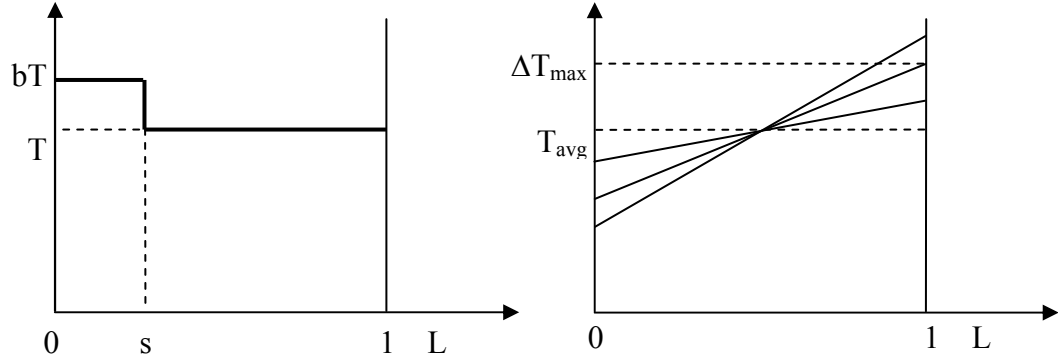
Figure 6. Idealized temperature profiles for the study of absorption. Left: profile of type (A) with a spike above a uniform profile. Right: profiles of type (B) with linear temperatures characterized by the mean and maximum deviation.

2.4 Requirements for Temperature Nonuniformity Sensing

To define the requirements of a temperature nonuniformity sensor for gas turbine engines, actual temperature distributions or measures of these distributions, such as the PF, are needed. A survey of published literature and consultations with experts resulted in limited data, as turbine inlet temperature profile information in gas turbine engines is a very closely guarded secret (for both proprietary and export control reasons).

An example of the temperature distribution in the exit of a gas turbine combustor is shown in Figure 7.[8] Although the average temperature is relatively low (~1900 °F or 1300 K), there are many deviations of more than 250 °F (~140 K), and the pattern factor for this profile is 0.13 (based on absolute temperatures).
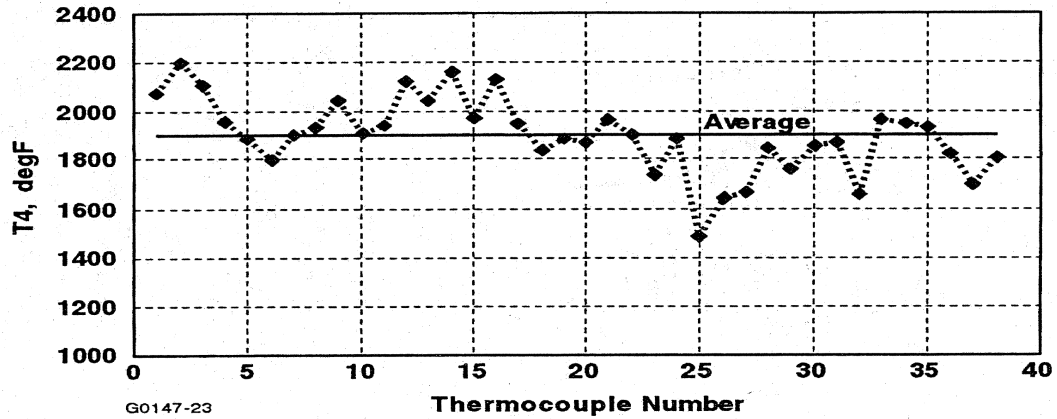
Figure 7. Combustor exit temperature measured by a series of 38 thermocouples placed circumferentially, one thermocouple downstream of each injector and one downstream and in-between adjacent injectors.[8]

Further information on PF levels comes from work comparing modelling and measurements for GE gas turbine combustors.[14] That work presents measured PF values in the range 0.1–0.4. Assuming an average temperature of roughly 1800 K, this translates into maximum deviations of 180-720 K. Another source describes modern combustors operating with pattern factors between 0.2 and 0.3.[56]

For the practical use of a nonuniformity sensor, the published data on pattern factor can be used to define a sensor requirements envelope: a nonuniformity sensor should be capable of measuring temperature profiles with temperature deviations between 150K and 700K, or pattern factors between 0.1 and 0.4. The smaller the minimum deviation sensed, the better the sensor performance.

2.5 Error Analysis

Absorption measurements are by no means exact. Errors in the instrumentation and in the approach limit the accuracy and precision of these measurements. The terms errors and uncertainty are used interchangeably to mean variations in the measured data.

32

For the scope of this work, errors will be classified as either random or systematic. Systematic errors are the result of measurement technique or instrumentation limitations which always result in the measured value being larger (or smaller) than the "true" value.

In general, there are multiple sources of errors affecting a measurement and there are variables, such as the nonuniformity parameter U, which depend on several other measured quantities. Let a quantity, X, be a function of several other measured variables, y_i, each one with uncertainty described by its variance, s_i^2. Then if the y_i variables are uncorrelated, the variance of the X measurement can be calculated using the following error propagation formula:

$$s_X^2 = \sum_{i=1}^{n} \left[\left(\frac{\partial X}{\partial y_i} \right)^2 s_i^2 \right] \tag{13}$$

By estimating the uncertainty in each measurement error source and measured absorption values, the above equation can be used to compute the overall sensor uncertainty.

CHAPTER 3: METHODOLOGY

This chapter describes the methods used in the development and analysis of the temperature nonuniformity sensing technique. A comprehensive approach was used, consisting of analytical work, experimental testing, and computer modelling.

3.1 Computer Modelling and Analysis Methods

Computer modeling is used to supplement experimental testing and to perform sensor virtual testing under a wide range of conditions. In particular, sensor models are used to validate the basic concept, to perform trade studies of sensor operation, and to study the effects of errors and uncertainty on sensor performance. Sensor modeling is also used to determine an envelope of sensor applicability and performance.

3.1.1 Sensor Model

Mirroring the physical setup of an absorption sensor, the modelling effort is broken down in two parts: (a) a model of the medium to be measured and its absorption, and (b) a model of the sensor hardware. A comparison between the physical sensor and the model is shown in Figure 8. The medium to be measured is a gas (combustor exhaust) with a given distribution of temperature and absorber concentration along the laser beam path (line-of-sight). The attenuation in the laser signal, I/I_0, or the absorption, α, is the integral along the path and is computed as the sum of the absorbances for a finite number n of length sections l_j with given temperatures T_j and concentrations x_j (discretized forms

of eq. 1 or 3). Either the wavelength dependent absorption, $k(v)$, or the integrated absorbance, α, can be computed as follows:

$$k(v) = -\ln\left(\frac{I}{I_0}(v)\right) = \sum_{j=1}^{n} k_j(v) = \sum_{j=1}^{n} p x_j S(T_j) \phi(v - v_0, T_j, x_j, p) l_j \qquad (14)$$

$$\alpha = \int_{-\infty}^{+\infty} -\ln\left(\frac{I}{I_0}(v)\right) dv = \int_{-\infty}^{+\infty} \sum_{j=1}^{n} k_j(v) dv = \sum_{j=1}^{n} p x_j S(T_j) l_j \qquad (15)$$

The spectroscopic properties of the absorption features are taken from the HITRAN database.[47] The line strength is computed with equation 2. The computation of the integrated absorbance (eq. 15) is relatively straight forward and is useful for analyzing overall sensor response. The spectral absorption coefficient is needed to simulate the spectral sensor signal, similar to how it is physically measured. The Kuntz implementation of the Humlicek algorithm is used to compute the Voigt line shape function, ϕ, and wavelength-dependent absorption.[57,58] The broadening parameters from the HITRAN database, although not always accurate, are used to compute the parameters for the Voigt profile, as described in Appendix A. Then given a specified laser incident signal $I_{0L}(v)$, the detected signal $I(v)$ can be computed using equation 1.

The hardware model allows the creation of any arbitrary laser baseline signal, I_{0L}, which can be wavelength dependent. Constant and linear profiles are used, as well as higher order polynomial profiles meant to approximate the measured experimental laser baseline. Errors can also be introduced in the simulated measurement in the form of a wavelength dependent gain, $G_e(v)$. For example, losses in the optics and detection system are approximated by a constant or weakly wavelength-dependent gain, G, that multiplies the transmitted signal. Absorption from gases outside the measurement region is

computed using either eq. (14) to determine the spectral effects, or using eq. (15) to add an overall effect. Other wavelength dependent effects can also be added to the transmitted signal I. The whole sensor system and response can then be modelled by combining the absorption model with the hardware model:

$$I_{simulated}(v) = I_{0L}(v)G_e(v)\exp\left[-\sum_{j=1}^{n} px_j S(T_j)\phi(v - v_0, T_j, x_j, p)l_j\right] \qquad (16)$$

These simulated sensor output laser transmission scans are reduced with the same sensor data analysis software used in the experiments (Figure 8).
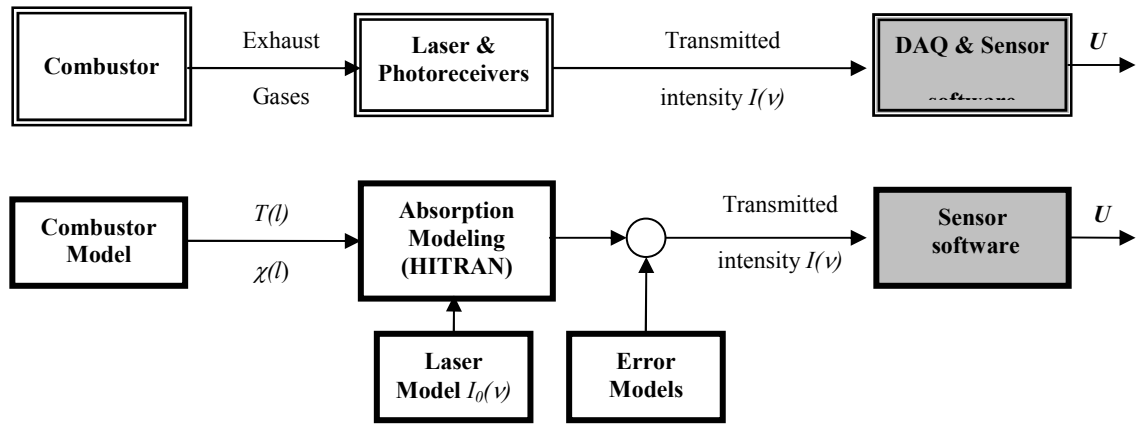
Figure 8. Physical sensor system and sensor model.

3.1.2 Synthetic Combustor Data for Sensor Simulations

The models described above are used to explore the sensor operation and performance under a variety of conditions described by the temperature and species profiles, as well as expected levels of measurement uncertainty. Three types of data are used for the study of sensor operation and performance: (i) simple synthetic data (temperature and species profiles, for example profiles of type (A) or (B)) generated to be representative of idealized combustor conditions, (ii) temperature data measured during

36

experiments and assumed corresponding concentration profiles, and (iii) data representative of realistic gas-turbine engine conditions obtained from CFD combustor simulations.

The CFD data used in this research is based on several combustor exit temperature and species profiles obtained from a Large Eddy Simulation (LES) of a turbulent, axisymmetric, premixed, gas fueled, swirl-stabilized combustor with adiabatic walls operating at 6 atmospheres.[59] Exit temperatures are on the order of 1000-2000 K. Several instantaneous profiles at three downstream stations near the exit are used for the sensor simulations (Figure 9). These stations are representative of different combustor conditions. The absorbances of water lines along a diameter of the combustor are calculated for the given temperature and concentration profiles using spectroscopic data from the HITRAN 2004 database and used to simulate the sensor output U.
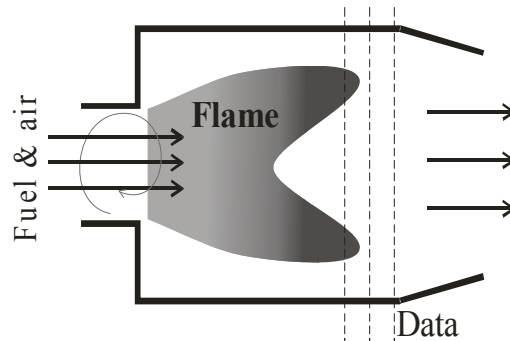
Figure 9. LES simulation of axysimmetric combustor. Temperature and species profiles from three downstream stations (dashed lines) are used for sensor simulations.

A representative set of instantaneous temperature profiles at three downstream stations (bottom is furthest) is shown in Figure 10. Water concentration profiles have the same shape because the simulation was performed for adiabatic walls.
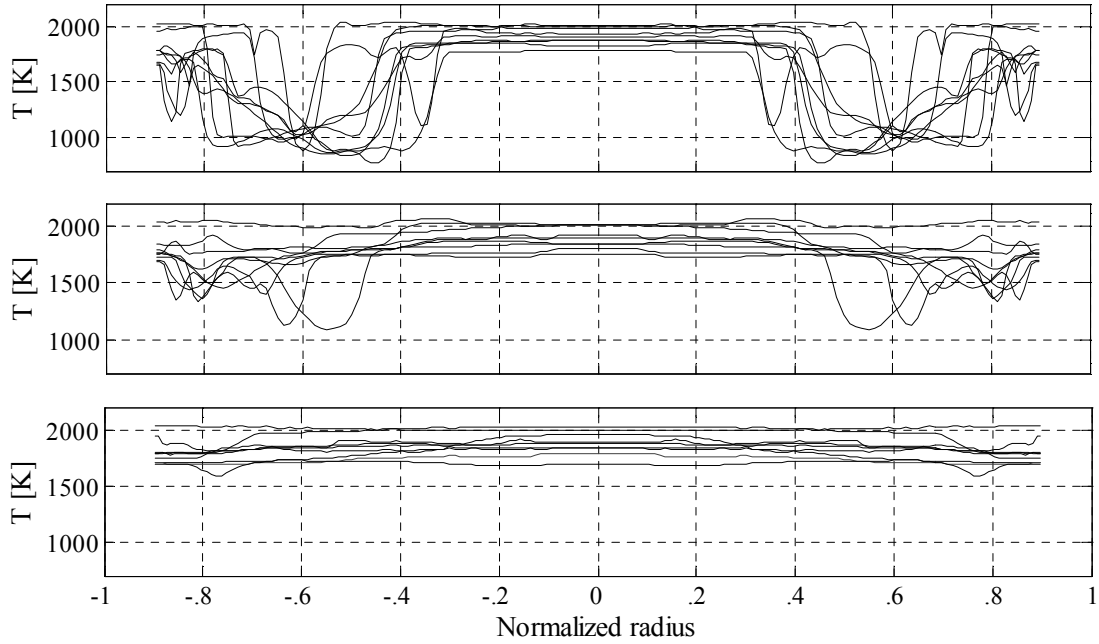
Figure 10. Example of instantaneous temperature profiles at three stations downstream of the combustor (bottom panel is farthest downstream). [59]

These temperature and concentration profiles are later used as inputs to eq. (16) for sensor simulations. The model described above is used to study the sensitivity of the sensor to the different sources of errors and to devise ways to minimize their effects. Furthermore, the model is used to determine minimum laser and hardware specifications needed for a required level of sensor performance and to optimize the sensor design. These results are presented in Chapters 4 and 5. Furthermore, this model can also be used to design and test a temperature nonuniformity control system. The simulations can also be used as a design tool to evaluate different sensor configurations without the lead time and expense of building new experimental facilities and buying new hardware.

3.2 Experimental Methods

Experimental testing is important for concept validation and for understanding limitations in implementing the concept. Although a series of experimental setups were constructed during the development process, only the tests conducted in a combustor rig will be described here as they are most relevant to realistic sensor applications.

A series of combustor experiments were conducted in order to gain an understanding of practical sensor implementations and to validate the sensor concept in realistic combustion conditions. A combustor capable of creating a series of different temperature profiles at the exit was used and subsequently modified to provide a wider range of conditions and allow for better control of the exit temperature profile. The initial experimental setup (configuration A) is presented in Figure 11 and consists of the sensor (laser, optics, detectors, and data acquisition and conditioning) and the test combustor.
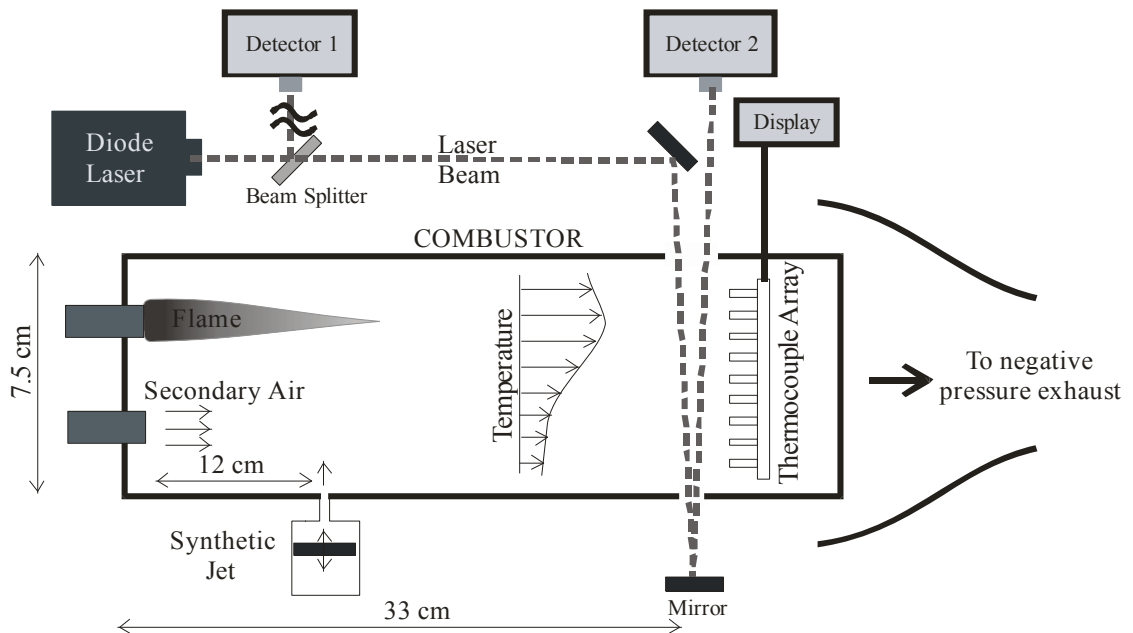
Figure 11. Experimental setup in configuration A.

3.2.1 Combustor Test Rig

The combustor has a rectangular cross-section (internal size 2"×3" or 5×7.5 cm) and two upstream injectors. The top and bottom walls are made of brass and the two side walls are fitted with 29 cm long and 8 cm high quartz windows. The primary fuel-air injector is located at the top of the combustor, and a secondary (dilution) air injector is located at the bottom. The injectors have an OD of 1" and extend into the combustor about 0.5"; they are placed vertically, 1.75" apart. Methane fuel and air are supplied to a control panel by laboratory lines at 25psig and 125psig respectively and at room temperature. The air flow is split into primary and secondary streams and regulated by two rotameters (Dyer RM Series) with nominal ranges of 0-100 and 0-400 scfh. Methane is regulated by a rotameter (Matheson 604) with a range of 0-70 scfh. The flow rates of methane, primary, and secondary air can all be varied independently.

At the combustor exhaust, there is a vertical array of nine type-K thermocouple wires, each with a wire diameter of 0.02". The thermocouples are located a few mm downstream of the laser path. The laser enters the combustor through two small holes (3mm × 12mm) in the top and bottom walls. Hot gasses may potentially escape through these holes, changing the effective laser path length and the thermocouple measurements. To prevent hot gasses from escaping or cold air from entering the combustor, the negative pressure duct was adjusted such that the top and bottom thermocouples registered the same temperatures when the holes were opened or covered. The thermocouples are distributed at the following normalized heights (with '0' representing the bottom wall and '1' representing the upper wall): 0.08, 0.23, 0.38, 0.54, 0.62, 0.69, 0.77, 0.85, 0.92. The thermocouple outputs are connected to a series of portable

thermocouple readers (Omega model HH12). The outputs (in °C) are recorded manually at the beginning and end of each set of laser line scans. The thermocouple readouts are averaged (manually) over several seconds.

The shape of the exhaust temperature profile is controlled in two ways. First, the relative flow rates of the primary and secondary air are changed. In this case, the total water content of the exhaust is kept constant if the total air supply rate remains the same (assuming complete combustion). Consequently the shape of the temperature and concentration profiles changes as the equivalence ratio changes and as the relative velocities of the two streams are adjusted. Another way to alter the temperature profile is to enhance mixing between the cold air stream and the flame products by downstream actuation. In the current setup, this is accomplished with an array of synthetic jets.[60,61]

A synthetic jet is a mixing actuator that requires no external mass flow. It typically consists of a cavity with a small orifice leading to the flow of interest. The cavity volume is modulated such that it draws in fluid from the flow field during its expansion and ejects it, in a jet like manner, during its compression. In the current implementation, the synthetic jet is a piston-cylinder system in the lower part of the combustion chamber (Figure 12). Therefore it can move cold fluid from the bottom of the stratified combustor into the hot region above and enhance the mixing. An electric motor is used to drive the piston and the fluid is ejected through an array of four small holes oriented perpendicular to the combustor flow. The mixing enhancement increases roughly with modulation frequency for our configuration, but at high frequencies the effects diminish.[61]
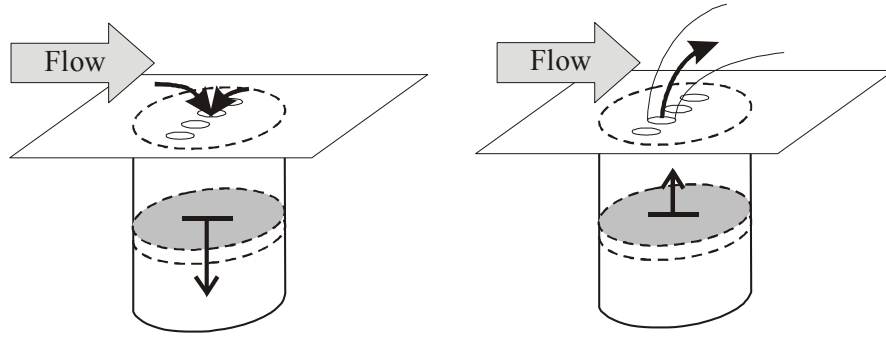
Figure 12. Synthetic jets for enhanced mixing.

In the initial configuration (A), mixing of the two jets was difficult, allowing for little control authority over the exit temperature profiles. Furthermore, because of the flow configuration and heat losses, the combustor could not achieve high exhaust temperatures.

The test rig was subsequently modified to provide higher temperature conditions and to allow for better control authority over the temperature profile (configuration B). This was achieved by distributing the dilution air uniformly around the primary methane-air injector. The modified experimental setup is presented in Figure 13. The primary methane-air injector is still located near the top of the combustor, but dilution air is injected through a 9" long region filled with 5mm diameter glass balls ending in a honeycomb flow straightener region 1" long. This air distribution region results in a parallel flow enveloping the primary injector flow. As before, the flow rates of methane, primary, and secondary air can all be varied independently using the rotameters, but are generally adjusted such that the velocities of the primary injector flow and dilution air are close to each other.

In configuration (B), before entering the combustor, the dilution air first passes through a tank of water at room temperature. This humidification process brings the

water vapor content of the dilution air close to saturation (about 2.5% water mole fraction, as measured with a hand-held hygrometer in the combustor exit). The water mole fraction in the dilution air is raised to make sure that there is a measurable amount of water throughout the measurement region, regardless of how well the flame exhaust and dilution air mix.
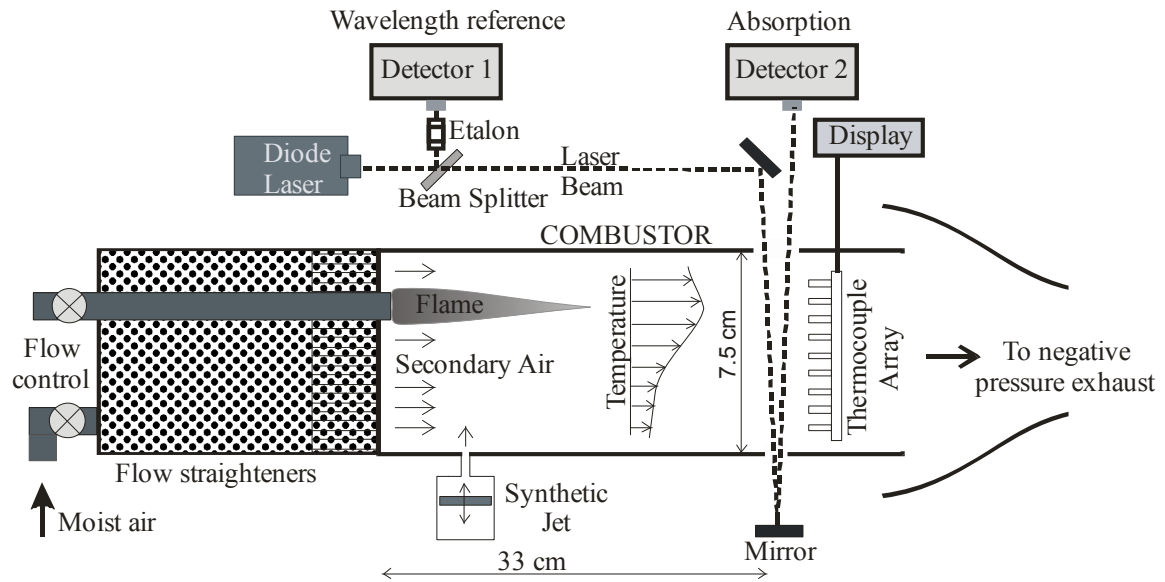
Figure 13. Modified combustor test rig, configuration B.

3.2.2 Sensor Hardware

The sensor consists of a light source (laser), optics, detectors, and signal conditioning (data acquisition and reduction). The light source is a New Focus Velocity model 6332, external cavity tunable diode laser with a maximum power of 3.5 mW and a useful tuning range of 1945–1985nm (total tuning range: 1945–2040nm). The useful range is defined as the region where the laser output is single mode and exhibits a relatively linear power versus wavelength baseline. The laser beam passes through a

beam-splitter (CVI Laser, 60% reflectance, 45º, unpolarized, centered at 2010nm, CaFl), with one beam sent to a New Focus InGaAs large-area photo receiver model 2034 used to monitor the background room-air absorption in configuration (A). The detector has a 3dB frequency response of 700kHz (low gain setting, as used in this work).

In the modified setup (confiuration B), a Fabry-Perot air-spaced etalon is added to the air path and the first detector now monitors relative wavelength instead of room absorption. The etalon is needed to measure the wavelength because the laser tuning speed is not constant, so a linear conversion from the time-scale of the acquired data to wavelength information is not accurate. An etalon is an interference cell made of two partially reflective surfaces with an optical medium between them (Figure 14). The intensity of the transmitted light is a function of the wavelength of the light, the reflectance of the surfaces, the width of the etalon, d, and the index of refraction of the medium between the surfaces, n. Maximum transmission occurs at resonance when there is constructive interference in the etalon. The distance between the transmission peaks is called the free spectral range (FSR) and can be used to measure the relative change in wavelength of the incoming light.

$$FSR_{wavenumbers} = 1/(2nd) \tag{17}$$
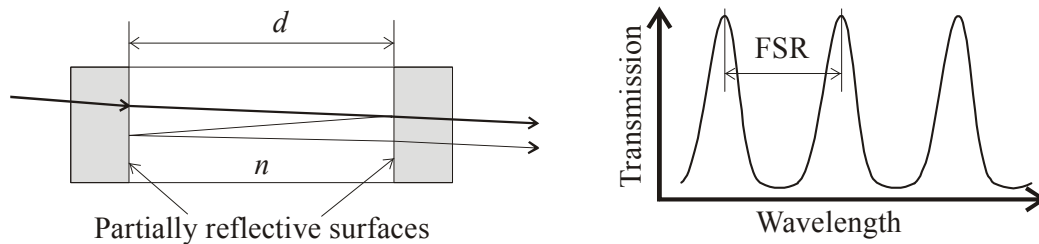
Figure 14. Etalon construction and operation.

A custom etalon was built using two partially reflective mirrors (CVI Laser, 70% reflectivity, centred at 1990nm). The distance between the mirrors is adjustable and was set to 20 cm resulting in a *FSR* of 0.025 cm^{-1}. Since a water absorption line scan is done over about 0.8 cm^{-1}, this results in more than 30 etalon peaks per line scan, sufficient to correct laser wavelength nonlinearity.

In both configurations, the second beam is double passed through the exhaust gases of the combustor and measured by a second identical detector (New Focus model 2034). The two detectors are placed such that the two laser beams travel the same distance through the room air. The voltage signal from the two detectors is captured by a National Instruments data acquisition card (PCI-MIO-16E-4) capable of measuring 250 kilo samples per second from 16 single-ended analogue inputs with a 12 bit A/D converter, installed in a Pentium 4 PC. The sensor output is captured and recorded by a LabView program and computed off-line by a data reduction program written in MATLAB.

The external cavity diode laser used here has two tuning modes: a slow tuning mode over the full tuning range of the laser (up to 40nm/s which corresponds to a repetition rate of ~4Hz over several closely-spaced water lines); and a fast tuning mode (up to ~150Hz) over about 0.3nm, sufficient for measuring one relatively narrow line. A sample wide and slow scan is shown in Figure 15. The large (saw-tooth like) changes in laser power with wavelength are due to etaloning effects in the laser cavity, and the small dips represent absorption lines. Measurement limitations arise because small changes in the absorption lines have to be measured over large changes in the incident laser power. Moreover, because of the difficulty in accurately fitting a background and because of

unsteadiness in the combustor, the slow tuning mode of this laser is more difficult to use for sensor measurements. The large change in laser power is characteristic for external cavity lasers. Most commercially available lasers (though often with smaller tuning range) have much better tuning characteristics and would likely result in better sensor performance.
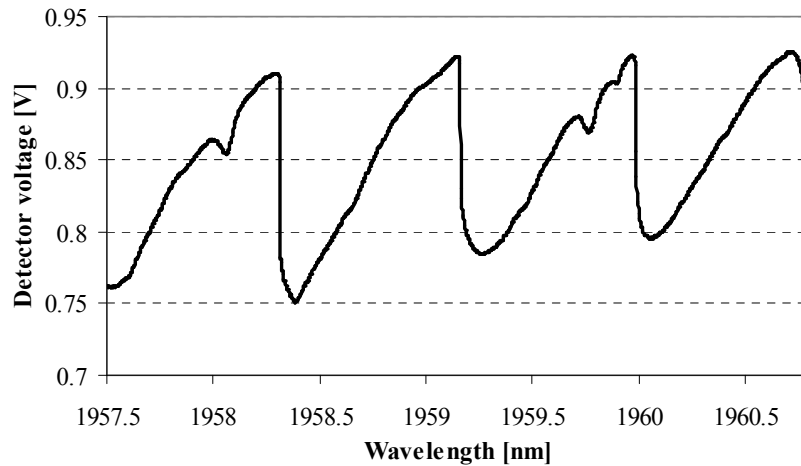
Figure 15. Typical laser signal output measured through a region of room air. The large signal drops are due to laser etaloning; the small dips are absorption lines of water vapor in the room air.

Fast tuning has the benefit of "freezing" the flow and reducing the effects of combustor unsteadiness and beam steering, resulting in much better data. Because of this, only fast tuning was used for sensor testing, despite limiting the measurements to scanning over one line at a time. The laser is fast tuned over an isolated line using a triangular driving wave at 70 or 80Hz (Figure 16). To obtain the three or more lines needed by the sensor, the laser is rapid tuned over one absorption line for one second or more, then the laser wavelength is slowly changed to a new line location and the fast scans are repeated.

46
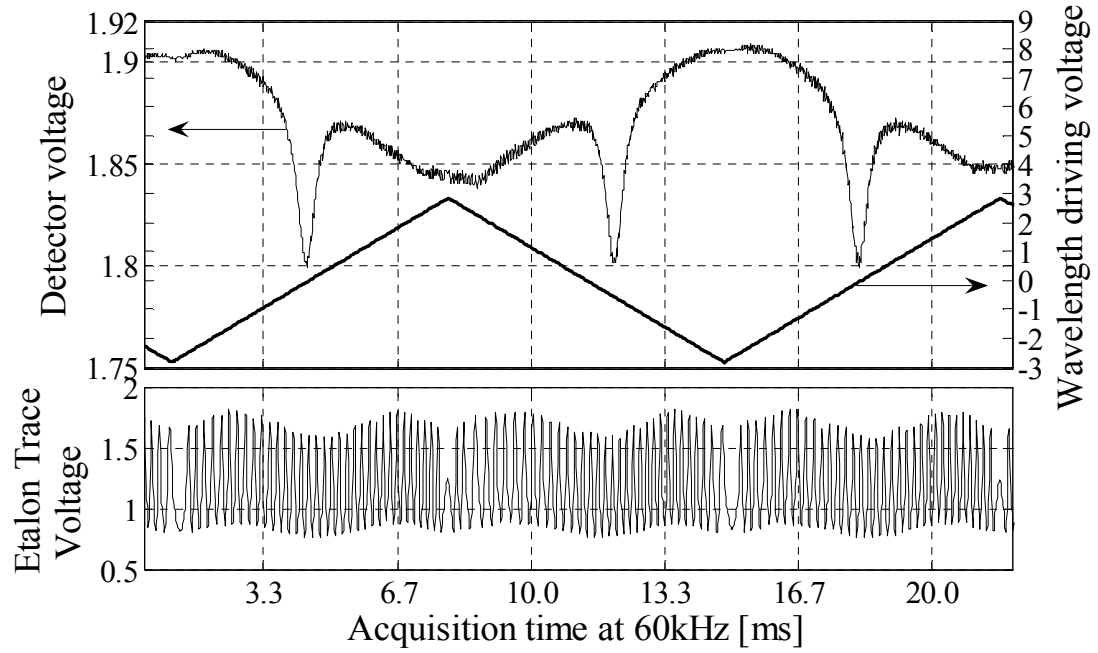
Figure 16. Time trace of transmitted laser signal, voltage signal that drives laser tuning, and etalon transmittance.

3.2.3 Sensor Data Reduction

Software programs were developed to control the laser, acquire the data, and process it to obtain the sensor output U. A LabView program is used to control the laser and capture the raw sensor data during measurements (the voltage signal from the two detectors, the laser coarse wavelength indicator voltage, and the laser wavelength driving voltage). Several MATLAB scripts process this data to obtain the sensor output U. The processing code evolved through several iterations by adding more complex analysis and error reduction techniques to improve accuracy and reduce uncertainty in U. The latest sensor data processing information flow is summarized in Table 1.

By fast tuning the laser for 1-1.5 seconds over each line, a signal trace $I(t)$ containing several hundred line scans is acquired for each line (Figure 16). This trace is then separated into a collection of individual line scans $I_j(t)$. The line center is identified

47

and given the known line wavelength position, v_0. The corresponding wavelength for each line scan is determined from the driving voltage and corrected by use of the etalon data. The result is a set of line transmission signals of the form $I_j(v)$, covering a spectral region Δv. To determine the absorption spectrum, $k(v) = -\ln(I(v)/I_0(v))$, a polynomial baseline is fitted to the far wings of each absorption line, which gives $I_0(v)$ (Figure 17). In some cases, baselines were obtained for each line when the combustor was off and subsequently shifted and used for all other operating conditions. This method better captures the actual shape of the laser baseline signal. A Voigt profile is then fitted to each absorption line scan. The fit is used to determine the integrated absorbance, α. Since the lines are not captured at the same time, the average absorbance of all lines measured at each operating condition are used to compute the U value representative of that condition. Averaging also decreases the effects of combustor unsteadiness, beam steering, and other errors.
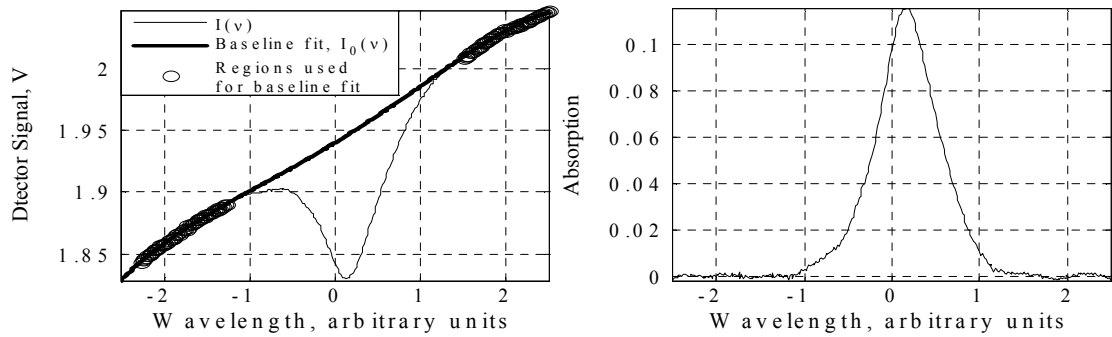
Figure 17. Half-period of fast laser scan over an isolated water absorption line. The top panel shows the detector trace and baseline fit, the bottom panel shows the resulting absorption, k_v = -ln(I/I_0).

Table 1. Data reduction methodology.

Measurements:

1. Measure absorption lines with the combustor off before and after testing session (use to subtract room air absorption from measurements)
2. Run combustor at multiple operating settings
3. Wait for temperatures to stabilize before taking data at each setting
4. Acquire data and write to file

    - Detector 1 voltage (room air absorption and laser baseline in initial configuration (A) / etalon trace in configuration (B))
    - Detector 2 voltage (combustor absorption trace)
    - Laser coarse wavelength voltage indicator
    - Laser fast tuning driver voltage

Off-line:

1. Analyze combustor-off data to obtain absorption baseline shapes

    1.1. Read data for each line at combustor-off condition

    1.2. Identify each line scan from transmission time trace

    1.3. Find line peak

    1.4. Cut off each line from data (peak ± number of points)

    1.5. Compute wavelength for each line based on laser tuning voltage

    1.6. Identify etalon peaks and correct wavelength based on etalon peaks

    1.7. Fit preliminary polynomial baseline to far wings of each line (least squares)

    1.8. Compute absorption trace ($-\log(I/I_0)$)

    1.9. Fit Voigt profile to absorption trace (3-parameter nonlinear least squares) with an option to correct baseline fitting parameters (2-3 parameters added to the Voigt fitting routine)

    1.10. Compute integrated absorbance for each line trace from the Voigt fit

    1.11. Clean data - throw away outliers

Table 1 Continued.

1.12. Average absorbances

1.13. Repeat for other lines

2. Analyze data for each combustor operating setting

   2.1. Read data for one line

   2.2. Repeat steps 1.2. to 1.6 above

   2.7. Use baseline from step 1. and shift to fit to points of least absorption

   2.8. Compute absorption trace ($-\log(I/I_0)$)

   2.9. Fit Voigt profile to absorption trace (3-parameter nonlinear least squares) with an option to shift baseline (1 parameter added)

   2.10. Compute integrated absorbance for each line trace from the Voigt fit and subtract absorption from room air

   2.11. Clean data - throw away outliers

   2.12. Average absorbances

   2.13. Repeat for other lines

3. Compute U for each combustor condition

CHAPTER 4: SENSOR DEVELOPMENT RESULTS

The results of this research effort are presented in two chapters. This chapter covers the development of the nonuniformity sensing concept, including an in-depth analysis of nonuniformity effects on absorption and the development of line selection criteria for nonuniformity sensing. Furthermore, results of simulations of sensor operation and experimental testing of a nonuniformity sensor are also presented in this chapter. Chapter 5 focuses on the detailed analysis of sensor performance under realistic conditions and the effect of errors on sensitivity and accuracy.

4.1 Single Line Response to Nonuniformity

A first step in developing a nonuniformity sensor is to understand how absorption lines respond and depend on nonuniform temperature profiles. The response to nonuniformity is investigated by comparing the absorption of a line through a gas with a uniform temperature, T_u, and a gas with a temperature profile of type (A) and with $\overline{T}_A = T_u$.

The magnitude of the difference between the absorbance for the uniform profile (T_u) and the two-temperature-regions profile (A) describes the sensitivity of one absorption line to this type of nonuniformity. Assuming uniform concentration, the sensitivity of a line to nonuniformity can be expressed as follows:

$$\frac{\alpha_{nonunif} - \alpha_{unif}}{\alpha_{unif}} = \frac{\alpha(T_u) - \int \alpha(T(l))dl}{\alpha(T_u)} = \frac{S(T_u) - \int_0^1 S(T(l))dl}{S(T_u)} =$$

$$= 1 - \frac{\int_0^1 \frac{1}{T(l)Q(T(l))}\exp\left(\frac{-1.44E''}{T(l)}\right)dl}{\frac{1}{T_u Q(T_u)}\exp\left(\frac{-1.44E''}{T_u}\right)} \qquad (18)$$

From the above equation, it can be noted that the sensitivity of a line to nonuniformity depends on the lower energy of the transition, E'', and on the average temperature of the gas, T_u. As such, different lines will exhibit different sensitivity to nonuniformity. For example, for water vapor, the sensitivity of absorbance to nonuniformity is plotted in Figure 18 for a number of absorption lines characterized by the lower state energy of the transition and for a series of average gas temperatures (from 500K to 2000K).
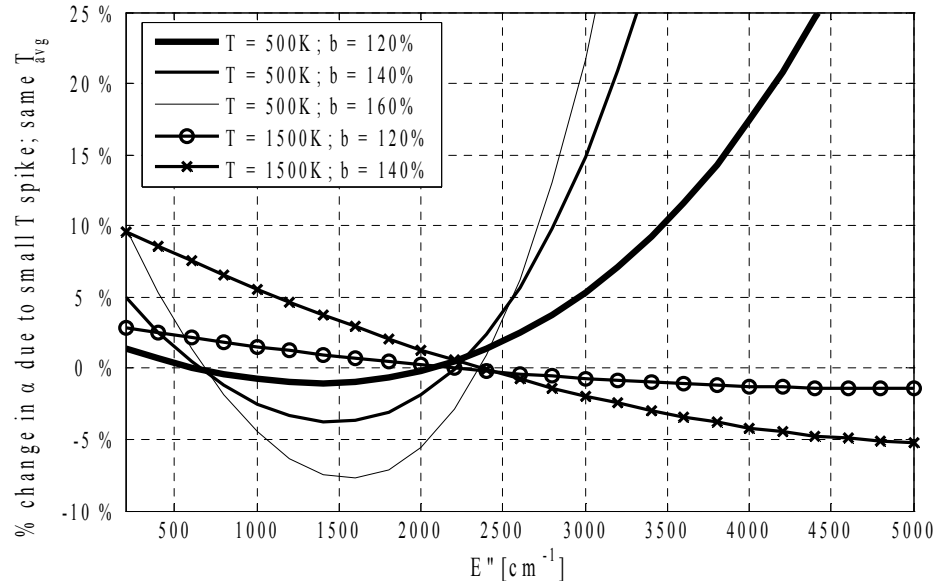
Figure 18. Absorption line response to a temperature profile of type (A) with a spike of temperature $b*T$ over $s = 20\%$ of the path plotted as % difference in absorbance as a function of the lower state energy of the transition.

52

Based on the results shown in Figure 18, two observations can be made about the water sensitivity to nonuniformity: (1) at lower temperatures, lines become more sensitive in general (solid lines with no symbols); (2) at any temperature, the dependence on E'' looks like a parabola, where larger (and very small) values of E'' give large positive sensitivities, while the magnitude of the negative sensitivity is always limited and occurs in a specific narrow range of E'' (temperature dependent). The sensitivity of a specific line to nonuniformity can be more clearly seen in Figure 19 by normalizing the x-axis. This plot shows that there are a few exceptional places, or $1.44E''/T_u$ value ranges, where maximum positive or negative sensitivities can be reached. In other words for temperature profiles in a narrow range of temperatures there exist a set of lines (E'') that will have the highest possible response to nonuniformity. In the normalized plot (Figure 19) profiles with different average temperatures (T_u of 1000 K vs. 2000 K) collapse close to the same line (the solid and dashed profiles) and the large effect on nonuniformity response of larger fractional temperature spikes (larger b values) can be clearly seen. The sensitivity to nonuniformity also determines the signal to noise ratio achievable in the measurements.
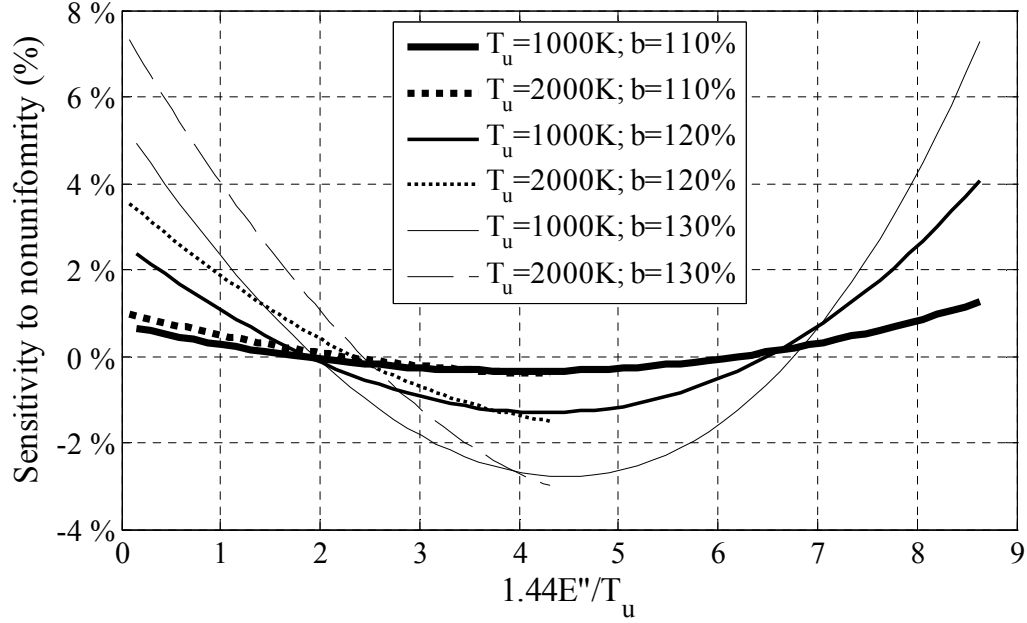
Figure 19. Absorption line response to a temperature profile of type (A) with a spike of temperature $b*T$ over $s = 20\%$ of the path plotted as % difference in absorbance as a function of the normalized lower state energy of the transition.

For practical measurements, it should be noted that the high E'' transitions are relatively weak (low absorption) at low temperatures (large $1.44E''/T$), while low E'' transitions are weak at high temperatures (small $1.44E''/T$). Using very large or small values of $1.44E''/T$ to increase sensitivity to nonuniformity requires measurement of small changes in absorbance, which is very difficult. For example, a line at 2μm with $E'' = 3000$ cm^{-1} and $S_0 \sim 10^{-23}$ cm^{-1}/molecule/cm^{-2} in a gas with 10% water over 10 cm at 500 K has an absorbance of ~2.5%; a 100K spike would change this absorbance by a few percent, requiring better than 10^{-4} measurement accuracies. For the higher temperatures typical of combustion processes (1200–2000 K), the maximum percentage change in absorbance due to a temperature spike is much less than for lower temperatures, on the order of a few percent (Figure 18 and Figure 19).

4.2 Line Selection

Sensitivity to temperature nonuniformity is important for two applications: most importantly, nonuniformity sensing as developed in this research and secondly, by understanding the response to nonuniformity, normal temperature sensors may benefit by reducing the biasing effects of boundary layers on traditional measurements. This second aspect has been briefly addressed previously.[53]

Line selection for two-line thermometry sensing was described in Chapter 2. Nonuniformity sensing requires a new line selection process for increasing sensitivity to nonuniformity – an aspect that has not been covered in the published literature. Based on the understanding of the sensitivity and response of a single absorption line to nonuniform temperature profiles, a novel process for line selection specifically designed for nonuniformity sensing is developed and presented below.

4.2.1 Analysis of Line Selection for Temperature Nonuniformity

When trying to measure departures from a uniform profile or changes in a nonuniform profile, it is more important for an absorption line to change more due to the nonuniformity than due to changes in the average temperature. Figure 18 showed the effects of nonuniformity on absorbance. It was also noted that the changes in absorbance due to nonuniformity changes are generally very small. Because of this, desirable lines should have a large enough absorbance at the experimental conditions such that a small percentage change in the absorption due to nonuniformity is detectable. In other words it is paramount to maximize the signal to noise ratio.

In section 2.1.3 it was shown that the higher derivatives of the absorbance with respect to temperature contain the information on nonuniformity effects. Based on this insight, the second derivative of the line strength function, S, can be used as a measure of the change in absorbance as a response to changes in the shape of the temperature profile, namely the sensitivity of an absorption line to nonuniformity. Let the normalized second derivative S_T'' be defined as follows, $S_T'' = \partial^2 S / \partial T^2 / S$. Lines with larger absolute values of S_T'' are more desirable. When measuring multiple lines, it is then important to choose ones that span a range of different S_T'' values, such that they respond differently to nonuniformity. If the values of the normalized second derivative S_T'' are plotted against the lower state energy, E'', for all water transitions between 0.7 and 7.7 nm (Figure 20), it can be seen that all absorption lines fall on a parabola of S_T'' as a function of E''. Lines with S_T'' close to zero will be very insensitive to temperature variations along the path. A pair of such lines that also have large first derivatives (sensitivity to average temperature) would be ideal for sensing the true average temperature by minimizing the nonuniformity effects associated with cold boundary layers or gas regions with temperatures far away from the range of interest. Alternately, lines with large absolute values of S_T'' will exhibit large changes in absorbance as a function of changes in the temperature distribution along the path, and therefore provide information on nonuniformity.

When measuring several two-line ratios to obtain nonuniformity information, it can also be seen that large but different $\Delta E''$ for the two pairs are advantageous. Different $\Delta E''$ are needed so that the effect of the nonuniformity is different between the pairs. For example, using water lines and sensing around 1500 K, lines with either very low or very high E'' have the best sensitivity to nonuniformity as measured by S_T'' (Figure 20 left). If

56

these lines also have low temperature sensitivity (low $\partial S/\partial T/S$), the changes in absorbance will be most reflective of nonuniformity changes and not small changes in average temperature (Figure 20 right).
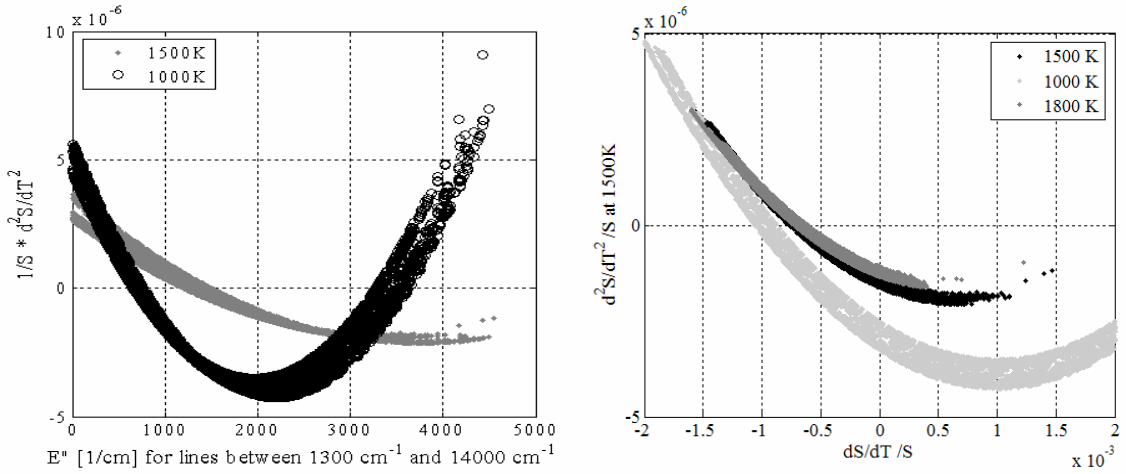
Figure 20. The second derivative of the line strength as a function of *E"* and its first derivative for water absorption lines between 1300 cm^{-1} and 14000 cm^{-1} (7.7μm to 0.7μm).

For a more detailed look at the difference between line sensitivity to nonuniformity (given by S_T") and sensitivity to average temperature (given by $\partial S/\partial T/S$), their ratio is plotted in Figure 21. A specific behavior stands out; although S_T" is generally much smaller than $\partial S/\partial T/S$, for every temperature there is a set of lines in a small range of *E"* that have a large response to nonuniformity. These lines are designated here as "nonuniformity discerning lines" for a given temperature. A zero (or close to zero) first derivative occurs when the absorbance peaks as a function of temperature (see Figure 24). In a range around this temperature where the absorbance peaks, the influence of nonuniformity relative to changes in the average temperature of the path distribution can be large.

When temperature deviations in a certain narrow range need to be measured, a nonuniformity discerning line can be chosen that yields maximum response for that particular range of fluctuations. Furthermore, since nonuniformity discernability for a certain temperature is a function of E'' and three lines with different E'' need to be used for sensing, it follows that such a sensor will always have heightened nonuniformity response in three (relatively narrow) temperature ranges. In the idealized case of a single temperature spike of T_s above a uniform temperature profile, assume a sensor with one line pair containing a nonuniformity discerning line tuned for T_s. Then the line pair not containing T_s will yield a temperature close to the true average, while the line pair containing the nonuniformity discerning line will respond to the temperature spike and yield a temperature away from the true average, thus resulting in good U response to deviations of that size.
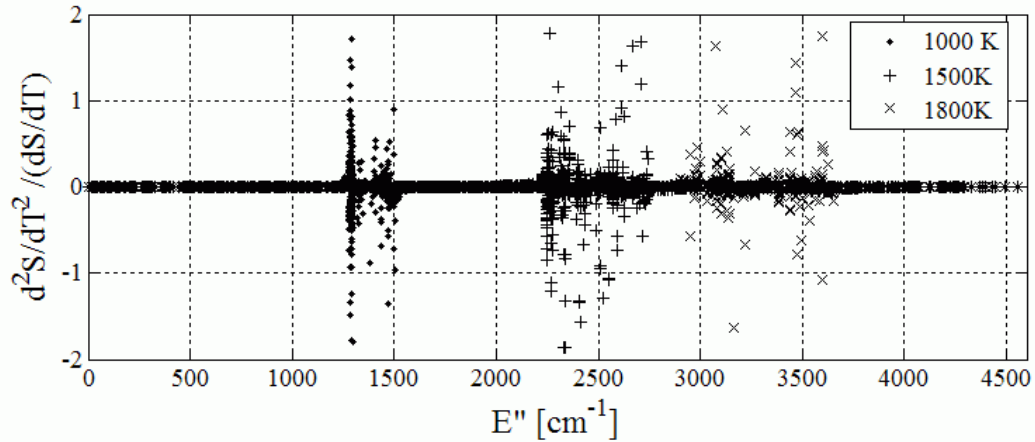
Figure 21. The ratio of the second to the first derivatives with respect to temperature for water absorption lines between 1300 cm^{-1} and 14000 cm^{-1} (7.7μm to 0.7μm) plotted against their lower state energies, E''.

58

4.2.2 Step by Step Line Selection Process

Although several approaches of line selection for temperature sensors have been described, to the author's knowledge, no approach has included criteria for maximizing sensitivity to *nonuniform* profiles. Based on the above analysis, a multi-step line selection approach was developed. In conjunction with a spectroscopic database such as HITRAN, the following down-selection process is used:

(1) select lines with sufficient absorption at the expected conditions (T, x_{H2O}, p, …) and within the laser interrogation range (sufficient absorption should be defined based on the capability of the measurement system);

(2) eliminate lines that have interference from other absorption features (e.g. keep lines or small groups of lines that do not have any other absorption features of significant strength at the expected conditions within a certain number of FWHM of the desired line); at least 10 FWHM separation is recommended;

(3) select the lines with the largest sensitivity to nonuniformity at the expected conditions (based on $\left|d^2 S_i/dT^2\right|/S_i$);

(4) select one or two lines with the largest possible $\left|\left(d^2 S_i/dT^2\right)/\left(dS_i/dT\right)\right|$ value at the expected fluctuation temperatures;

(5) select lines with the largest possible range of E'' values;

(6) simulate sensor response for expected conditions and temperature and species distributions based on the reduced set of lines as a final selection step.

It should be noted that the spectroscopic parameters in the HITRAN database are not always correct, especially at combustion temperatures. Furthermore there might be lines that are not included in the database, so for sensitive measurements the spectroscopic properties and spectral isolation of the chosen lines should always be checked experimentally.

4.2.3 Selection of Lines for Simulation and Sensor Analysis

The above process of line selection was used to choose six water lines that give good sensitivity to nonuniformity at temperatures around 1600 K. Although for all these lines sensitivity increases as the temperature decreases, for lower temperatures a different set of lines would yield better overall sensitivity and error rejection. The spectroscopic parameters of these lines are summarized in Table 2 below. These lines are used in the rest of the thesis to illustrate the sensitivity and effects of errors on nonuniformity measurements.

Table 2. Selected water lines.

#	Wavenumber $[cm^{-1}]$	Wavelength $[\mu m]$	E'' $[cm^{-1}]$	S_0 $[cm/molec]$	S (1600K)	$d^2S/dT^2/S$ (1600K)
1	2391.123	4.18214	3654	4.00×10^{-27}	3.77×10^{-22}	-1.87×10^{-6}
2	4038.381	2.47624	3264	7.74×10^{-26}	1.72×10^{-21}	-1.70×10^{-06}
3	5604.517	1.78428	1581	5.69×10^{-23}	1.64×10^{-21}	-3.67×10^{-07}
4	3920.089	2.55096	704	2.58×10^{-20}	2.25×10^{-20}	1.08×10^{-06}
5	3081.342	3.24534	300	5.69×10^{-22}	9.68×10^{-23}	2.02×10^{-06}
6	3837.869	2.60561	136	2.45×10^{-19}	2.25×10^{-20}	2.26×10^{-06}

These lines were selected as good candidates under the assumption that appropriate lasers are available to probe these transitions. These lines are not necessarily the best line for nonuniformity in this spectral range. They represent a sampling of good lines selected under a very specific set of criteria (minimum absorbance, response around 1600 K, large range of E'' values). For practical sensors, line selection would be limited to wavelengths accessible by the available lasers, generally resulting in lines with lower performance than the ones chosen above.

The sensitivity of these lines to temperature nonuniformity is plotted in Figure 22. Although these lines were selected for sensing at 1600 K, their sensitivity increases at lower temperatures, as is the case for most absorption lines. This trend also shows that colder regions of the profile will be more heavily weighted than hot regions.
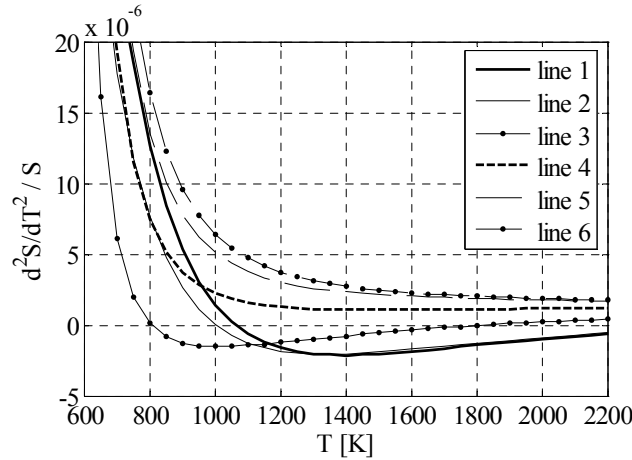
Figure 22. The second derivative of the line strength for chosen water absorption lines.

4.2.4 Line Selection for Experiments

For the experiments conducted as part of this development effort, the limiting factor in the line selection process was the tuning range of the available laser. The diode laser used in the experiments has a useful tuning range of 1945–1985 nm (single-mode

and relatively linear power output as a function of wavelength) – so only absorption lines in this range could be chosen. Furthermore, the laser exhibits strong internal etaloning effects when tuning over this range (as described in Chapter 3). Only lines located in the relatively linear rising part of the laser sweep, away from etalon edges (Figure 15), could be used for measurements.

In this spectral range, water has the strongest and most numerous absorption lines and was chosen as the marker species for the experiments. In general, water makes a good marker species for combustion applications because it is abundant in exhaust gases and it has numerous and strong absorption features throughout the spectrum, but the results of this research apply to any other molecule (as explained in Chapter 2). A plot of the water absorption spectrum at 700 ºC in the laser range is shown in Figure 23.
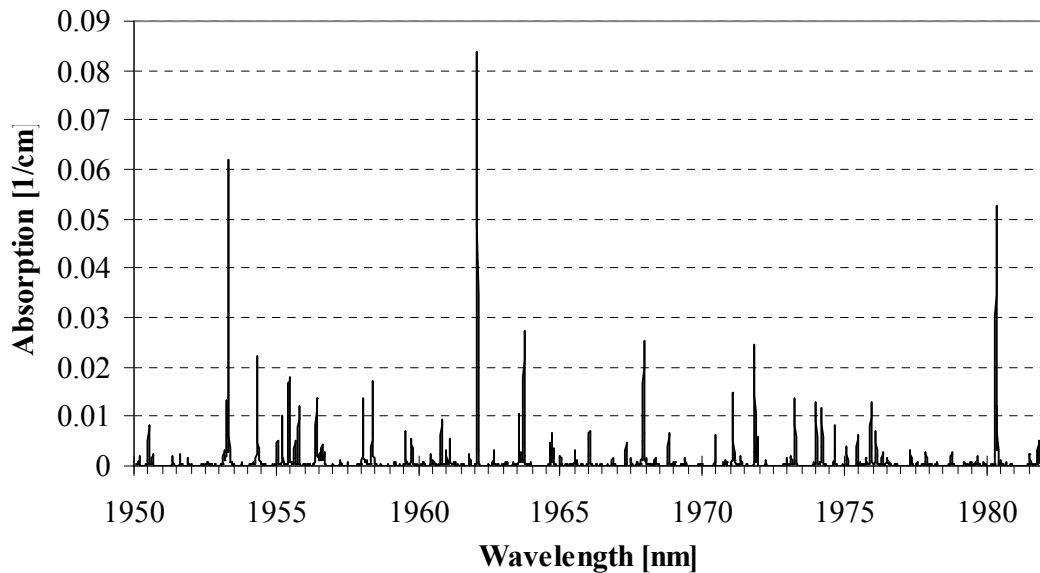
Figure 23. Water absorption spectrum at 700 ºC.

The strongest interference in this spectral range comes from a few relatively weak CO_2 absorption lines, especially at the longer wavelengths. This factor is considered in the selection criteria.

In the selected wavelength range, there are about 720 potential absorption lines strong enough to measure. Using criteria (1) and (2) from above on the spectral region accessible to the laser (i.e, selecting lines with sufficient absorption at the expected conditions and eliminating lines that have interference from other absorption features) results in about 25 candidate lines. Further, eliminating lines that overlap the laser etalon edges reduces the number of measurable candidates to only about 6-12 lines, depending on the selection criteria. These lines are listed in Table 3. Out of these lines, only six were successfully used for measurements. Lines h2, h5, h7, and h8 are best suited to nonuniformity measurements and can be measured with the least errors. These lines are not ideal for such measurements, but they represent the best choices given the constraints imposed by the laser.

Table 3. Water lines selected for experiments.

Wavenumber [cm^{-1}]	S_0(296K) [cm^{-1}/(molec·cm^{-2})]	E'' [cm^{-1}]	Line Designation
5093.326	2.26×10^{-22}	285	c1
5104.160	2.13×10^{-22}	446	c2
5050.694	1.56×10^{-22}	488	c3
5105.399	6.79×10^{-23}	704	c4
5116.795	3.99×10^{-22}	1201	h1
5113.870	2.78×10^{-22}	1293	h2
5107.070	1.28×10^{-22}	1446	h3
5114.487	2.68×10^{-23}	1718	h4
5043.738	3.74×10^{-24}	2246	h5
5092.791	3.49×10^{-23}	1525	h6
5092.360	1.05×10^{-22}	1524	h7
5074.950	9.96×10^{-25}	2433	h8

The absorbance of a few of these lines is plotted as a function of temperature in Figure 24. From this plot it can be observed that all the plotted lines have their highest sensitivity to temperature (slope) at relatively low temperatures (below about 800 °C), in the regions to the right and left of their peaks. Also, all the lines slowly decrease in intensity at high temperatures.
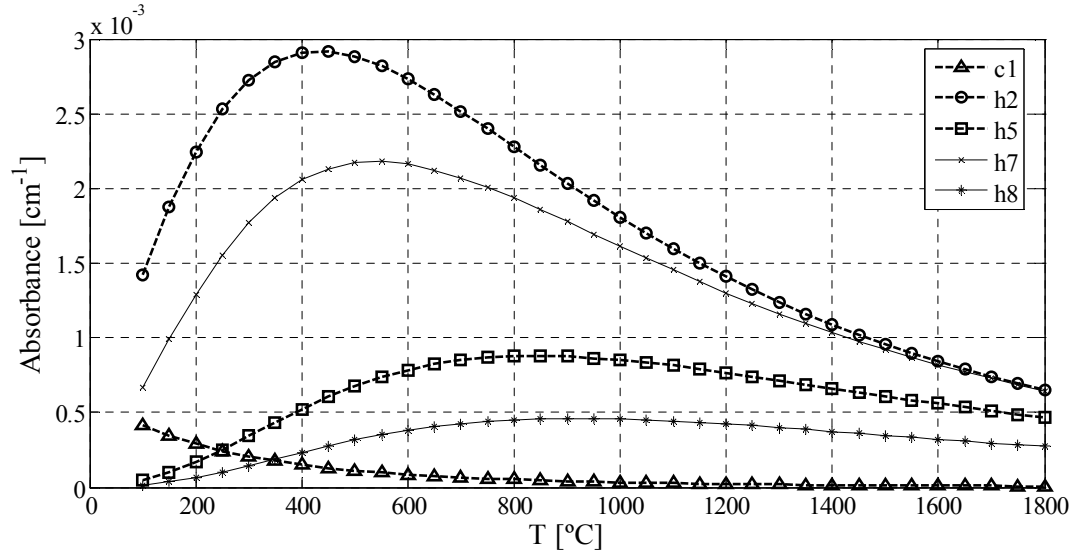
Figure 24. Absorbance of water as a function of temperature.

The second derivative of several selected absorption lines normalized by their absorbance is plotted in Figure 25. As outline above, this represents the line's sensitivity to nonuniformity; it can be seen that lines h5 and h8 have large sensitivities at very low temperatures, decreasing rapidly as the temperatures increase beyond about 500 ºC. Furthermore, because they cross zero, these lines would not be appropriate for temperature profiles centered around 300 ºC. Line c1 has moderate sensitivity throughout most of the temperature range.
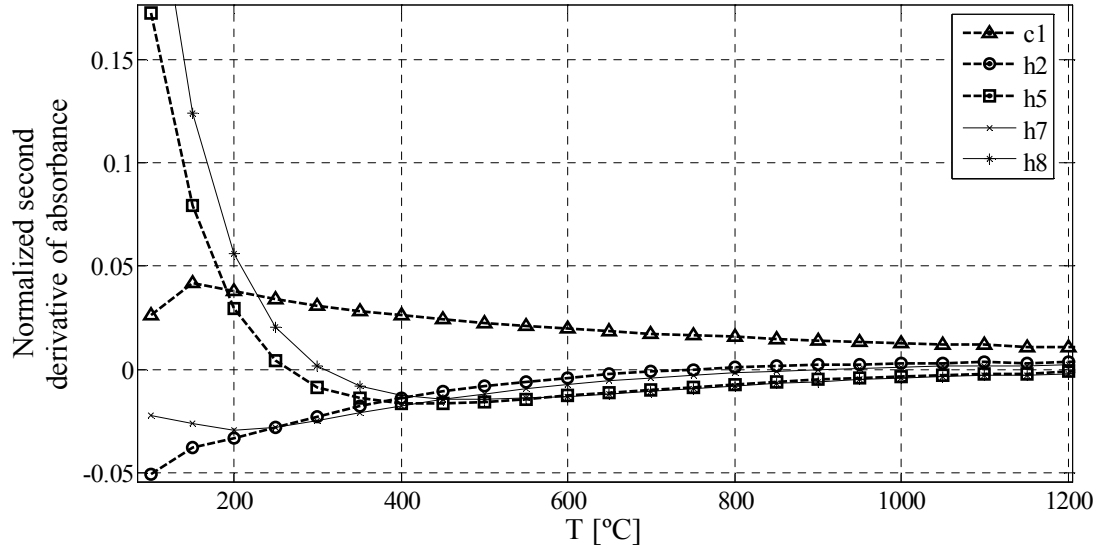
Figure 25. Sensitivity to temperature nonuniformity of selected absorption lines.

Finally, it is interesting to look at the difference between sensitivity to nonuniformity and sensitivity to temperature for these lines. The second derivative of absorbance with respect to temperature is divided by the first derivative and plotted in Figure 26. From here it can be seen that each line changes much less with nonuniformity than with average temperature throughout most of the temperature range except within a narrow band. Temperature fluctuations with peaks close to the narrow temperature ranges where each line responds to nonuniformity will be very easy to pick up. This fact may be used to pick one line that has a good nonuniformity response in the expected range of fluctuations (e.g. line h8 around 900 ℃). Then such a nonuniformity discerning line will contribute the nonuniformity information and the other two lines will yield information more characteristic of the average temperature. The location of the nonuniformity sensitivity peaks is described by the lower state energy of the line, *E"*.

66
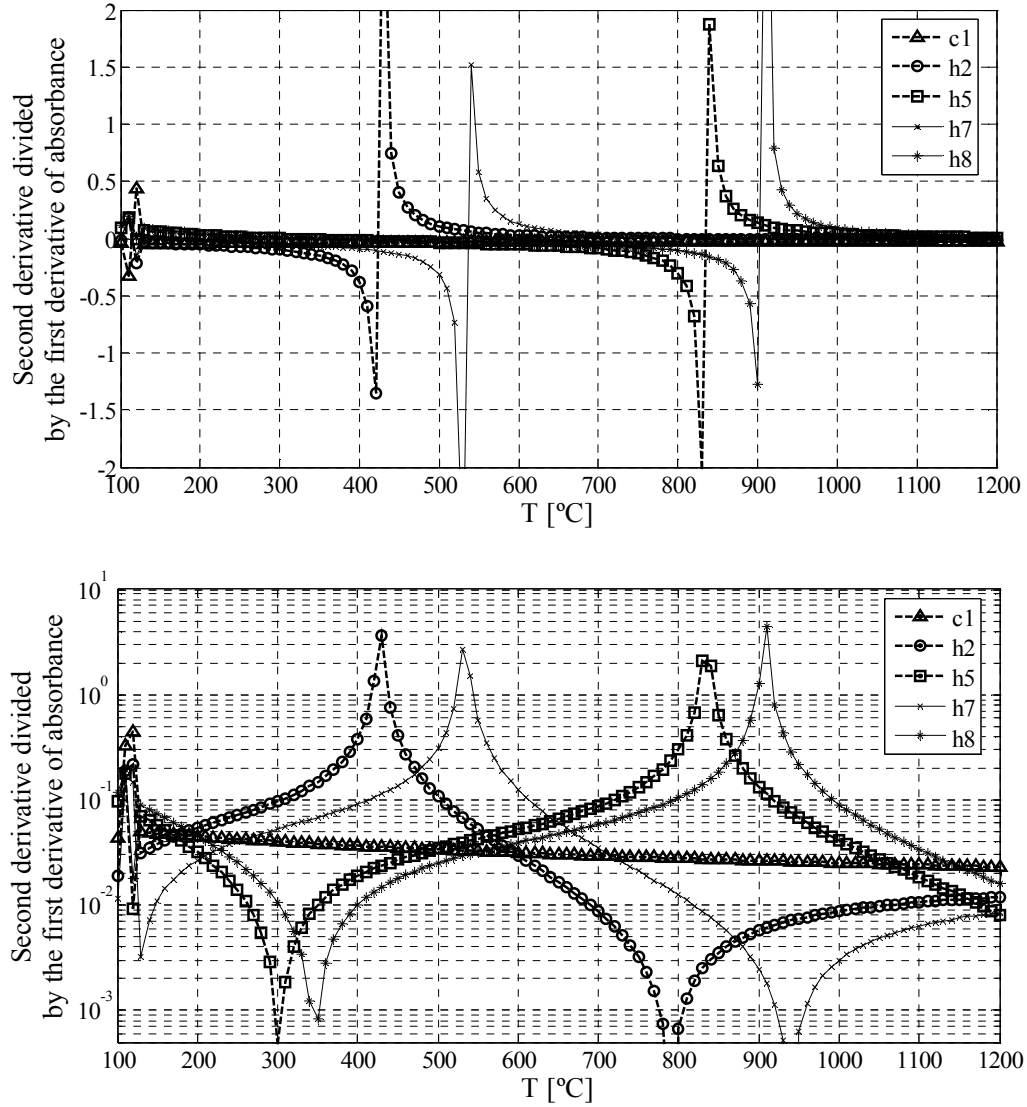
Figure 26. The second derivative of the absorbance with respect to temperature divided by the first derivative. The absolute values are plotted on the semi log scale.

4.3 Modelling Results

This section presents results based on computer modeling of the sensor. The sensor concept is first validated through simulations of the sensor output under ideal error-free conditions. U is computed for several simple temperature profiles with the same average temperature of 1500 K and small deviations from the mean of 10% and

20% in temperature spanning 5% and 10% of the path (Figure 27). The path length was chosen to be 20 cm, and the water concentration was a constant for this comparison.

As the size and extent of the temperature deviations increases, as measured by the coefficient of variation of the temperature profile, $CV_T=T_{std}/T_{avg}$, so does U. This simple simulation demonstrates the fact that U varies monotonically with the extent of temperature deviations.
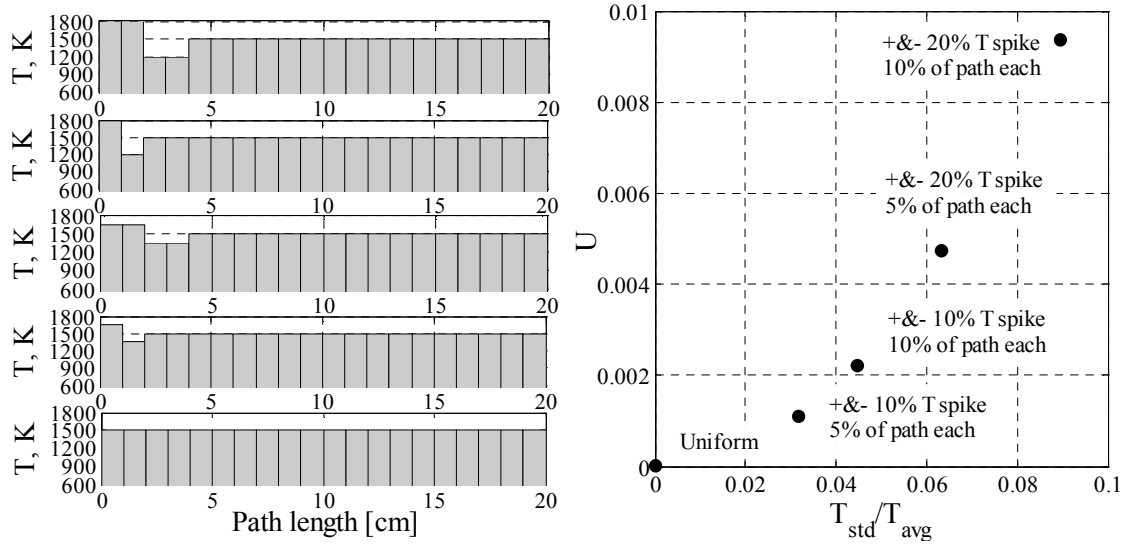
Figure 27. *U values for several simulated temperature profiles with spikes of increasing magnitude and width. The water concentration was assumed constant.*

To confirm that U is a sensible parameter for tracking nonuniformity under realistic combustor conditions, the sensor is also simulated for temperature and concentration profiles obtained from CFD combustion simulations. The CFD data used here comes from the LES simulation described in Chapter 3. U is computed for several instantaneous temperatures and water mole fraction profiles from the CFD data (Figure 28). Because the combustor walls are adiabatic, water concentration is directly proportional to temperature. It is important to note that each of the profiles has a different average temperature, as well as a different degree of nonuniformity. The resulting U

68

values for each profile increase monotonically with T_{std}/T_{avg} as shown in Figure 28. When used as an input to a control system, this means that driving down the value of U (through some means of actuation) results in a profile with smaller temperature extremes.
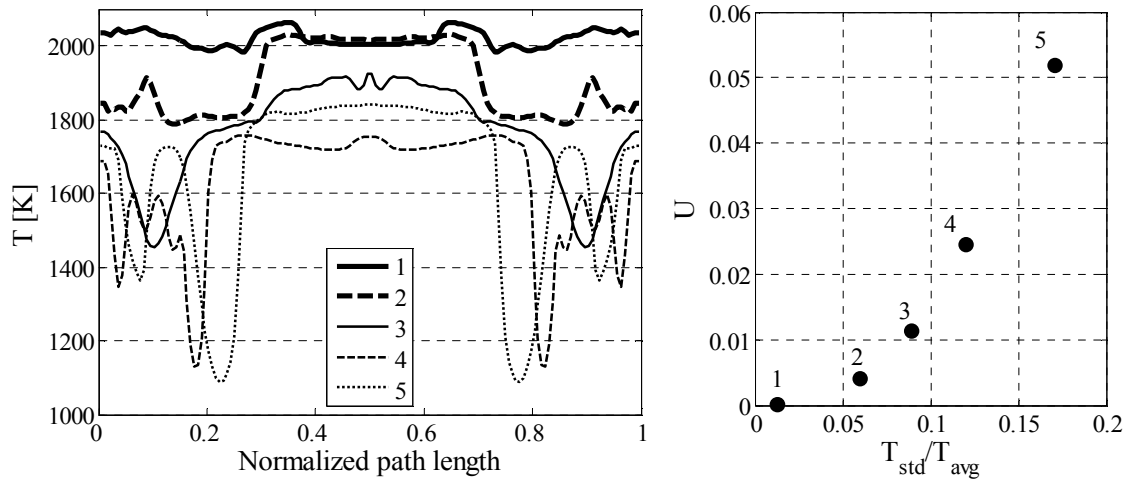
Figure 28. CFD exit temperature profiles and corresponding simulated U values.

The sensor model is also used to study the sensor response to changes in the average gas temperature compared to changes in temperature nonuniformity. The sensor generally tracks the level of nonuniformity, even when the average temperature of the profile changes. This can be seen in Figure 28; the five profiles have average temperatures, T_{avg} = 2021, 1905, 1765, 1626, 1642 K for profile 1 to 5. Even though the temperature profiles have different means, the U variable is still an indicator of their nonuniformity; for example, for most of these profiles the mean decreases, while U increases but from profile 4 to 5 the mean increases, yet the trend in U follows the nonuniformity and does not seem to be influenced by the mean temperature of the profiles.

In summary, modeling of error-free sensor operation shows that U monotonically tracks the level of nonuniformity for a series of synthetic temperature profiles and profiles characteristic of gas turbine engines. To further develop this sensing concept, experiments are performed to validate the modeling results and further investigate the sensing technique.

4.4 Experimental Results

The experimental setup described in Chapter 3 was used to validate the sensor concept by measuring absorption under a variety of conditions (temperatures and water concentrations). The results presented below are from tests run in the exhaust of the combustor rig, under initial and modified configurations (A & B).

In the initial configuration (A), the combustor was run with two injectors, one for premixed methane-air and one for secondary (dilution) air. The laser was rapidly tuned over each isolated line using a triangular driving wave at 80Hz (160 line sweeps per second). Regions far from the line center are used to fit a polynomial background with data from both detectors. The absorption, $-\ln(I/I_0)$, is then computed with data from both detectors. Finally, room water absorption is subtracted from the total absorption to determine the absorption in the combustor. The wavelength is determined from the laser piezo-driver signal. No etalon correction for the wavelength is used in this setup.

The lines used in these experiments are h1, h2, h3, h5, c1, and c4 (Table 3). The line-pairs used to determine the temperatures T_{ij} used in the computation of U are listed in Table 4. For a given set of combustor operating conditions, the average exhaust temperature profiles were obtained from the thermocouple data. These were then used to

compute T_{std}/T_{avg} and interpret and compare the results of the laser sensor. Results are presented for the two mixing control methods described in Chapter 3: variations of the upstream air flow rates, and mixing control with the synthetic jet array.

Table 4. Line pairs (ratios) used to determine the nonuniformity parameter U.

Line pairs	S_{0i}/S_{0j}	$\Delta E"$ [cm^{-1}]
h1/c1	1.79	916.50
h1/c4	11.80	497.71
h2/c1	1.24	1008.22
h2/c4	8.17	589.42
h3/c4	3.73	741.92
h5/c4	0.10	1542.67

4.4.1 Air Injection Control

In this approach, the total flow rates of methane and air were maintained at a constant value (4 scfh fuel, 152 scfh air), while the ratio of air supplied to the premixed burner (primary) and secondary air injector was varied. Changing the air distribution affects the temperature of the upper (burning) stream, as well as the relative flow velocities of the two streams and the mixing characteristics between them. Two cases were examined, 54% and 44% of the air was supplied to the premixed (primary) injector. The resulting temperature profiles for the two cases are shown in Figure 29. As the flame is located in the top part of the combustor, the maximum temperatures can be seen in that region, with the peak at a nondimensional vertical location (normalized by the combustor height) of 0.7. In the first case (54% primary air), when there is a higher flow rate through the upper portion of the combustor (compared to the bottom), the combustion

71

products expand downward and mix with the cold stream, resulting in a nearly uniform

temperature profile (T_{avg} = 109 ℃, T_{std} = 12 ℃). It should be noted that there is

significant heat loss to the uninsulated combustor walls. This has a large influence on the

overall temperature profile. In the second case (44% primary air), the flame gases are

hotter (the flame burns closer to stoichiometric), and results in a more stratified flow. The

high temperature point near the bottom is possibly due to radiative heating of the bottom

wall. This profile has T_{avg}=152 ℃ and T_{std}=36 ℃. The sensor output was computed for

two different line-pair groups (i.e., two ways to measure U). U_A is based on temperatures

interpolated from line ratios h1/c1 and h1/c4, while U_B is based on h2/c1 and h2/c4

(Table 3 and Table 4). These results are shown in Figure 29 plotted versus T_{std}/T_{avg}

obtained from the thermocouple readings. The measurements show a significant increase

in U_A and U_B with the increase in the temperature nonuniformity of the flow. It should be

noted that the average temperature also changes between the two profiles but this fact is

believed to have at most a small influence on U as discussed above.
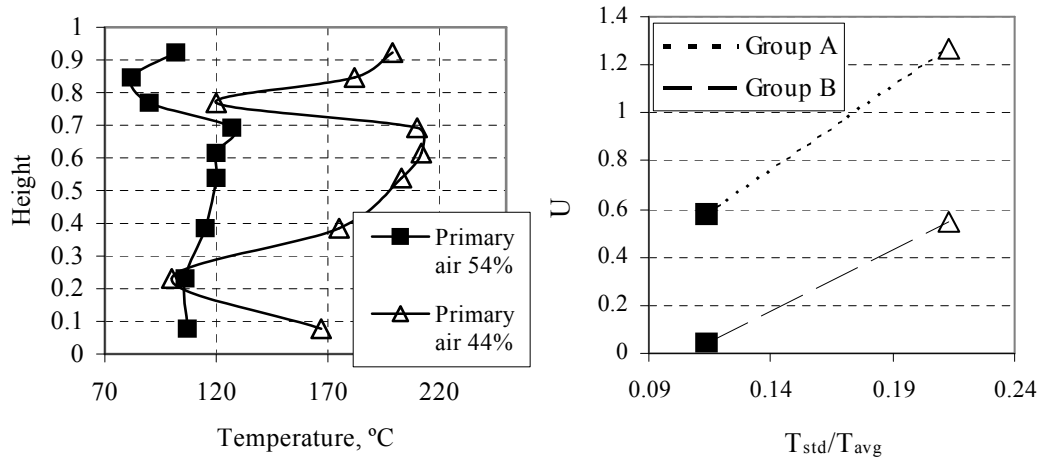
Figure 29. Left: temperature profile resulting from different air flow-rate ratios to the premixer and secondary air injector. Right: Nonuniformity parameter U_A (open symbols) and U_B (filled symbols) for relatively uniform flow (squares) and less uniform (triangles).

In these first tests, the overall temperature in the combustor exit was very low, and thus not similar to realistic conditions. Furthermore, there was a significant change in the average temperature between the two conditions, which has some influence on the absorption measurements. Higher overall temperatures and variations mostly in the profile shape and not the average temperature are needed for better study of the sensor operation. This was first attempted using different flow rates and synthetic jet mixing control.

4.4.2 Synthetic Jet Mixing Control

In these experiments, all flow rates remained fixed (8 scfh methane, 60 scfh premixer air, and 80 scfh secondary air). Mixing control was implemented using the synthetic jet. Results were obtained with no actuation (0 Hz) and for two jet frequencies (40 and 60 Hz). Nominally, this approach should only change the mixing of the hot and cold streams. As seen in the thermocouple temperature profiles (Figure 30), the synthetic jet array also causes a change in average temperature due to the enhanced heat loss to the combustor walls with the increase in mixing, but to a much lesser degree than in the previous case. Note that the average temperature for these cases (>200 ºC) is higher than for air injection control, since the total air flow rate is lower.

As the frequency of the synthetic jet changes from 0 to 60 Hz, mixing increases, and the nonuniformity variable U decreases (Figure 30). The synthetic jets tend to have a larger influence towards the bottom of the combustor, since they are located there. Two effects are noticeable: the hot region gets wider with the largest effect near the bottom wall, while the peak temperature is driven down. For this case, three nonuniformity

variables were computed: U_A is based on line pairs h1/c1 and h1/c4 (also used in the air injection control results), U_C based on pairs h1/c4 and h3/c4, and U_D (pairs h3/c4 and h5/c4).
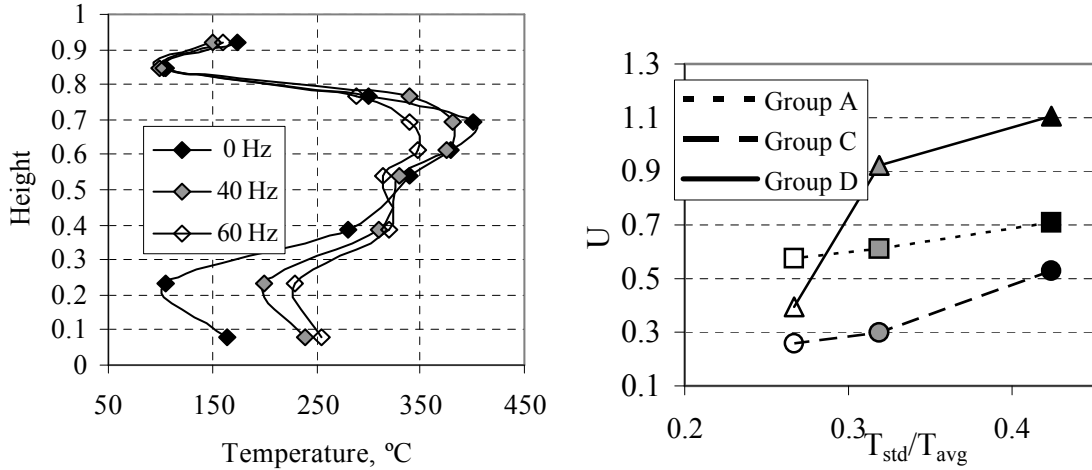
Figure 30. Left: temperature profile resulting from running the synthetic jet at different frequencies. Right: nonuniformity parameters *U* for conditions corresponding to running the synthetic jet at 0 Hz (black symbols), 40 Hz (grey symbols), and 60 Hz (open symbols).

While U appears to track T_{std}/T_{avg} in both control cases, the correspondence of U to T_{std}/T_{avg} is not unique. This can be seen by comparing the results for a fixed group of line pairs (i.e., U_A) for air injection control and synthetic jet mixing control (Figure 29 and Figure 30). For example at T_{std}/T_{avg} of ~0.2, $U_A = 1.2$ for air injection control, while $U_A = 0.5$ for the synthetic jet mixing. It is likely that the range of U also depends on T_{avg}, since the two flows cases have very different average temperatures. There could also be an influence due to the different water concentration profiles for the two control cases. The dependence of U on these factors is studied using the simulation methods, as presented in the next chapter.

Although promising, these initial experiments exhibited several limitations. First as noted above, the available laser system limited measurements to one absorption line at a time. This limited the U values to average measurements. Because of combustor unsteadiness each line might be measured at slightly different conditions. In addition, sensor sensitivity and noise rejection were severely limited by the available absorption lines in the laser wavelength range. Also as explained above, the combustor rig used in the initial experiments allowed for limited control authority over the exit temperature profiles.

The test rig was improved to configuration (B) as described in Chapter 3; exit temperature profiles obtained after the modifications are shown in Figure 31. As suggested, the new configuration increased the range of temperature nonuniformity in the combustor exhaust, as well as increasing the maximum exhaust temperatures. However, the exhaust temperatures are still less than the adiabatic flame temperature based on the overall air and fuel flow rates. This is due to significant heat losses at the combustor walls. The adiabatic flame temperature based on the primary injector flame is 2000K and based on the overall fuel and air is estimated at around 900 K. The average measured temperature in the exhaust was about 720 K (447 ºC).
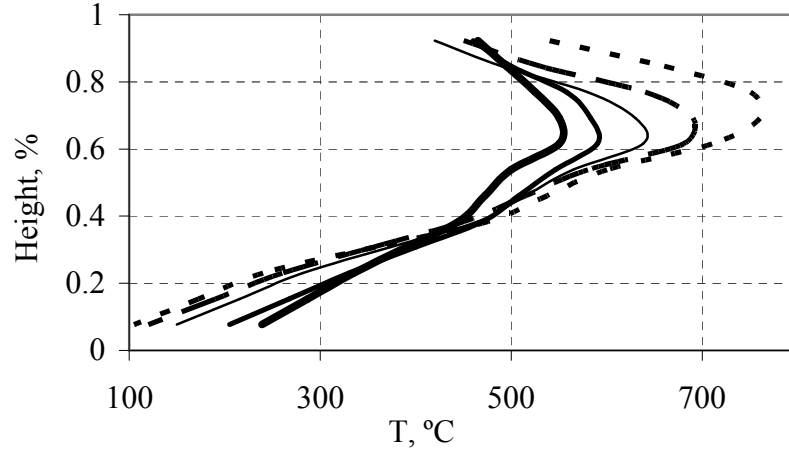
Figure 31. Typical combustor exit temperature profiles.

Measurements in the modified setup yielded mixed results. In certain cases (Figure 32 left), the U parameter exhibited the desired trend (increasing with T_{std}/T_{avg}), except for isolated tests (e.g., the peak point in Figure 32 left). In other cases, there was a larger scatter of the measured U values, and the correlation with the degree of temperature nonuniformity is poor (Figure 32, right).
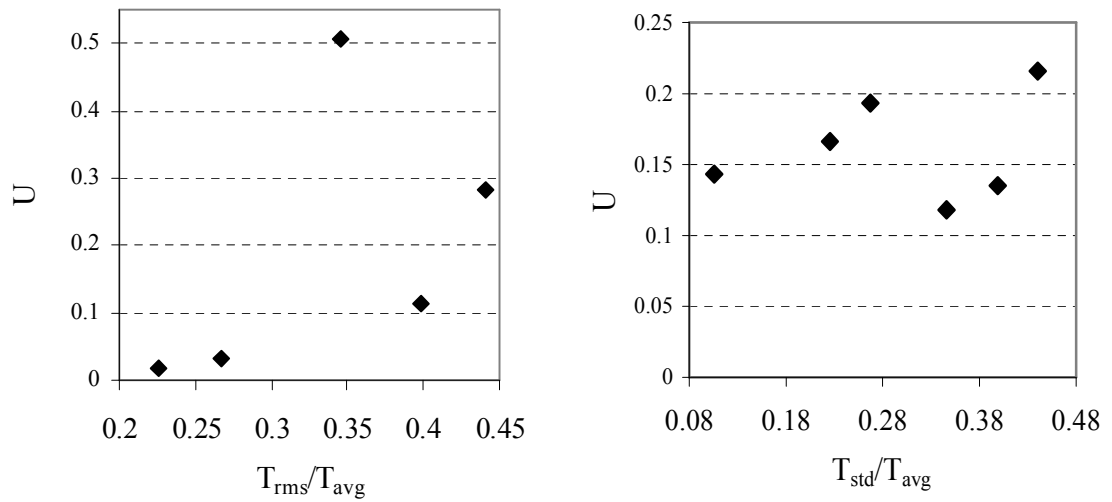
Figure 32. Measurements of U in the exit of a temperature stratified methane-air combustor. The two plots are based on different sets of lines to form U.

4.5 Summary

Computer modeling results demonstrate how the sensor would operate and how the nonuniformity variable U monotonically tracks T_{std}/T_{avg}. A fundamental analysis of how nonuniformity affects absorption indicates that the second derivative of the absorption with respect to temperature is an important factor controlling line response to nonuniformity. The understanding of nonuniformity effects on absorbance was used to develop a new line selection process that maximizes sensitivity to nonuniformity. This process was used to determine a set of good lines for a generic application and also for selecting the best lines for experiments based on the available hardware.

Experimental testing of this sensor demonstrated its use and performance in a combustor exhaust flow. The sensor generally tracked the temperature nonuniformity of the exhaust when either of two actuation methods was used for changing the temperature profile (injection control and synthetic jets). The experiments also raised awareness of the most important issues affecting a practical sensor: hardware limitations and measurement uncertainties. Measurement uncertainty and its effect on accuracy of this sensing method is an issue that needs further study. An in depth analysis of uncertainty and sensor performance is performed in the next chapter.

CHAPTER 5: SENSITIVITY AND ERROR ANALYSIS RESULTS

In the preceding chapter, the basic sensor concept was demonstrated through a combination of modeling and experimental results. The measured data suggested that experimental errors and hardware limitations have a significant impact on the performance and accuracy of this sensing approach. This chapter describes an in-depth analysis of the sensing technique carried out to determine the capabilities of the technology. To understand the factors limiting sensor performance, the possible sources of errors that resulted in the large experimental scatter are identified and examined in this chapter. Factors affecting sensitivity to errors and methods to decrease the errors, either through improved experimental design or data processing, are also developed and described. This work is further extended through development of a comprehensive analysis of the effects of errors and uncertainty on the operation and performance of absorption nonuniformity sensors. This framework is then used to explore the performance envelope of the nonuniformity sensor based on the use of state of the art technologies. Most of the analysis performed in this chapter is applicable to any direct absorption temperature sensing technique and, as such, its usefulness extends beyond the sensing technique described in this thesis.

5.1 Overview of Error Sources

Tunable diode laser absorption sensors (TDLAS), especially direct absorption, are very sensitive to noise and measurement errors. The effect of errors is especially large and detrimental to measurements of temperature nonuniformity because of the small

changes in absorption that have to be resolved. Understanding the effect of errors allows better design of sensors and experiments, as well as setting realistic expectations on sensor performance (sensitivity and accuracy).

Measuring absorption lines typically entails making multiple scans over several absorption lines. This work focuses primarily on identifying and analyzing the sources of errors and uncertainty affecting a single line scan. Fluctuations and their sources from scan to scan or for measurements taken on different days are not addressed in detail; if each line measurement is improved, then long time-frame fluctuations in the measurements represent real changes in the flow or environment and not intrinsic measurement errors.

Every component of the measurement system and the environment introduces some level of uncertainty in the sensor output. Figure 33 illustrates the components of an absorption sensor system and the corresponding sources of errors. This figure is also representative of the experimental setup used in Chapter 4.
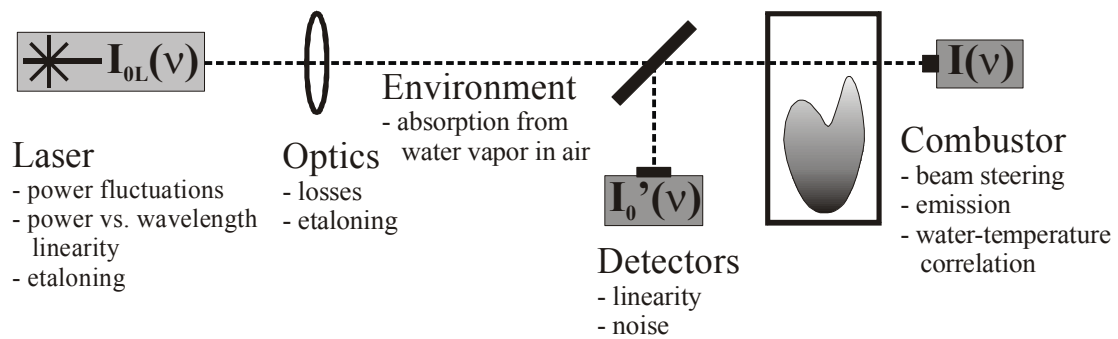
Figure 33. Absorption sensor system components and the errors they introduce.

All of these potential sources of error accumulate to affect the final, acquired transmittance signal, $I(\nu)$, and the corresponding baseline, $I_0(\nu)$, as depicted in Figure 34.

Starting from a theoretical transmittance shape in the absence of any errors (Figure 34 left), different signals characteristic of error sources (Figure 34 center) may transform the transmittance resulting in the measured transmittance signal (Figure 34 right). The theoretical baseline undergoes the same changes as the transmittance such that if the final shape of the theoretical baseline were known, the error-free transmittance signal could be recreated. The challenge is to identify a baseline to the measured transmittance that captures the changes due to errors by either physically eliminating the error sources or measuring their contributions. Finally, whatever errors can not be eliminated or inferred will limit sensor accuracy and uncertainty.
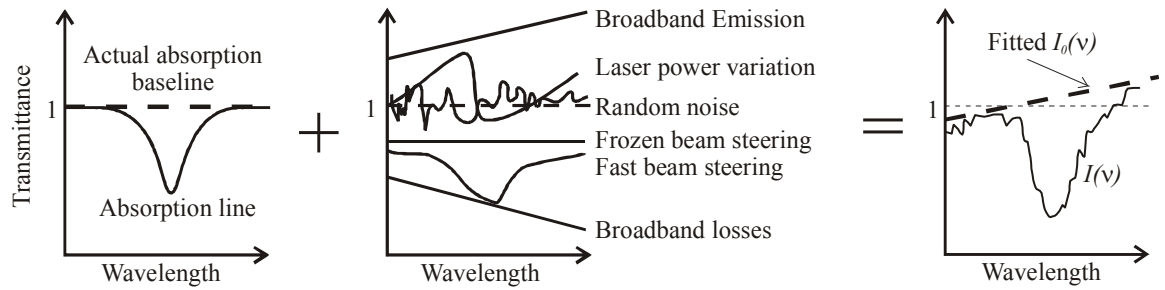
Figure 34. Actual absorption line (just from combustor gasses and error-free) plus effects on this signal due to errors, hardware, and environment results in the actual measured transmittance signal.

The measured signal, $I(v)$, depends on the absorption line transmission, $e^{-k(v)l}$, as well as all the errors through the measurement system. The contribution of errors to the transmitted signal, $I(v)$, can be expressed as indicated in equation (19). This expression does not explicitly show errors that affect the actual line absorption, such as uncertainty in the spectroscopic parameters or changes in the temperature profile during a line scan.

$$I(v) = I_{0L}(v) \cdot K_{ext}(v) \cdot A_{optics}(v) \cdot A_{BS}(t) \cdot I_{flow}(v) \cdot G_{det}(v) \cdot R(t) \cdot e^{-k(v)l} \qquad (19)$$

Each of the quantities in equation (19) is identified below and analyzed in the subsequent sections. First, the effective laser output signal, $I_{0L}(v)$, which is generally not linear, has to be determined. The laser beam may be directed to the measurement area through air (or some other gaseous medium) or through optical fibers. Interference may occur if species in the gas outside the measurement region absorb at the measurement wavelengths, thus superimposing a frequency dependent external absorption signal, $K_{ext}(v)$. If fibers are used, they also introduce noise such as scattering (Raman and Brillouin), the Kerr effect, and parametric nonlinearities leading to wavelength dependent signal losses. The sensor optics usually introduce broadband losses and may exhibit etaloning effects. These are combined in the optical attenuation loss function, $A_{optics}(v)$. The last part of the instrument train, the detectors, may also introduce uncertainties due to nonlinearity in the response – the gain changing with wavelength, $G(v)$, and noise. The measurement region (combustor) is also a source of errors due to beam steering, $A_{BS}(t)$ and broadband emission from the hot gases and surfaces, $I_{flow}(v)$. Finally, there are random measurement errors and electronic and quantization noise. All random errors are represented by $R(t)$. The product of all these terms represents the signal baseline, $I_0(v)$, that has to be determined from the measurements.

The absorbances α_i, and U are computed from the ratio $I(v)/I_0(v)$. In the rest of this chapter the sources of errors are analyzed in terms of their physical sources and what can be done at the experimental/hardware level to reduce them. Their effects on $I(v)$ and $I_0(v)$ and how these can be reduced through smart signal processing are also analyzed.

A note should be made about the difference between frequency and time dependence of the error terms. For wavelength scanning techniques, frequency and time

are related through the scanning speed, so $v = f(t)$. When the scan speed is constant, the wavelength and time are interchangeable; this will be the working assumption for the current research. When the scan speed exhibits fluctuations or tuning is driven by a nonlinear function (e.g. a sinusoid) then fluctuations in time will exhibit a different distribution when mapped to the frequency, for example a uniform error distribution in time will result in a distribution with multiple peaks over frequency under sinusoidal driving, with more errors occurring at the peaks of the sinusoid. In practice, linear triangular driving signals are used to scan back and forth over one or more absorption lines and although at the turn-around point the tuning speed goes to zero, these frequency regions are small and can be eliminated from the scan.

5.2 Analysis of Errors

The errors identified above can be classified as random or systematic (as discussed in Chapter 2. Random errors are addressed first. Systematic effects on the measured absorbances are more difficult to control than random errors and will be addressed one by one in the following sections.

5.2.1 Random Errors

Random error sources include the electronics (detector noise, $1/f$ noise), random fluctuations in laser power and beam direction, and flow and environmental factors. Most random errors occur as a function of time and others as a function of wavelength. As discussed above, under the assumption of linear tuning (used in these experiments),

random errors occurring as a function of time or wavelength can be treated the same, as a random scatter occurring throughout the measured scan $I(v)$.

In the experiments described in the previous chapter, the random errors were much smaller than the systematic errors. For example, the experiments used two identical detectors whose inherent noise level is very low (±0.07 mV), much lower than the A/D converter steps of 1.2 mV. For a measured signal of around 2V, the limiting S/N ratio of the detector is 3×10^5, while the quantization S/N is 1700 (or 0.06% of measured voltage). Measurements in the test combustor exhibited a noise level of the laser baseline measurements of about ±0.15% of the detector voltage readout (S/N of 670) with the combustor off (no flow or beams steering effects). The same level of errors was also observed in the far wings of absorption scans with the combustor running, which indicates that no other flow related errors, such as beam steering, act on the timescale of a small fraction of a line scan (in the current experiments a line is acquired at 300Hz or 3ms). This level of noise translates in about 0.03% standard deviation of the measured peak absorbance for the average line heights in these experiments.

Random errors are generally reduced by two methods: averaging measurements from multiple scans and smoothing data from a single scan. The method used by the author is to fit each line trace with the line-shape function. In this case, fitting is the primary random error filter. An example of the fitting process for a line with uniform random noise up to ±0.5% on the voltage signal is presented in Figure 35. The fit eliminates most errors and recovers the original line. In the case shown below, there is a small difference in peak height between the fit and the original line. This peak difference between the original and the fit results in an area difference of less than 0.1%. For

random noise levels similar to the ones measured in the test combustor, fitting can reduce errors in the area (integrated absorbance) to less than 0.01%.
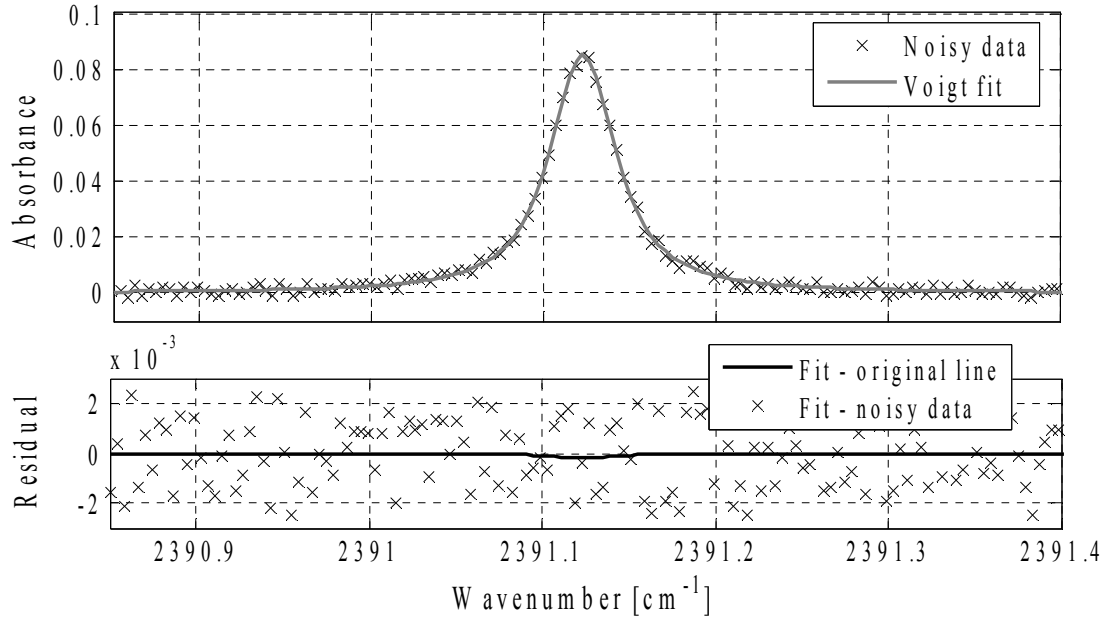
Figure 35. Absorption line with uniform random noise up to ±0.5% on the voltage signal *I*(*ν*) and the Voigt fit through the resulting absorption, -ln(*I*(*ν*)/*I₀*(*ν*)). The residual between the fit and the noisy data has a distribution that looks uniform and the residual between the fit and the original noise-free line is very small, exhibiting a shape characteristic of an error in the peak height.

Thus the measured random errors are small and fitting the data to an analytic (Voigt) function does a good job of reducing them. As a result, random errors are considered a minor error source and the following effort concentrates on reducing systematic errors for each single line-trace.

5.2.2 Linear Bias Errors

To analyze the contributions of the systematic errors to the sensor performance, it is useful to divide these into errors with linear and nonlinear behaviour. Many of the error

sources identified in equation (19) may be essentially constant or linear with wavelength during a single line scan. The optics will generally have a transmittance or reflectivity of less than 100%, which is a function of wavelength: $A_{optics}(v)$. Typical fused silica glass or other optical materials have very flat transmittance over several microns or at least hundreds of nanometers. Over the bandwidth of one line scan (~1nm), the transmittance of an optical element can be considered constant (independent of wavelength) or at least linear with wavelength. The gain of photo-detectors, $G(v)$, is a weak function of wavelength (through their quantum efficiency) in the operating range and thus can be considered linear over one line scan. For example, the detectors used in the current experiments have a gain that changes approximately 0.3% over a 10nm bandwidth near 2000nm. The combustion exhaust gases, the walls, and the windows, might exhibit broadband emission (black body). Whether the emission is relatively linear over the scan range or nonlinear, it will have a constant effect on the measurements because the detector is broadband. As such emission will always be aggregated by the detector and result in a constant bias.

All these linear and constant contributions to the measured transmittance can easily be determined and eliminated through baseline fitting to the far wings of the absorption line. Assume the only errors are in the form of a linear "gain": $A_{lin}(v) = a_1 \cdot v + a_0$ and the laser baseline, $I_{0L}(v)$, is constant. Then the measured signal becomes:

$$I(v) = A_{lin}(v)I_{0L}(v)e^{-k(v)l} = \left(c_1 v + c_2\right)e^{-k(v)l} \tag{20}$$

Because in the far wings of the line there is no absorption, the measured signal is $I(v) = \left(c_1 v + c_2\right)$ and can be extracted with a simple linear fit. Thus linear errors can be reduced and have a negligible effect on the measurements. As a result, random errors and

85

systematic linear error sources are either very small or are eliminated through baseline and profile fitting. The other factors contributing to measurement uncertainty are characterized by nonlinear signal distortions and are much more difficult to eliminate. These are discussed next.

5.2.3 Beam Steering

Beam steering is the result of temperature gradients along the line of sight that change the index of refraction of the gas and result in the beam walking off the detector. Changes in beam steering are a function of the bulk flow speed as well as the unsteadiness and turbulence level. Thus the attenuation in the signal due to beam steering can be written: $A_{BS}(t) = A_{BS}(\nu)$. Beam steering effects are only considered here for completeness and as an aggregate effect to characterize the overall uncertainty introduced in the measurements. It is not the author's intention to analyze beam steering in detail – there are many good sources in literature that describe and characterize beam steering effects.[62-65]

For the purpose of this error analysis, beam steering is separated into two contributions. If the beam steering time-scale is of the same order of magnitude as the time it takes to scan over one line (300Hz or 3ms for the New Focus laser used here; 100kHz – 10μs or faster for other readily available laser sources) then the amount of beam steering changes during the scan resulting in a nonlinear decrease in the detector signal. The decrease in transmitted signal associated with this "fast" beam steering increases the measured absorbance. If the beam steering timescale is much longer then the scan time, the beam steering is slow or "frozen" and only a constant fractional

decrease in transmittance is registered. This latter case of constant bias falls into the linear error regime analyzed above.

In practical applications, fast laser tuning (hundreds of kHz or better) and optical system design (focusing the laser beam, using large collecting optics, etc.) is used to freeze the flow and reduce beam steering effects. For some lasers, the output beam direction changes slightly with wavelength, a behavior called "beam walk." The effects of beam walk are very similar to beam steering (moving the beam off the detector) and can be treated in the same way as fast beam steering because it may change during a line scan.

If beam steering can not be effectively eliminated, then measurements where beam steering can be identified should be discarded based on physics-based rules. For example, if the line shape is not similar to a Voigt (i.e., the Voigt fit results in large residual error between the data and fit), or the absorption-free spectral region close to the absorption feature is far from the nominal zero level, these measurements can be discarded. Small beam steering effects would also be reduced by averaging multiple measurements. Nevertheless, fast beam steering remains one of the major sources of uncertainty in all highly turbulent combustion flows.

5.2.4 The Laser System

The laser system is probably the most important piece of equipment for absorption spectroscopy sensors. The laser performance in terms of accessible wavelengths, tuning speed, tuning range, and baseline shape is the primary factor in overall sensor performance. The limitations of the laser used in the above experimental work are analyzed below. Nevertheless, since much better laser technology is available,

87

overall performance and uncertainty for nonuniformity sensing is derived based on available state of the art systems.

The shape of the laser baseline, or optical power as a function of wavelength, is very important for absorption spectroscopy. The laser baseline, $I_{0L}(\nu)$, is a major source of nonlinear errors in the above experiments and as such its accurate determination is essential for absorption spectroscopy sensing.

5.2.4.1 Measurement Baseline Determination

The laser used in the current experiments has an output power that is a highly nonlinear function of wavelength and it also exhibits large and closely spaced power drops due to internal etaloning. A sample laser scan is shown in Figure 36. It is a source of errors due to the difficulty in its determination and because small changes in absorption are generally more difficult to measure when the laser baseline changes significantly.
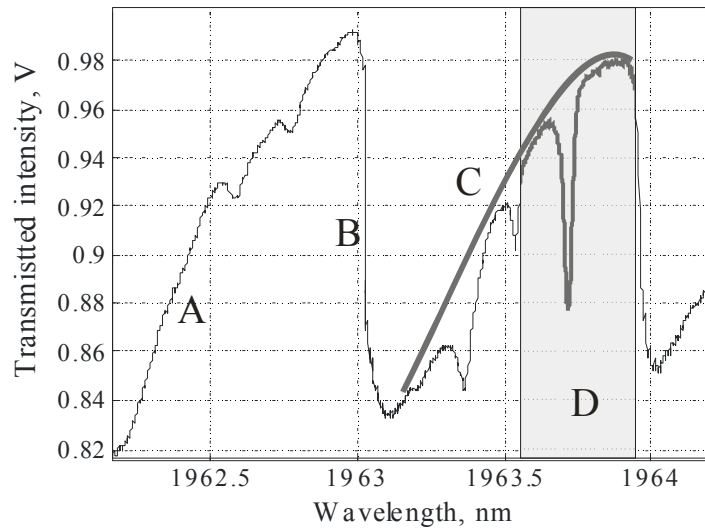
Figure 36. Laser transmission trace. A: laser baseline signal, $I_{0L}(\nu)$, as a function of wavelength; B: etaloning in the laser; C: fitted laser baseline; D: absorption line and shaded range of fast laser tuning.

In any direct absorption measurement, the overall baseline signal, $I_0(v)$, can be obtained in two ways. The laser beam can be split before the measurement region and the laser power of the beam that bypasses the measurement region can be measured directly with a second detector. The baseline can also be determined by fitting a function (generally a polynomial) to the far wings of an isolated absorption feature. A combination of the two methods yields the best results in terms of accuracy and sensitivity.

To use a separate measurement of the laser power for baseline determination, the two detectors used have to be matched to have the same response and calibrated to yield the same final output in the absence of absorption. For sensitive measurements, two methods of reducing baseline errors are available: balanced radiometric detection, and modulation spectroscopy with higher harmonic detection. These methods can usually increase the signal to noise ratio of absorption measurements in combustion flows by about 1-2 orders of magnitude. Balanced radiometric detection was developed by Hobbs[66] and an application to absorption spectroscopy is described in Reference 67. The method uses two detectors, one for the measurement beam and one to monitor laser power, as part of a circuit that that electronically cancels the photodetector currents. Modulation spectroscopy encompasses several techniques, such as wavelength modulation spectroscopy, frequency modulation spectroscopy, and two-tone frequency modulation spectroscopy. Reference 68 gives a review of these methods as they apply to trace gas detection.

If no fitting is used and the baseline is measured only by a separate detector, such a baseline signal does not include information about errors originating in the combustor, such as beam steering. It only contains information on the laser baseline $I_{0L}(v)$ and some

optics losses A_{optics}. The main advantage of a separate baseline measurement is that it captures the actual shape of the laser power curve and any etaloning effects occurring before the beam splits. The more nonlinear the laser power is with wavelength, the more important is such a measurement. Furthermore, if the laser does not scan far enough to use the wings of absorption features for baseline fitting, a separate measurement may be the only way to determine the baseline signal. This is also the case for some high pressure applications when the absorption features undergo significant broadening. A separate measurement also accounts for absorption from sources outside the measurement region, $K_{ext}(\nu)$, such as water in the room air if the laser path is exposed.

The second way of determining the baseline, by fitting a polynomial to the far wings of an absorption feature, has the advantage of capturing changes in the signal due to absorption from global emission in the combustor aggregated by the detector, I_{flow}, absorption in the optics, A_{optics}, and slow beam-steering that is frozen in time during a line scan, $A_{BS\text{-}frozen}$. The major drawbacks, especially in the above experiments, result from the necessity to scan far enough from line-center to capture regions of no absorption for the fit and the inability to account for other absorption sources (e.g. room air) and laser power nonlinearity.

When the two methods are combined, then most of the factors affecting the signal are captured: $I_{0L}(\nu)$, A_{optics}, I_{flow}, $A_{BS\text{-}frozen}$, and $K_{ext}(\nu)$. The only unaccounted error contributions to the transmittance remain from fast beam steering, $A_{BS}(\nu)$, some random noise, and flow unsteadiness and turbulence affecting the actual absorption.

5.2.4.2 <u>Effects of Tuning Limitations on Baseline</u>

Another limitation of the laser used in the above experiments that is a source of errors is its limited fast tuning range and speed (shaded region in Figure 36). The laser can only fast tune over one line ($\Delta\lambda$=0.3nm) at a time at a repetition rate of 150Hz, resulting in single line data acquired in roughly half the time, 1/300 sec (or 2 scans per sweep cycle). This limited tuning capability is directly responsible for two types of errors: (i) the small tuning range is not always sufficient to capture the whole line shape and absorption-free background in the far wings and (ii) the low tuning speed allows for some errors due to beam steering and combustor unsteadiness.

If the far wings are not captured completely, because of the limited tuning range, and the baseline is fitted to regions that exhibit non-negligible absorption, the resulting integrated absorption will be smaller than the true value. This error in absorption is illustrated in Figure 37. The percent error in absorbance is computed for a baseline that is fitted to points in the wings that are a given number of FWHM away from center, thus not capturing the whole absorbance area. From this figure it can also be seen that to capture most of the absorbance in the absence of other errors, one has to tune more than 30 FWHM away from center (if no other techniques are used to account for the difference in baseline position).
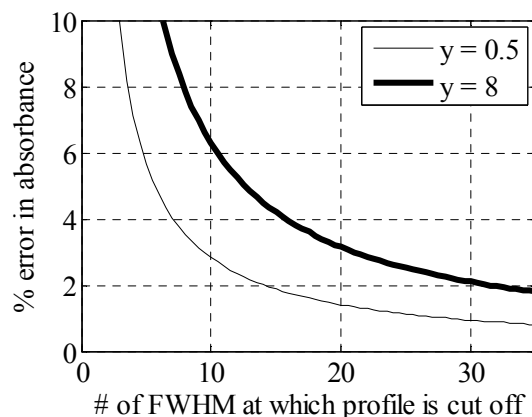
Figure 37. Absorbance error resulting from baseline fitted to wings, a given number of FWHM from center. The '*y*' parameter represents the ratio of Lorentz to Doppler widths for a Voigt profile. For most water absorption lines of interest, the Voigt '*y*' parameter is between 0.5 and 8.

A typical water line has a Voigt FWHM at 1000K of 0.02–0.04nm, so the laser scan of 0.3nm encompasses only about 10 FWHM, or 5 FWHM to each side of a line. From Figure 37 it can be seen that this limited scan range alone can introduce biased negative errors in the absorbance of 4–10%. These numbers represent an upper bound (worst case). As demonstrated in the measurements described in Chapter 4, these errors are alleviated in two ways. First, the baseline fit parameters are allowed to be optimized during the Voigt fitting process. By bounding the Voigt fitting parameters based on an assumed minimum and maximum temperature, to increase the goodness of the fit the baseline is forced away from the initial guess (based on the points at 5 FWHM from center) and closer to its error-free position. Although this method does not completely eliminate this error, it does decrease it significantly (estimated decrease in absorbance errors by more than half). To further reduce errors due to baseline nonlinearity and placement, the laser baseline, $I_{0L}(\nu)$, is measured independently with the combustor off before and after a set of measurements are performed. The absorption line of interest is

measured uncentered, such that one of the wings is measured farther from the center. This region of lower absorption is used to anchor the predetermined baseline shape during the Voigt fitting process. The baseline fit parameters are still allowed to be optimized during the Voigt fit. Results from the two methods are shown in Figure 38. Although the fit is good and reduces the errors due to the limited scan range in both cases, using a separate measurement of the baseline shape and anchoring it to the measured transmittance is preferable (in general and especially in the current experiments) because it yields Voigt fits based on a real baseline shape and data from one far wing.
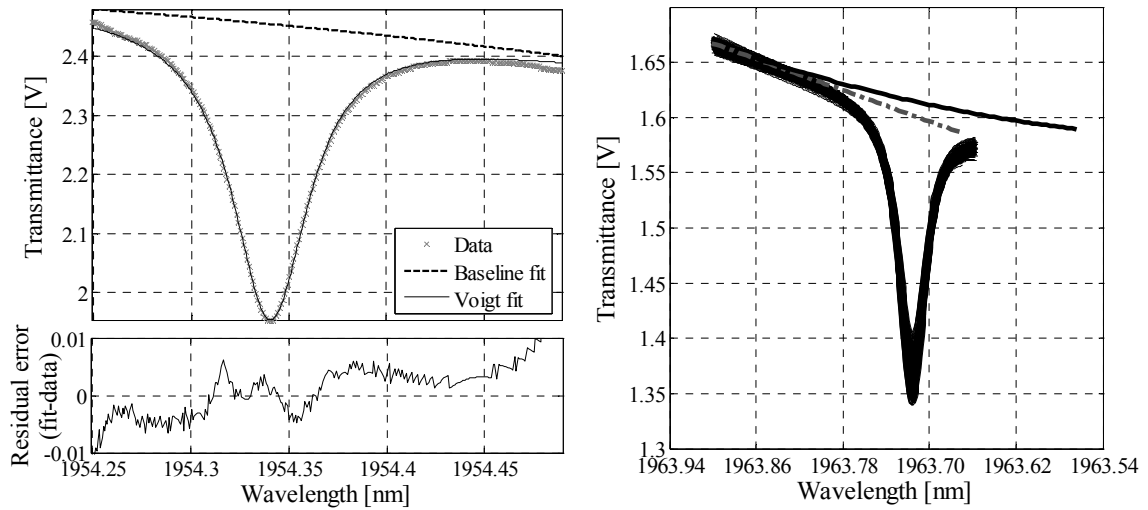
Figure 38. Left: Voigt fit to transmittance data with baseline position optimized during the Voigt fitting. Right: multiple Voigt fits (black lines) to a series of scans over one line. The solid black baseline is the average of baselines determined from combustor off measurements and anchored to far left wing of the line. The dash-dot line represents the average of the baselines that would have been fitted to the far wings of this measurement.

Currently available diode lasers can exhibit very linear power. Nevertheless, even when using available lasers with better tuning characteristics, the comparison above suggests that measuring the baseline with a separate detector and allowing for small adjustments during the Voigt fitting process would improve the overall accuracy.

A higher tuning speed also allows the flow and beam steering effects to be effectively frozen during a line-sweep – in other words, the time it takes to scan over a line should be shorter than the time-frame of significant changes in the flow. This is important because all absorption lines should be scanned through essentially the same gas region with steady temperature and concentration profiles and fixed beam steering. Generally, tuning speeds in excess of a few hundred kHz over several lines (~2-10nm) are desirable. For a combustor exhaust flow of 30m/s, a laser scanning at 100kHz would complete a scan in 0.01ms, a time in which the bulk flow would advance only 0.3 mm. This movement is relatively small compared to the expected size of most turbulent structures, as well as the typical laser beam size (~1 mm). Thus it should not cause significant errors in the absorbance. In the test combustor the flow velocity was on the order of 1m/s. During a single scan of one line taking ~3ms, the bulk flow moved about 3mm. When tuning back and forth over one absorption line, changes in the flow were observed spanning several singe line scans (on the order of 3-6 scans or 9-18ms). From this measure it is estimated that the size of flow structures that may result in beam steering or temperature and concentration changes are on the order of 1-2cm (less than 25% of the diameter). These relatively slow flow variations validate the assumption that changes in the temperature profile during one such scan are likely to be low. Nevertheless, flow unsteadiness is one source of error that directly affects the absorption $k(\nu)$ in the current experiments.

5.2.5 Limits of Voigt Fitting

The shape of absorption lines at a given temperature are given by the Voigt profile, as described in Chapter 2. When the measured absorbance is the integral over a

path with nonuniform temperature and absorber concentration (equation 3), the shape of the path-integrated line can not be perfectly represented by a Voigt profile. If the line shape for absorption through a nonuniform medium could still be perfectly represented by a Voigt function, then there would always exist a uniform profile with temperature, T_V, corresponding to the resulting line shape. It can be proven that such a T_V does not exist.

The absorption line shape through a nonuniform medium is given by the path integral in eq. (1) and can be approximated as a sum over a finite number n of regions of equal path $l_i = L/n$ with temperatures T_i. For simplicity assume a uniform mole fraction x:

$$-\ln\left(\frac{I(v)}{I_0(v)}\right) = \int_0^L xS(T(l))\phi(v, T(l), x)dl = \sum_{i=1}^n xS(T_i)\phi(v, T_i, x)(L/n) \qquad (21)$$

If this resulting line shape were represented by a Voigt profile characteristic of a temperature T_V, then the difference between the two profiles would be zero:

$$\frac{L}{n}\sum_{i=1}^n xS(T_i)\phi(v, T_i, x) - LxS(T_V)\phi(v, T_V, x) = 0$$

$$\sum_{i=1}^n \left[S(T_i)\phi(v, T_i, x) - S(T_V)\phi(v, T_V, x)\right] = 0 \qquad (22)$$

T_V could be found by performing a Taylor series expansion of $(S\phi)(T)$ around the average temperature of the nonuniform profile, T_{avg}, where A_i is the ith derivative of $(S\phi)$ evaluated at T_{avg}.

$$S\phi(T) = S\phi(T_{avg}) + \sum_j A_j / j! \cdot (T - T_{avg})^j \qquad (23)$$

Then the difference between the profiles can be written as:

$$\sum_{i=1}^n \sum_j \frac{A_j}{j!}\left[(T_i - T_{avg})^j - (T_V - T_{avg})^j\right] = 0 \qquad (24)$$

95

This expression is true if and only if $T_i = T_{avg} = T_V$, i.e., a Voigt profile can only represent the absorption line shape if the flow is uniform. Consequently, equation (24) represents the difference between the two profiles. Because the derivatives of the product of S and ϕ are very difficult to compute, the left side of equation (24) is not used to analytically determine the errors associated with fitting a Voigt profile to the absorption line shape through a nonuniform medium.

Instead, a simulation was conducted to examine the accuracy of a Voigt fit for absorbances through nonuniform media. The line shape for a single absorption line is computed first for a medium having a uniform temperature of 1600 K and then for a medium of the same length, with average temperature of 1600 K and a linear temperature profile from 1200 K to 2000 K. As expected, the area under the curves for the two lines is different because of the nonuniformity effects on absorbance (Figure 39, left). A Voigt profile was fit to the line through the uniform medium. This fit had a residual error in area of 0.00003% when compared to the original line; this small difference is caused by the discretization of the signal and numerical (e.g., round-off) errors in the simulation. The same fitting process was applied to the line computed for the linear temperature profile. The result of this fit is plotted in the right panel of Figure 39. The resulting error between the real absorbance area and the fitted area was 0.001%, larger but still relatively small. The residual in this case exhibits a small structure that may indicate that a different line shape function, such as a Galatry profile,[21] may be a better representation of the convolution line shape through a nonuniform medium. Nevertheless, the very small difference in areas suggests that Voigt fitting can be used and does not contribute significantly to the systematic error.

96
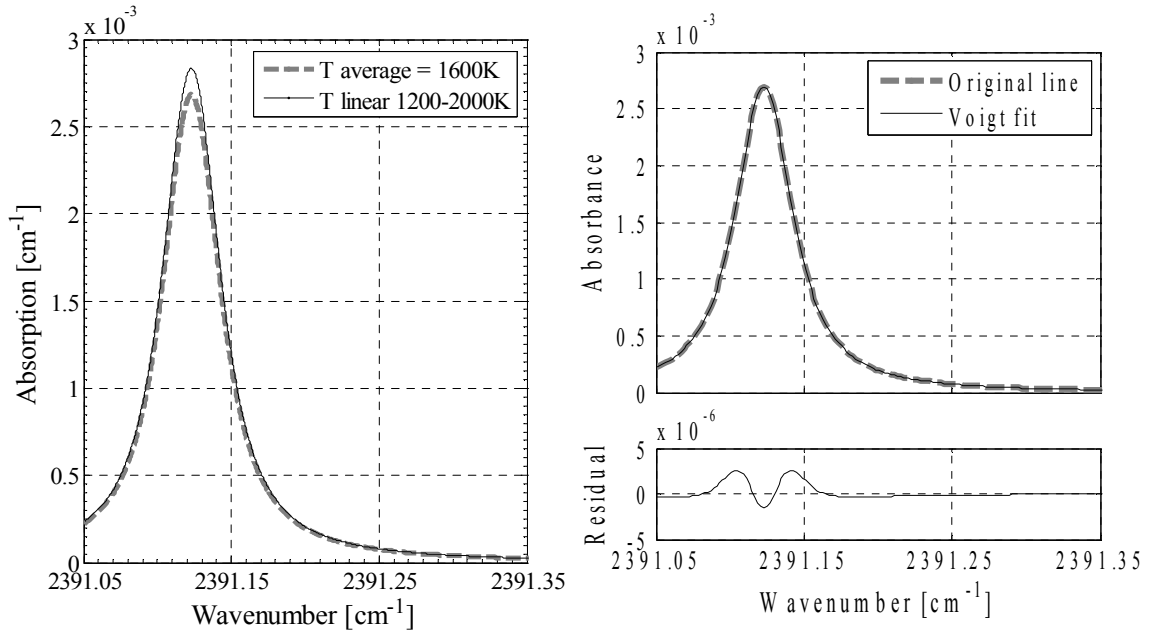
Figure 39. Left: comparison of absorption line shape for a uniform temperature of 1600K and the same line for a linear temperature profile over the same path in 33 increments between 1200K and 2000K. Right: Voigt fit to the line corresponding to the linear temperature profile to check if the line shape changes from a Voigt. The shape of the residual may indicate that a Galatry profile might provide a more accurate fit. Area difference between line shape and fit was 0.001%.

5.2.6 Changes in Concentration versus Temperature Profiles

In the combustor test rig (Chapter 4), severe heat losses at the walls have a large effect on the exit temperature profile (reducing the local temperature in the near wall region, and also the bulk average temperature). However, the water mole fraction profile is relatively unaffected by the heat transfer; loss of heat from the gas near the wall does not reduce its water content. Thus, the heat losses can significantly alter the correlation between the species composition and the temperature field. As combustor operating conditions change, changes in wall cooling have larger effects on the temperature profile than on the absorber distribution. Effectively, this means that under different operating

conditions, the local correlation between the temperature and species mole fraction may also be different.

In general, all absorption-based sensors are influenced by both the temperature field and the concentration field. If the temperature and concentration are correlated and the correlation never changes, it is equivalent to saying that the concentration is a set function of temperature, so a nonuniformity absorption sensor will be a measure of changes in the temperature profile. When this correlation changes (i.e., from one combustor operating point to another), than the absorbance (or U) becomes a composite measure of changes in the temperature field combined with "independent" changes in the concentration field, raising the question whether U is still indicative of temperature nonuniformity. In most practical gas turbine combustors with limited heat losses, the temperature and species concentrations are strongly correlated (i.e. hotter regions have more water), regardless of operating conditions. Because the experimental setup used for this sensor exhibits unusually large heat losses and possibly large changes in correlation between different operating conditions, these effects are investigated as a possible major experimental error source in the measurements presented in Chapter 4.

The effects of changes in correlation on U are investigated using the measured combustor exit temperatures (Figure 31) and simulating the sensor operation for several water distributions at every operating condition. For example, for a given temperature profile characterized by a T_{std}/T_{avg} value, U is computed for a uniform water distribution, for a water mole fraction that varies linearly and quadratically with temperature, and for several random water distributions. In all cases, the mean water mole fraction is the same. The resulting U values for each operating condition (T_{std}/T_{avg}) are shown in Figure 40.

The plot shows that when going from one combustor condition to another (i.e. from one T_{std}/T_{avg} to another) and the correlation is different, even considering the largest possible unfavorable change in correlation, the U values still generally track the actual T_{std}/T_{avg} values.
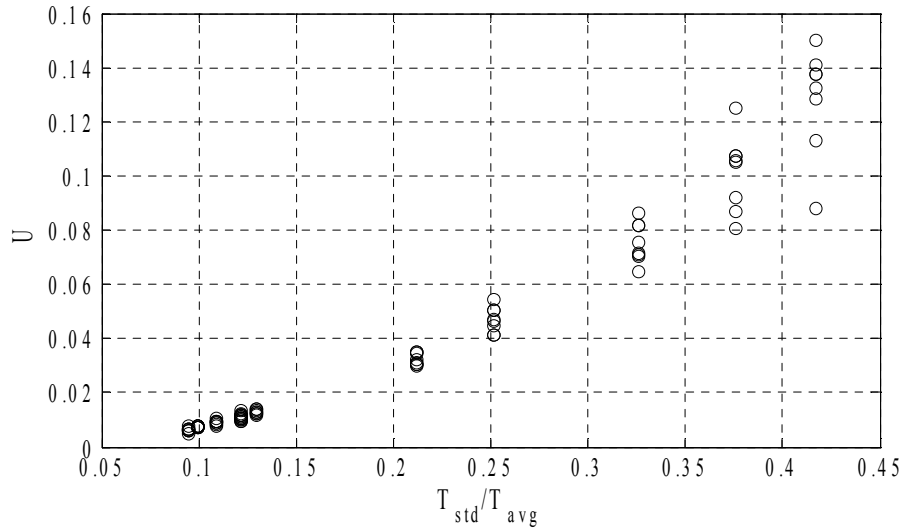
Figure 40. U for several correlations between temperature and concentration.

Although this simulation employs extreme changes in the water-temperature correlation, the U values still increase with temperature nonuniformity and exhibit limited scatter. This suggests that the changing correlation is not a major problem in the current experiments and other error sources have a larger contribution to the errors observed in the measured U values.

Based on this analysis, it is therefore concluded that in general, for a set of lines with good sensitivity, the effects of small to moderate changes in correlation do not significantly affect the trend of U. Furthermore, this problem becomes even less significant for practical gas-turbine combustors where heat loses at the walls are small and large changes in correlation are not expected.

99

5.2.7 Other Error Sources

For the sake of completeness, several other sources of errors and the established ways to reduce them are summarized in this section. The optics used in the sensor may create undesired etaloning, superimposing a wavelength-dependent, sinusoidally varying baseline that would adversely affect the measurements. When observed in experiments, such etalons is eliminated through changes in the optical layout, for example by slanting the optics relative to the laser propagation direction, changing the distance between optical elements, and using wedged optics. Fiber optics or purging the air path outside the measurement region with an inert gas can be used to eliminate external absorption (K_{ext}), for example due to water in the room air for the current experiments.

Another source of uncertainty is inherent in the use of published spectroscopic parameters. The parameters for each line listed in the HITRAN database, such as reference line strength, S_0, line position, lower state energy E'', and especially broadening parameters, are not always reliable. Uncertainty in these parameters directly affects $k(v)$ and propagates into the absorbance values and U. In general, the spectroscopic parameters of the lines used should be verified experimentally. Furthermore, attention should be taken to correctly identify each line used and to experimentally check for interference from lines that may not be listed in the database. It should be noted that for nonuniformity measurements changes temperature are important, not the absolute value. Because of this fact, some constant systematic errors (such as spectroscopic parameters) have a smaller effect on nonuniformity sensing.

5.3 Global Uncertainty Analysis

Most of the sources of errors discussed above ultimately affect the computation of the baseline I_0, which is the most critical information needed for accurate absorption measurements and good sensitivity. The physical causes of errors and estimated magnitudes were described above, together with amelioration methods at the hardware and experimental design level. The remaining cumulative uncertainty on the senor is analyzed below to determine a performance envelope for nonuniformity sensing in terms of accuracy and minimum expected uncertainty. This analysis is performed based on capabilities of current state of the art hardware, which is taken to define the limits of this sensing technique.

5.3.1 Baseline Fitting Errors

As described by eq. (19), the baseline containing the effects of all the errors has to be determined to compute the actual absorption. In the above sections it was shown that 1) random errors, $R(t)$, result in a cumulative absorbance uncertainty of 0.01% or less; 2) $A_{optics}(v)$, $G_{det}(v)$, $A_{BS-frozen}$, and I_{flow} are linear bias errors and are eliminated through baseline fitting to the far wings; and 3) Voigt fitting of the line shape through a nonuniform medium results in less than 0.001% errors in absorbance. Since all these errors are very low, it is the contribution of nonlinear systematic errors (fast beam steering, laser baseline shape) that is addressed below by analyzing its global effect on the baseline fit and ultimately on U.

The effects of errors in baseline measurements on absorbance and temperature sensing are determined based on computer simulations and analytical computations of

error propagation (eq. (13)). Errors due to broadband absorption or from fitting the baseline to a region not sufficiently far in the wings of an absorption feature are modeled first. These errors result in a misidentified baseline that is shifted from the error-free signal. If such a shift can be estimated, the percent error in absorbance is then computed based on the shift in baseline measured as a fraction of the actual peak height of the absorption line. Figure 41 shows the fractional error in absorbance resulting from shifting the absorption baseline (I_0) by a certain percent of the peak absorbance. The shift levels shown in the plot are relatively large, but were experienced in the experiments when certain lines exhibited a partial overlap with laser etalon drops. In those cases simple baseline fitting to the ends of a scan (Figure 38) resulted in large baseline and absorbance errors.

Figure 41 further shows that even small errors in the baseline placement characteristic of better systems results in much larger (~10 times) errors in the absorbance and consequently in the computed temperature. This plot shows that good baseline measurements are critical in obtaining accurate absorption values. If we define the percent error in baseline signal at line center, e_b, as:

$$e_b = \frac{I_{peak}/I_{0,shifted} - I_{peak}/I_{0,true}}{I_{peak}/I_{0,true}} = \frac{I_{0,true}}{I_{0,shifted}} - 1 \qquad (25)$$

and the percent error in peak absorption as e_p, then $e_p = \dfrac{\ln(e_b+1)}{-\ln(I_{peak}/I_0)}$ (26). It can be seen that the peak absorption error depends both on the error in the baseline as well as in the magnitude of the transmittance, I_{peak}/I_0. For example, a 0.1% error in the baseline of a line with 90% peak transmittance will result in approximately 0.1% peak absorption

error, or about 1% (integrated) absorbance error (Figure 41 right). These errors can be reduced using the techniques described in section 5.2.4.2.

Figure 41 and equation (26) are used to compute the propagation effect of baseline uncertainty into absorbance, regardless of the source of uncertainty in the baseline. This establishes the link between signal errors and absorbance uncertainty. The uncertainty in absorbances is then propagated to U to determine the overall capabilities of the sensor.
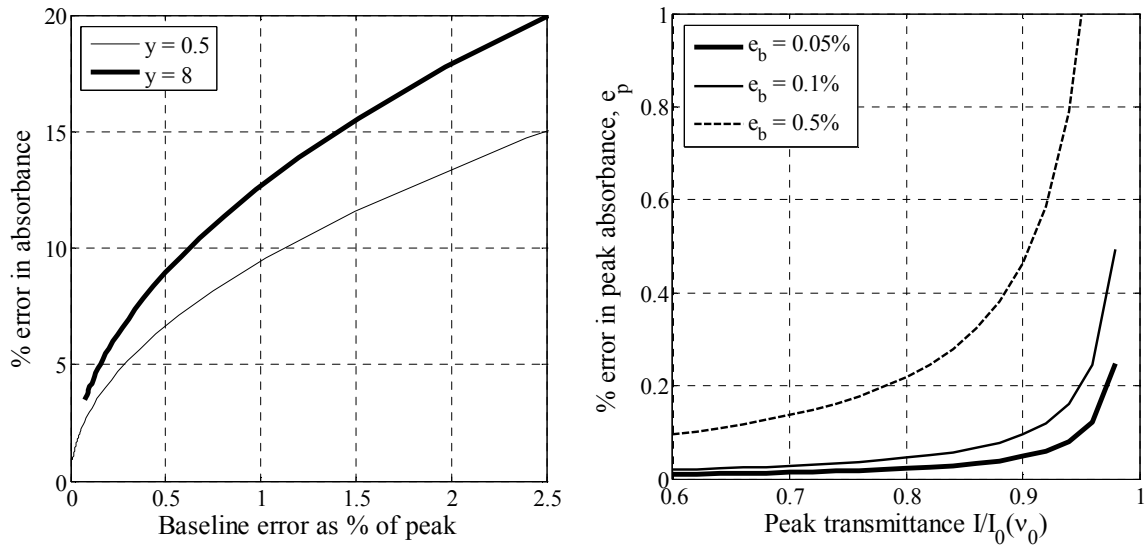
Figure 41. Left: effect of a shift in baseline equivalent to a given percent of the real absorption peak. y is the ratio of the collision to the Doppler widths used for the Voigt profile (see Appendix A). Right: effect of a shift in baseline equivalent to a given percent of the real peak on absorption.

5.3.1.1 Effects of Baseline Uncertainty on Nonuniformity Measurements

The uncertainty in absorbance is a result of all the errors (mostly nonlinear) that can not be eliminated. These absorbance uncertainties can be estimated for a certain experiment by some of the methods described earlier. Based on published literature, absorbance uncertainty in combustion flows is around 1-3%, although these values are

103

understood to contain the effects of flow unsteadiness as they are based on measurements averaged in time.[27,39] Therefore for some of the reasons given above (error rejection optimized for each scan, relative versus absolute measurements), it is assumed here that the effective uncertainty in absorbance for nonuniformity sensing using state of the art hardware is below 1%.

When measurement errors affect the baseline and the resulting absorbances, measurements of the temperature distribution will also be affected. The effects of errors on the nonuniformity variable "U" are illustrated using temperature profiles of type (A) and (B), as described in Chapter 2.

A set of three profiles of type (A) are used: one uniform profile with T, and two profiles with spikes over $x = 30\%$ of the path and spike temperatures bT, where $b = 120\%$ and 140%. Two values of T are used for illustration: $T = 1500K$ and $T = 1000K$. For each profile, U is computed first for the error-free case and then for 100-500 cases where we introduce an independent, uniformly distributed uncertainty (e.g. -0.1% to 0.1%) for each absorbance value and then compute the corresponding U (based on lines 1, 4, & 6).

For the profiles based on $T = 1500K$, a uniform distribution of errors of up to 0.2% in absorbances results in significant scatter of the U values (Figure 42 left). The spread in U can be characterized by its standard deviation, s_U. If we consider that most values lie within two standard deviations of the mean, then a nonuniformity sensor would potentially be able to differentiate between profiles that have U values different by at least $2*s_U$. For a range of error levels and temperature profiles based on $T = 1500K$ and 1000K, the resulting U values and their standard deviations are plotted in Figure 42 (right). A nonuniformity sensor would be able to differentiate between profiles to the

right of the dashed line. It should also be noted that the coefficient of variation

(s_U/mean(U)) decreases with temperature due to the increased sensitivity of the lines, so

while a 20% spike over 1500K with 0.5% errors may not be measured, a 20% spike over

1000K with 0.5% errors is measurable (Figure 42 right). This means that it becomes

harder to measure the same percent spike (bT) at higher temperatures, given the same

level of uncertainty (e.g. solid versus open circles).
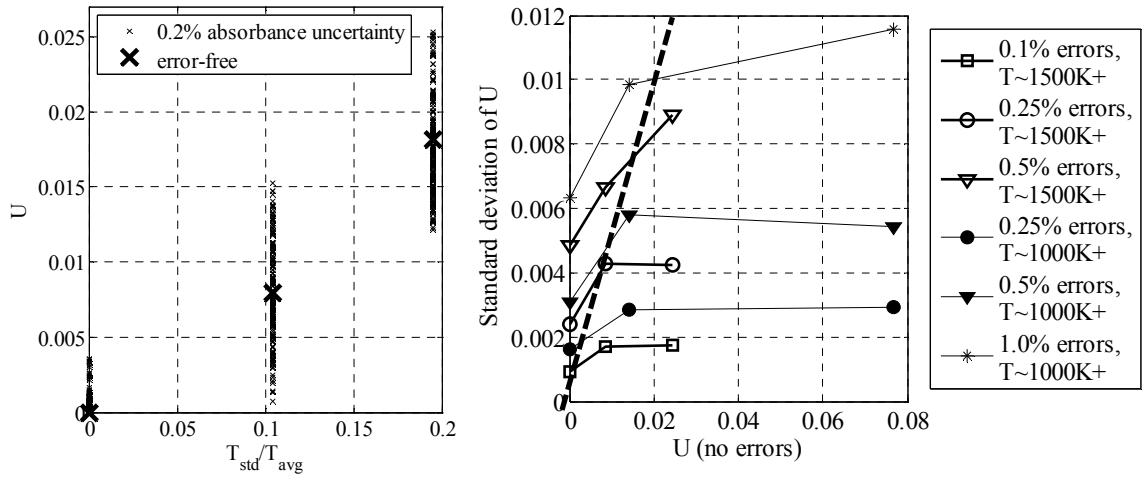
Figure 42. Left: *U* values for measured absorbance uncertainty of ±0.2% for three profiles of class (A) based on T = 1500K, and b = 120% and 140% for x = 30%. Right: The standard deviation of the *U* distributions for each profile given different levels of uncertainty, based on T = 1500K and T = 1000K. The dotted line represents *U*=2*s_U; profiles with *U* to the right of the line have low enough errors such that a sensor can differentiate between them, i.e. differentiate between a 20% and 40% temperature spike.

The same procedure is applied for a set of four profiles of type (B) with an

average temperature of 1500K and linear temperature distributions with ranges of 0K

(uniform), ±100K, ±250K, and ±500K. The nonuniformity parameters for these profiles

given an absorbance uncertainty of up to 1% are computed and plotted in Figure 43. The

standard deviation of *U* corresponding to the four profiles shows that the differences

between some of these profiles can be measured even for errors up to 0.5% (Figure 43).

105

The nonuniformity sensor has a better ability to differentiate between these profiles than in the case of simple spikes because of the higher sensitivity to lower temperatures.
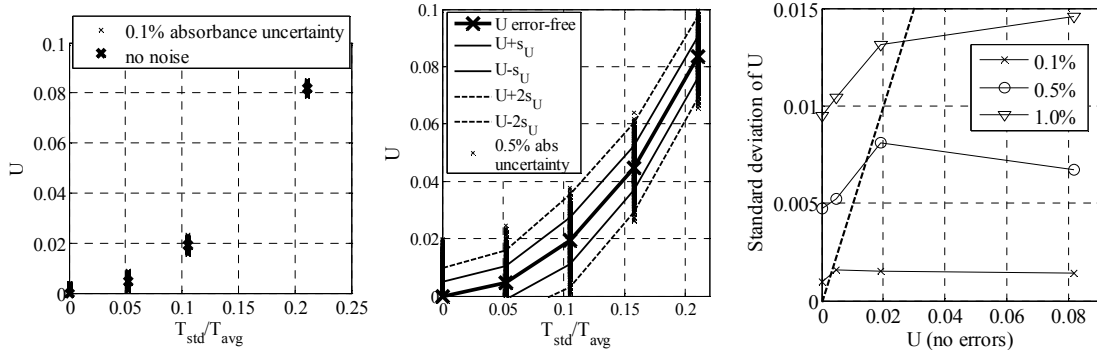
Figure 43. *U* values (and spread due to errors – 'x') for four profiles with linear temperature distributions with an average of 1500K and ranges of 0K, ±100K, ±250K, and ±500K – the higher the spread the higher the T_{std}/T_{avg}. On the right the plot represents the standard deviation of *U* due to various levels of uncertainty in absorbance; the dotted line represents $U=2*s_U$; profiles with *U* to the right of the line have low enough errors such that a sensor can differentiate between them, i.e. differentiate between a profiles with a range of +/- 100K and +/- 250K.

In the case of small absorbance uncertainties of 0.1%, even the smallest temperature deviations (±100 K) can be sensed. For a moderate level of uncertainty in absorbances (0.5%), the spread of the *U* values increases but the trend in *U* is still clearly visible and slightly larger temperature deviations (±250 K) can be sensed. The same simulation for profiles centered around 1000 K shows that smaller relative changes in the temperature profiles can be sensed for the same level of absorbance uncertainty. This is due to the fact that line sensitivity to nonuniformity increases at lower temperatures, effectively increasing the signal to noise ratio.

The simulations performed above demonstrate that even in the presence of significant uncertainty in absorbance (~ 1%), this sensing technique is still capable to differentiate and track relevant changes in the temperature profile.

106

5.4 Sensing Capability and Needs

The previous sections analyze the errors affecting each absorption measurement and employ simulations to illustrate how the sensor output is influenced by total uncertainty in the measured absorbance values. Although these simulations show good sensor performance is possible for the synthetic profiles, a more rigorous error propagation analysis is performed below to provide a performance bound, independent of the type of temperature profiles encountered.

5.4.1 Global Sensor Performance Analysis

Mathematically, assuming that the uncertainty sources in absorbance are independent, the standard deviation of U, s_U, can be derived as a function of the uncertainty in measured absorbances:

$$s_U^2 = \sum_{i=1}^{3} \left(\frac{\partial U}{\partial \alpha_i} \right)^2 s_{\alpha i}^2 \qquad (27)$$

where $s_U{}^2$ is the standard deviation in U and $s_{\alpha i}{}^2$ is the standard deviation in α_i. Expanding this expression yields:

$$\frac{s_U^2}{U^2} = \frac{4 \cdot T_{12}^2 \cdot T_{13}^2}{\left(T_{12}^2 - T_{13}^2\right)^2} \left[\frac{T_{12}^2}{1.44^2 \Delta E_{12}^2} \left(\frac{s_{\alpha 1}^2}{\alpha_1^2} + \frac{s_{\alpha 2}^2}{\alpha_2^2} \right) + \frac{T_{13}^2}{1.44^2 \Delta E_{13}^2} \left(\frac{s_{\alpha 1}^2}{\alpha_1^2} + \frac{s_{\alpha 3}^2}{\alpha_3^2} \right) \right] \qquad (28)$$

If we assume that the percent uncertainty is the same for each absorbance, written as $e_\alpha = s_\alpha / \alpha$, and writing $T_{13} = T_{12} + \Delta T$ and the normalized difference between the measured temperatures $T_d = \Delta T / T_{12}$, then:

$$e_U^2 = 8e_\alpha^2 \frac{1+2T_d+T_d^2}{T_d^4+4T_d^3+4T_d^2} \left[\frac{T_{12}^2}{1.44^2\Delta E_{12}^2} + \frac{T_{13}^2}{1.44^2\Delta E_{13}^2} \right]$$

$$\cong 8e_\alpha^2 \frac{1}{4T_d^2} \left[\frac{T_{12}^2}{1.44^2\Delta E_{12}^2} + \frac{T_{13}^2}{1.44^2\Delta E_{13}^2} \right] \tag{29}$$

This equation shows how the uncertainty in U depends on the uncertainty in absorbances, the choice of lines (E_i''), and the operating temperatures. For a given level of fractional uncertainty in the absorbances (e_α^2), the uncertainty in U can be decreased by minimizing the right side of the equation. This can be achieved by: 1) increasing the response to nonuniformity (increasing T_d), 2) maximizing each $\Delta E''$, and 3) operating at overall lower temperatures. The requirements of maximizing T_d and $\Delta E''$ show the importance of understanding the effects of nonuniformity on absorbance and developing a line selection process customized for nonuniformity sensing (the analysis and results shown in Chapter 4).

The simulations from the previous section show that useful measurements can be performed when the uncertainty in U is less than two standard deviations, or $e_U<0.5$. In other words, by imposing this lower limit on the accuracy of the measurements, the overall capability of this sensing technique is investigated for a variety of applications. Equation 29 is used to create a map of sensor performance in terms of what levels of temperature nonuniformity can be sensed under a given level of absorbance uncertainty, σ_α, regardless of the source of uncertainty or the type of profiles to be sensed. It should be noted that this map does depend on the chosen lines through the $\Delta E''$ values, so it needs to be recreated based on the available lines for the specific application. This map is shown in Figure 44 and is computed for moderate $\Delta E''$ values (in the range 1000–2000cm^{-1}).
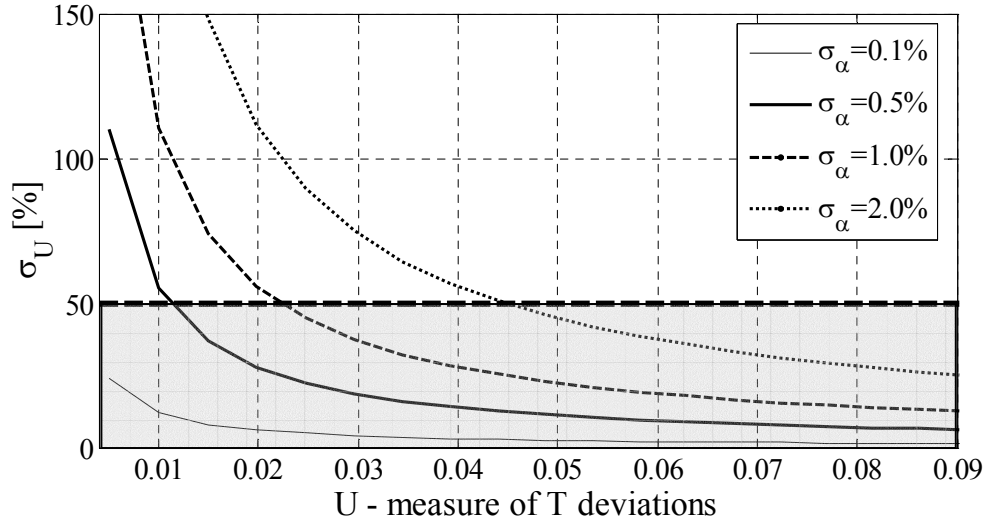
Figure 44. Map of sensor applicability. Given an expected uncertainty in absorbance, temperature profiles with *U* values in the shaded region can be measured with a S/N ratio greater than 2.

The plot can be used to asses the need and capability of a system for a specific application before any hardware is purchased. For example, from this plot it can be seen that for an expected level of absorbance uncertainties of 1% (dashed line), a nonuniformity sensor can be used to measure profiles with nonuniformity *U* greater than about 0.022 (for the assumed line parameters). This plot and eq. (29) are useful for performing trade-off analysis between the accuracy of a system and its capability in terms of temperature fluctuation sensing. Such a map is essential in designing a nonuniformity sensor for a given application.

5.4.2 Nonuniformity Sensing Capability and Requirements

In this section, the performance map developed above is used to translate sensor capabilities in terms of the *U* output into pattern factor and minimum measurable

temperature fluctuations. Stating the sensor capability in these terms allows comparison with the needs of the gas turbine industry, as defined in section 2.4.

The uncertainty in absorbance can either be computed for an existing absorption system, or can be estimated for a new system based on current state of the art. Published minimum detectable absorbances were summarized in section 2.1.2. In terms of uncertainty, from published literature, absorption spectroscopy sensors can achieve absorption uncertainties of much less than 0.1% for laminar flows.[50-52] This uncertainty value is a lower bound for instrumentation and measurement errors. In combustion flows, additional sources of errors are beam steering and flow unsteadiness and turbulence.

For realistic, fully turbulent combustion applications the limited published uncertainty data suggests that the absorbance can be measured to within about 1-3%.[25,27,39,48] This rather large uncertainty stems from the fact that many of the experiments were not optimized for accuracy. Furthermore, the published uncertainties were based the distribution of absorbance values in time, which is mostly a function of combustor unsteadiness and not the inherent errors in the absorption measurement. The uncertainty of each absorbance value is not well known, but for a single line scan it is believed to be lower than 1% because beam steering and flow effects can be controlled to a large extent by the use of fast tuning lasers. Furthermore, certain error sources introduce a constant error in absorbance that affects temperature measurements but not as much nonuniformity measurements where the relative change in absorbances is important and not the absolute value of the temperature.

Assuming that through careful design absorption nonuniformity sensing can achieve uncertainties of about 1% or better, as shown above this translates in measurable

profiles with $U > 0.02$. For uniformly distributed temperature fluctuations, this translates in profiles with pattern factors of 0.17 or larger. As shown in section 2.4, gas turbine combustors operate with pattern factors of about 0.1 to 0.4. The capabilities of the developed sensor are well within this range. As such this technology becomes a very useful tool for gas turbine combustion sensing and control. A visual summary of the capabilities and needs for this nonuniformity sensing technique is shown in Figure 45.

Capabilities:
• Absorbance uncertainty ~ 1.5%
• Measure in typical combustor exhaust flows:
    • $T_{max} - T_{avg} > \sim$ **180** K at $T_{avg} \sim 1200$ K (**PF ~ 0.15**)
    • $T_{max} - T_{avg} > \sim$ **330** K at $T_{avg} \sim 1800$ K (**PF ~ 0.18**)

Apply Technique Here

Current Measurement Capabilities

Pattern Factor: 0   0.1   0.2   0.3   0.4

Current and Future GT Operation

Use in Practical Applications

Needs:
• Measure & reduce PF in Gas-Turbine engines
• Reported **PF ~ 0.1 – 0.4**
    • @1200 K => $(T_{max}-T_{4avg}) \sim$ **120 – 480** K
   • @1800 K => $(T_{max}-T_{4avg}) \sim$ **180 – 720** K

Figure 45. Nonuniformity sensing capabilities and needs.

CHAPTER 6: CONCLUSIONS AND RECCOMENDATIONS

This chapter summarizes the results of this research effort and proposes possible directions for future development of this technology.

6.1 Accomplishments

The overall result of this work is the development of a sensor approach for temperature nonuniformity in combustion applications. Absorption spectroscopy using tunable laser absorption was extended to the sensing of temperature nonuniformity along the laser line of sight, based on a previous approach that looked at the difference in temperature between a set of cold and hot lines.[55]

The research effort described in this thesis advances the knowledge of absorption spectroscopy by thoroughly analyzing the behaviour, shape, and response of absorption line through mediums with nonuniform temperature profiles and by developing a new line selection process for nonuniformity sensing. A sensor for temperature nonuniformity was proposed and demonstrated through computer simulations and experiments in the exhaust of a laboratory-scale combustor. Finally, the capabilities of this sensing technique were determined based on a comprehensive analysis of errors and their effect on sensor performance. Methods to mitigate these errors were described, and the overall sensor capability was determined based on the characteristics of state of the art diode laser and absorption sensor technology. Furthermore, the results and knowledge presented in this thesis apply to other absorption based sensing techniques.

6.1.1 Results of Absorption through Nonuniform Mediums

To understand how a nonuniformity absorption based sensor would function, a detailed mathematical analysis was performed to study the effects of nonuniform temperature along the line of sight on a single absorption line. It was determined that the second and higher derivatives of the absorption with respect to temperature determine the response of a line to a nonuniform temperature profile. Furthermore, there is a strict correspondence between the energy of the lower quantum state of an absorption transition and the peak relative response to nonuniformity versus average temperature – a single line exhibits the best response to nonuniformity (named nonuniformity discerning) when its absorption peaks as a function of temperature. Since this peak occurs at a specific temperature for each line, as characterized by its lower state energy, there is a correspondence between nonuniformity response for temperatures in a given limited range and the lower energy of the transition. This correspondence and the importance of the second derivative of the absorbance with respect to temperature are crucial for a novel line selection process that was developed for maximizing the response of any absorption sensor to temperature nonuniformity. These results greatly improve the understanding on nonuniformity effects on absorption measurements and allow the development of better sensors.

6.1.2 Results of Sensor Development

The fact that absorption is a nonlinear function of temperature was used to propose a sensor concept based on measuring three absorption lines for combustion sensing and control applications. A nonuniformity variable U was defined and designed

to monotonically track the level of temperature nonuniformity along the sensor line of sight. The concept was first validated through computer modelling. An implementation of the sensor concept was also successfully tested in the exhaust of a temperature stratified methane-air laboratory combustor. The modelling and experiments demonstrated the ability of the sensor output, U, to track the level of temperature nonuniformity, regardless of the method used to create or modify the temperature distribution. The experiments also demonstrated the potential use of the sensor for control applications where a simple output proportional to the level of nonuniformity can be easily incorporated in a closed loop control system. As part of this effort, a physics-based set of modelling and analysis tools was developed to aid in the study of the dependencies between the physical parameters, the hardware characteristics, and the application environment. These modelling tools also allow simulation of the sensor performance for many applications and can be used to simplify and optimize sensor design.

6.1.3 Results of Sensor Performance Analysis

Mathematical analysis and modelling tools were used to perform a comprehensive analysis of the major sources of errors affecting the operation of absorption spectroscopy sensors and prescribe amelioration methods. Of all the potential sources of errors in a typical absorption sensor, it was determined that random and systematic linear errors, given appropriate error reduction techniques, have a negligible contribution on the overall measurement uncertainty (less than 0.01% uncertainty). Furthermore, it was shown that Voigt fitting of line shapes resulting from absorption through nonuniform mediums, although not perfect, is an appropriate approximation of the line shape and independently introduces only minimal errors in the absorbance (<0.001%). Furthermore, effects of

small to moderate changes in the water concentration versus temperature profiles with changing combustor operating conditions are not significant sources of errors.

The major measurement errors were determined to derive from sources with nonlinear systematic effects on absorption, such as beam steering on the same time scale as the measurements, poor determination of nonlinear laser baseline, and flow unsteadiness and turbulence that change the temperature and composition along the line of sight during a laser line scan.

The laser system is the single most important piece of hardware limiting the senor performance. A laser with fast tuning in the hundreds of kHz or better range over several nanometers is needed to reduce errors and obtain good sensor performance in terms of accuracy and reduced uncertainty. For fully turbulent combustion flows, current technology seems to limit measurement uncertainty to about 1% in measured absorbance.

The overall sensor performance was analyzed through simulations and mathematical error propagation analysis. Estimated errors resulting from the identified physical sources were propagated to determine their effect on baseline and integrated absorbance uncertainty. Absorbance uncertainty was further propagated to understand the overall capability of this class of sensors in terms of the minimum levels of uncertainty that can be sensed or distinguished. Based on this analysis the sensor was shown capable of measuring relevant changes in the temperature profiles (as small as ±100 K) that match industry needs for such measurements. This translates in a sensor capable of measuring temperature nonuniformities with minimum deviations greater than about 180-330K or pattern factors greater than about 0.17. This capability matches a wide range of current industry needs. For example, gas-turbine combustors currently operate with

circumferential pattern factors as large as 0.3 – 0.4 (temperature deviations of 120-700K); the current sensing technique can be used throughout most of the needed PF range thus enabling pattern factor control. PF control is considered a key technology for future gas-turbine engines. This result is especially significant because even small reductions in pattern factor result in increased engine performance, longer component life, and significant cost savings.

6.1.4 Conclusions

In conclusion, the field of absorption spectroscopy was advanced by the development of a simple sensor for temperature nonuniformity using one laser beam with the potential to enable active pattern factor control. A thorough analysis of the technique resulted in a better understanding of nonuniformity effects on absorption and the development of a new line selection methodology for absorption nonuniformity sensing. A set of tools and techniques for the design and analysis of such sensors was also developed. Finally, the sensing technique was shown to be capable of operating under a set of conditions characteristic of sensing needs in the gas-turbine community, enabling new control systems and opening the way for potential improvements in gas turbine engine performance.

6.2 Recommendations for Future Work

Two directions for future work should be considered: sensing method improvements and extension of the technique to for spatial sensing and applications outside the gas turbine industry. There are several ways to improve the accuracy of the

method that would allow for a wider range of applications. Primarily the use of modulation spectroscopy with higher harmonic detection under certain conditions may improve the signal to noise ratio by a factor of two to ten. An intrinsic advantage of modulation spectroscopy is the fact that by measuring the derivative of the signal, baseline determination is virtually eliminated, reducing many potential errors. Another method of improving sensing performance would be to use wavelength-agile laser tuning. Wavelength-agile lasers refer to systems capable of tuning over hundreds of nanometers in a very short time (tenths of kHz to MHz).[69,70] Such systems enable the measurement of whole absorption bands and although the resolution of individual lines is relatively lower than traditional narrow-band tuning, the wealth of data enables more accurate measurements. Furthermore, data on many lines can be used to build a histogram of the temperature profile along the line of sight.[33] With such a wide spectral measurement, derivatives of the absorption signal with respect to temperature may also be used to reduce baseline induced errors and extract nonuniformity data.

Alternately, the analysis framework and modelling tools developed could be used to extend nonuniformity sensing to obtaining spatial temperature distributions in combustion exhaust. For example, an array of lasers could be arranged to provide circumferential cuts downstream from several injectors in an annular gas-turbine combustor (some possible arrangements are shown in Figure 46). Such an arrangement would provide information about the overall circumferential pattern factor and about the location of the larger deviations from the mean temperatures. This nonuniformity sensing technique may be combined with other instrumentation, such as thermocouples or

pyrometry, to provide a more complete picture of the combustor health and operating performance.
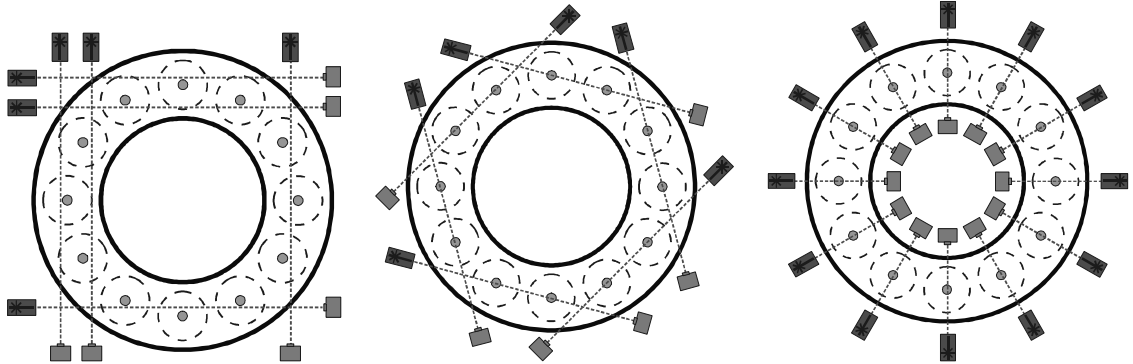
Figure 46. Spatial temperature sensing alternatives.

Furthermore, in an extension to this work, active sensing techniques may also be investigated. This technique refers to using small actuation efforts combined with coarse sensing to pinpoint desired effects. For example, a sensor across three injectors can determine that there is a problem, but not which injector is the source. By introducing subsequent small variations in each of the injectors and observing changes in the sensor output, one can potentially determine which injector is the source of the problems.

Finally, applications outside the combustion field should be investigated where such a sensing technique may provide a unique capability, such as the glass and metal smelting industries and petrochemical processing.

APPENDIX A

Peak Absorption Ratios

The vast majority of previous work on diode laser sensors in combustion uses integrated absorbances for determining temperature. An alternate approach is the use of the maximum absorption at the line peak, $k(v_0)$, instead of the absorbances:

$$k(v_0) = -\ln\left(\frac{I}{I_0}(v_0)\right) = \int_0^L p \cdot x \cdot S(T)\phi(v = v_0, T, x, p)dl \qquad (30)$$

The ratio of the absorption peaks of two lines is:

$$A_{ij} = \frac{k_i(v_{0i})}{k_j(v_{0j})} = \frac{\int_0^L x \cdot S_i(T)\phi_i(v = v_{0i}, T, x, p)dx}{\int_0^L x \cdot S_j(T)\phi_j(v = v_{0j}, T, x, p)dx} \xrightarrow{\text{uniform x}} \frac{S_i(T_{ij})\phi_i(v_{0i}, x, T_{ij})}{S_j(T_{ij})\phi_j(v_{0j}, x, T_{ij})} \quad (31)$$

The use of integrated absorbances results in more accurate temperature measurements because the line-shape function, ϕ, depends on broadening parameters that are usually not very well known and on the path-dependent properties (T, x).

Using peak absorption ratios to determine the temperature reduces computational time, hardware complexity, and the time response of the sensor. When using a single tuning laser to measure several absorption peaks, it is straightforward to identify the peak wavelength, eliminating the need for an etalon or wavemeter to monitor laser wavelength during tuning. Alternately, multiple (fixed wavelength) lasers can be used to monitor several line-peaks.

Another advantage of using peak absorptions is that a sensor based on line-peaks instead of absorbances will also work well at high pressures where lines broaden

significantly and individual features are very difficult to distinguish.[34] Also, in many cases, the ratio of peak absorptions can be approximated by the ratio of absorbances, or, if the lines are chosen to be rather insensitive to pressure and to have similar broadening characteristics, a simple correction can be used to yield results comparable to using integrated absorbances.[24,33]

Broadening Effects

If using peak ratios, or any time the spectral absorption coefficient has to be measured or computed, one must consider line broadening characteristics when selecting appropriate absorption lines for the sensor. Broadening comes into play through the ratio of line shape functions in Eq. (31). At combustion temperatures, both Doppler and pressure broadening are important. The line shape function (ϕ) can be represented by a Voigt profile, the convolution of Lorentzian collision broadening and Gaussian Doppler broadening, as given by:

$$\phi(D,B) = \frac{1}{\Delta v_D}\sqrt{\frac{\ln 2}{\pi}}K(D,B) = \frac{1}{\Delta v_D}\sqrt{\frac{\ln 2}{\pi}}\frac{B}{\pi}\int_{-\infty}^{\infty}\frac{e^{-y^2}}{B^2+(D-y)^2}dy \qquad (32)$$

$$D = \sqrt{\ln 2}\,\frac{v-v_0}{\Delta v_D} \qquad \text{and} \qquad B = \sqrt{\ln 2}\,\frac{\Delta v_c}{\Delta v_D} \qquad (33)$$

where Δv_D and Δv_c are the Doppler and collision broadening half-widths in cm^{-1}. The Doppler half-width of a line is a function of the root of the temperature and the molecular weight of the absorber, M:

$$\Delta v_D = 3.581179\times 10^{-7}v_0\sqrt{T/M} \qquad (34)$$

Collision broadening of an absorbing molecule depends on gas composition; broadening is a function of each collision partner, characterized by a half-width γ_k and a temperature coefficient n_k for each partner with a mole fraction x_k. This dependence takes the general form of Eq. (35):

$$\Delta v_c = \sum_k \left[\gamma_k \frac{P}{P_0} \left(\frac{T_0}{T} \right)^{n_k} x_k \right]$$

(35)

Because it is difficult to determine the broadening parameters for each collision partner, and when the exact gas composition is not well known, the HITRAN parameters are used. HITRAN only lists three parameters for each molecular transition: a self broadening half-width, γ_{self}, an aggregated half-width for collision with molecules in standard air, γ_{air}, and an aggregated temperature dependence coefficient, n. As a result, the collision half-width takes the following form:

$$\Delta v_c = \frac{P}{P_0} \left(\frac{T_0}{T} \right)^n \left[\gamma_{air} (1-x) + \gamma_{self} x \right]$$

(36)

This equation is used in this thesis as an approximation for computing collision broadening under any conditions.

At the line peak, $D = 0$, $\phi(0,B) = \phi(v=v_0,B)$, and peak absorption becomes a function of the broadening half-width ratio, B. The absorbance ratio can now be related to the peak ratio of two lines:

$$R_{ij} \cong A_{ij} \frac{K(0,B_i)}{K(0,B_j)} = A_{ij} \frac{B_i \int_{-\infty}^{\infty} \frac{e^{-y^2}}{B_i^2 + y^2} dy}{B_j \int_{-\infty}^{\infty} \frac{e^{-y^2}}{B_j^2 + y^2} dy}$$

(37)

121

In a nonuniform flow, there are several factors that affect the K ratio in Eq. (37). First, uncertainties in the broadening characteristics of the lines (for example the temperature coefficient n, or the species broadening coefficients) will introduce uncertainties in the values of B. Another source of errors is the unknown concentration and composition distribution along the path. Variable water mole-fraction and unknown concentration of other species will change the value of B. Overall, if the temperature coefficient n is similar then the other unknowns have little effect on the B_i/B_j ratio that appears in Eq. (37). The largest effect comes from the integral part of K (Eqs. (32) and (37)). A sample line pair A/R ratio is plotted in Figure 47. The two curves are for cases with different broadening parameters due to composition or other uncertainties of about 25%. This figure shows that using the peak ratio (A) instead of integrated absorbance (R) will introduce errors. By selecting pairs of lines with similar broadening behavior, however, these errors can be kept small (~2%). Furthermore, broadening effects will have an even smaller effect on measuring changes in the temperature profile.
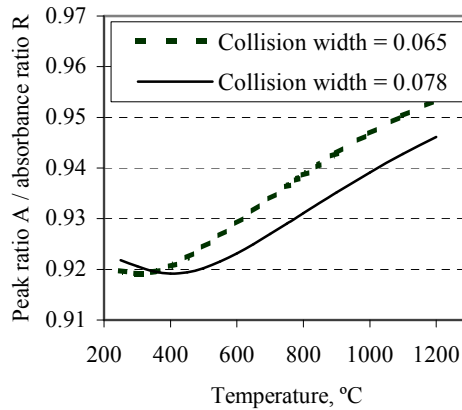

Figure 47. Broadening effects on peak ratio

High Pressure Sensing

In certain cases, absorption measurements have to be performed in high pressure environments, such as land-based gas turbines or aircraft engines. High pressure environments are more challenging to absorption spectroscopy sensing because of the pressure broadening of the absorption lines. As the pressure increases, the width of each absorption line increases, and lines start to merge together making it more difficult to determine the area of each absorption line (Figure 48). For moderate pressures, say up to about 10 atm, the techniques and discussion in this thesis still applies directly.

At high pressures when lines overlap significantly, wide laser scans, monitoring the peaks of abortion lines or using modulation techniques are more appropriate techniques. Line narrowing also has to be considered at high pressure. Absorption spectroscopy for monitoring temperature and species has been demonstrated in several high pressure applications.[37,71]
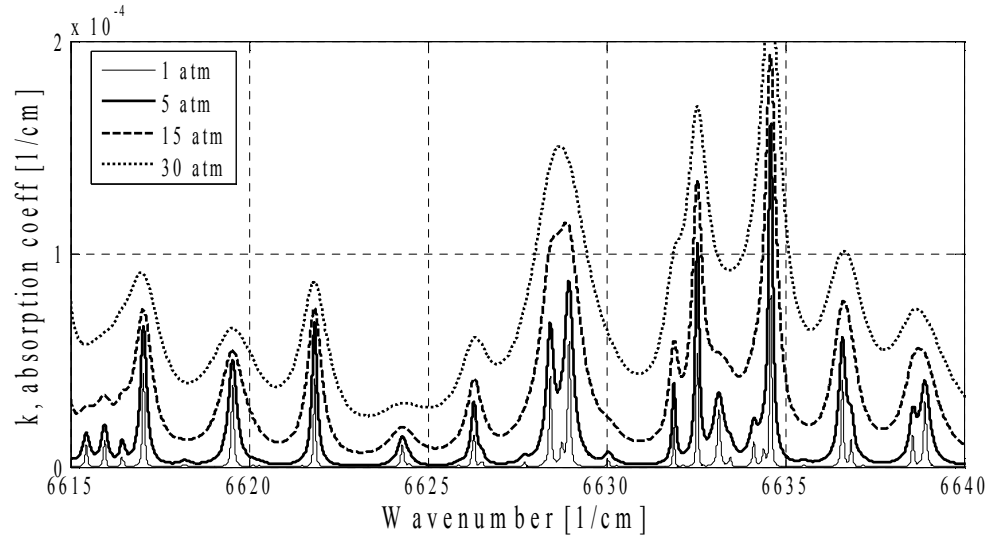
Figure 48. Absorption spectrum as a function of pressure for 10% water in air at 1800K.

The research described in this thesis concentrates on atmospheric or low pressure (a few atmospheres) sensing that is appropriate for cruse flight conditions in aircraft engines and many other industrial applications.

REFERENCES

[1] Skinner, G., Combustion control, *Trans. Instn Chem. Engrs*, , No. 772, Oct 2005.

[2] Docquier, N. and Candel, S., Combustion control and sensors: A review, *Progress in Energy and Combustion Science*, Vol. 28, No. 2, 2002, pp. 107–150.

[3] NASA, G. R. C., Combustion Science: Taming the Flames, Online. Internet. Retrieved 9/25/2006 from http://www.nasa.gov/centers/glenn/research/combustion.html.

[4] Garg, S., Propulsion Controls and Health Management Research at NASA Glenn Research Center, Tech. rep., NASA Glenn Research Center, Jul 2002.

[5] Lord, W. K., MacMartin, D. G., and Tillman, G., Flow Control Opportunities in Gas Turbine Engines, *Fluids*, 2000.

[6] DeLaat, J. C., Breisacher, K. J., Saus, J. R., and Paxson, D. E., Active Combustion Control for Aircraft Gas Turbine Engines, *36th Joint Propulsion Conference and Exhibition*, 2000.

[7] Kiel, B. V., Review of Advances In Combustion Control, Actuation, Sensing, Modeling And Related Technologies For Air Breathing Gas Turbines, *39th AIAA Aerospace Sciences Meeting and Exhibit*, 2001.

[8] McCarty, B., Tomondi, C., and McGinley, R., Reliable and Affordable Control Systems Active Combustor Pattern Factor Control, Tech. Rep. NASA/CR—2004-213097, NASA, 2004.

[9] Cox, G. B. J., Tiller, A. R., LeTourneau, J. J., and Ogg, J. S., Pattern Factor Improvement in the F-100 Primary Combustion System, *Journal of Engineering for Power, Transactions ASME*, Vol. 103, No. 4, 1981, pp. 739 – 748.

[10] Crocker, D. S., Smith, C. E., and Myers, G. D., Pattern factor reduction in a reverse flow gas turbine combustor using angled dilution jets, *American Society of Mechanical Engineers*, 1994, pp. 1–10.

[11] Lefebvre, A. H., Fuel Effects on Gas Turbine Combustion - Liner Temperature, Pattern Factor and Pollutant Emissions, *AIAA Paper*, 1984, pp. 18 –.

[12] McManus, K. and Lo, E., Closed-loop system for control of combustor pattern factor, *Proceedings of the 4th IEEE Conference on Control Applications*, 1995, pp. 699–704.

[13]   Mongia, H. C., TAPS – A 4th Generation Propulsion Combustor Technology for Low Emissions, *AIAA/ICAS International Air and Space Symposium and Exposition*, 2003.

[14]   Mongia, H. C., Perspective of combustion modeling for gas turbine combustors, *42nd AIAA Aerospace Sciences Meeting and Exhibit*, Reno, NV, United States, 2004, pp. 1759–1791.

[15]   Ng, D., A New Method to Measure Temperature and Burner Pattern Factor Sensing for Active Engine Control, Tech. Rep. NASA/TM—1999-209090, NASA, 1999.

[16]   Lyons, V. J. and Niedzwiecki, R. W., Combustor Technology for Future Small Gas Turbine Aircraft, Technical Memorandum NASA TM-106312, NASA Lewis Research Center, Aug 1993.

[17]   QinetiQ, Case Studiey: Future Developments in Industrial Gas Turbine Engines, Online. Internet. Retrieved on 9/26/2006 from http://www.qinetiq.com/home/case_studies/energy/future_developments_in_indus trial_gas_turbine_engines.html.

[18]   Johnson, L. P. and Diller, T. E., Measurements with a heat flux microsensor deposited on a transonic turbine blade, *International Congress on Instrumentation in Aerospace Simulation Facilities*, edited by IEEE, No. 37, IEEE, Jul 1995, pp. 1–7.

[19]   LAND Instruments, I., Combustion turbine blade temperature analysis, Product Brochure.

[20]   Sands, D., *Diode Lasers*, Series in Optics and Optoelctronics, Institute of Physics, 2004.

[21]   Mayinger, F. and Feldmann, O., *Optical Measurements: Techniques and Applications, 2nd edn*, Springer-Verlag, 2nd ed., 2001.

[22]   Teichert, H., Fernholz, T., and Ebert, V., Simultaneous in situ measurement of CO, H2O, and gas temperatures in a full-sized coal-fired power plant by near-infrared diode lasers, *Applied Optics*, Vol. 42, No. 12, April 2003, pp. 2043–51.

[23]   Allen, M. G., Diode laser absorption sensors for gas-dynamic and combustion flows, *Measurement Science and Technology*, Vol. 9, No. 4, 1998, pp. 545–562.

[24]   Zhou, X., Liu, X., Jeffries, J. B., and Hanson, R., Development of a sensor for temperature and water concentration in combustion gases using a single tunable diode laser, *Measurement Science and Technology*, Vol. 14, No. 8, 2003, pp. 1459–1468.

[25] Rieker, G. B., Liu, J. T., Jeffries, J. B., Hanson, R. K., Mathur, T., Gruber, M. R., and Carter, C. D., Diode Laser Sensor for Gas Temperature and H2O Concentration in a Scramjet Combustor Using Wavelength Modulation Spectroscopy, *41st AIAA/ASME/SAE/ASEE Joint Propulsion Conference and Exhibit*, 2005.

[26] Griffiths, A. D. and Houwing, A. F. P., Diode laser absorption spectroscopy of water vapor in a scramjet combustor, *Applied Optics*, Vol. 44, No. 31, 2005, pp. 6653–6659.

[27] Liu, J. T., Rieker, G. B., Jeffries, J. B., Gruber, M. R., Carter, C. D., Mathur, T., and Hanson, R. K., Near-infrared diode laser absorption diagnostic for temperature and water vapor in a scramjet combustor, *Applied Optics*, Vol. 44, No. 31, 2005, pp. 6701–6711.

[28] Liu, J., Jeffries, J., Hanson, R., Creighton, S., Lovett, J., and Shouse, D., Diode laser absorption diagnostics for measurements in practical combustion flow fields, *39th AIAA/ASME/SAE/ASEE Joint Propulsion Conference and Exhibit*, 2003.

[29] Bowman, C. and Hanson, R., Shock Tubes and Lasers: New Opportunities for High Temperature Kinetics Studies, *16th International Symposium on Gas Kinetics*, Invited Plenary Lecture, 2000.

[30] Oehlschlaeger, M., Davidson, D., and Jeffries, J., Temperature measurement using ultraviolet laser absorption of carbon dioxide behind shock waves, *Applied Optics*, Vol. 44, No. 31, Nov. 2005, pp. 6599–6605.

[31] Schulz, C., Jeffries, J., Davidson, D., Koch, J., Wolfrum, J., and Hanson, R., Impact of UV absorption by CO2 and H2O on NO LIF in high-pressure combustion applications, *Proceedings of the Combustion Institute*, Vol. 29, Combustion Institute, Sapporo, Japan, 2002, pp. 2735–2741.

[32] Sanders, S., Mattison, D., Jeffries, J., and Hanson, R., Time-of-flight diode-laser velocimeter using a locally seeded atomic absorber: Application in a pulse detonation engine, *Shock Waves*, Vol. 12, No. 6, May 2003, pp. 435–41.

[33] Sanders, S. T., Wang, J., Jeffries, J. B., and Hanson, R. K., Diode-laser absorption sensor for line-of-sight gas temperature distributions, *Applied Optics*, Vol. 40, No. 24, 2001, pp. 4404–4415.

[34] Nagali, V. and Hanson, R. K., Design of a diode-laser sensor to monitor water vapor in high-pressure combustion gases, *Applied Optics*, Vol. 36, No. 36, Dec 1997, pp. 9518–9527.

[35] Mihalcea, R. M., Baer, D. S., and Hanson, R. K., Diode-Laser Absorption Measurements of CO2 Near 2.0 um at Elevated Temperatures, *Applied Optics*, Vol. 37, No. 36, Dec 1998, pp. 8341–8347.

[36]   Hanson, R. K. and Jeffries, J. B., Diode Laser Sensors for Ground Testing, *25th AIAA Aerodynamic Measurement Technology and Ground Testing Conference*, 2006.

[37]   Li, H., Rieker, G. B., Liu, X., Jeffries, J. B., and Hanson, R. K., Extension of wavelength-modulation spectroscopy to large modulation depth for diode laser absorption measurements in high-pressure gases, *Applied Optics*, Vol. 45, No. 5, 2006, pp. 1052–1061.

[38]   Li, H., Zhou, X., Jeffries, J. B., and Hanson, R. K., Sensing and Control of Combustion Instabilities in Swirl-Stabilized Combustors Using Diode-Laser Absorption, *42nd AIAA/ASME/SAE/ASEE Joint Propulsion Conference & Exhibit*, edited by AIAA, 2006, AIAA 2006-4395.

[39]   Liu, X., Jeffries, J., Hanson, R., Hinckley, K., and Woodmansee, M., Development of a tunable diode laser sensor for measurements of gas turbine exhaust temperature, *Applied Physics B: Lasers and Optics*, Vol. 82, No. 3, 2006, pp. 469–478.

[40]   Frish, M., Wainner, R., Green, B., Stafford-Evans, J., Laderer, M., and Allen, M., Progress in reducing the size and cost of trace gas analyzers based on Tunable Diode Laser Absorption Spectroscopy, *SPIE Optics East Advanced Environmental, Chemical, and Biological Sensing Technologies II*, Philadelphia, PA, 2004.

[41]   Caswell, A. W., Sanders, S. T., and Chiaverini, M. J., Swept-Wavelength Laser Absorption Tomography for Imaging Rocket Plume Gas Properties, *41st AIAA/ASME/SAE/ASEE Joint Propulsion Conference & Exhibit*, 2005.

[42]   Bryner, E., Diskin, G. S., Goyne, C. P., and McDaniel, J. C., Development of an Infrared Laser Absorption Tomography System for a Scramjet Combustor, *25th AIAA Aerodynamic Measurement Technology and Ground Testing Conference*, 2006.

[43]   Palaghita, T. and Seitzman, J. M., Control of temperature nonuniformity based on line-of-sight absorption, *40th AIAA/ASME/SAE/ASEE Joint Propulsion Conference and Exhibit*, 2004.

[44]   Palaghita, T. and Seitzman, J. M., Pattern Factor Sensing and Control Based on Diode Laser Absorption, *41st AIAA/ASME/SAE/ASEE Joint Propulsion Conference and Exhibit*, 2005.

[45]   Liu, X., Jeffries, J. B., and Hanson, R. K., Measurement of Non-uniform Temperature Distributions Using Line-of-sight Absorption Spectroscopy,*44th AIAA Aerospace Sciences Meeting and Exhibit*, 2006.

[46]   Svanberg, S., *Atomic and molecular spectroscopy: basic aspects and practical applications*, Springer, 4th ed., 2004.

[47] Rothman, L., Jacquemart, D., Barbe, A., D. Chris Bennerc, M. B., Brown, L., Carleer, M., Jr., C. C., Chance, K., Coudert, L., Dana, V., Devi, V., Flaud, J.-M., Gamache, R., Goldman, A., Hartmann, J.-M., Jucks, K., Maki, A., Mandin, J.-Y., Massie, S., Orphal, J., Perrin, A., Rinsland, C., Smith, M., Tennyson, J., Tolchenov, R., Toth, R., Auwera, J. V., Varanasi, P., and Wagner, G., The HITRAN 2004 molecular spectroscopic database, *Journal of Quantitative Spectroscopy & Radiative Transfer*, Vol. 96, 2005, pp. 139–204.

[48] Zhou, X., Jeffries, J., and Hanson, R., Development of a fast temperature sensor for combustion gases using a single tunable diode laser, *Applied Physics B: Lasers and Optics*, Vol. 81, No. 5, 2005, pp. 711–722.

[49] Arroyo, M. P. and Hanson, R. K., Absorption measurements of water-vapor concentration, temperature, and line-shape parameters using a tunable InGaAsP diode laser, *Applied Optics*, Vol. 32, No. 30, 1993, pp. 6104–6116.

[50] Shao, J., Zhang, W.-J., Gao, X.-M., Ning, L.-X., and Yuan, Y.-Q., Absorption measurements for highly sensitive diode laser of CO2 near 1.3 microns at room temperature, *Chinese Physics*, Vol. 14, No. 3, 2005, pp. 482–486.

[51] Garnache, A., Liu, A., Cerutti, L., and Campargue, A., Intracavity laser absorption spectroscopy with a vertical external cavity surface emitting laser at 2.3 microns: Application to water and carbon dioxide, *Chemical Physics Letters*, Vol. 416, 2005, pp. 22–27.

[52] Shixin, P., Fenping, C., Xiaoming, G., Weixiong, Z., Yong, Y., Teng, H., Wei, H., and Weijun, Z., The detection of carbon monoxide by cavity enhanced absorption spectroscopy with a DFB diode laser, *Vibrational Spectroscopy*, Vol. 40, No. 2, 2006, pp. 192–196.

[53] Ouyang, X. and Varghese, P. L., Line-of-sight absorption measurements of high temperature gases with thermal and concentration boundary layers, *Applied Optics*, Vol. 28, No. 18, 1989, pp. 3979–3984.

[54] Seitzman, J. M., Tamma, R., and Scully, B., Broadband infrared sensor for active control of high pressure combustors, *36th Aerospace Sciences Meeting & Exhibit*, 1998.

[55] Seitzman, J. M. and Scully, B. T., Broadband infrared absorption sensor for high-pressure combustion control, *Journal of Propulsion and Power*, Vol. 16, No. 6, 2000, pp. 994–1001.

[56] O'Halloran, B., Thermostatic control of turbine cooling air, Patent 5,022,817, US Patent, June 1991.

[57] Kuntz, M., A new implementation of the Humlicek algorithm for the calculation of the Voigt profile function, *Journal of Quantitative Spectroscopy and Radiative Transfer*, Vol. 57, No. 6, 1997, pp. 819–822.

[58]   Ruyten, W., Comment on "A new implementation of the Humlicek algorithm for the calculation of the Voigt profile function" by M. Kuntz [JQSRT 57(6) (1997) 819-824], *Journal of Quantitative Spectroscopy and Radiative Transfer*, Vol. 86, No. 2, June 2004, pp. 231–233.

[59]   Eggenspieler, G. and Menon, S., Parallel Numerical Simulation of Flame Extinction and Flame Lift-Off, *Proceedings of the Parallel Computational Fluid Dynamic Conference*, 2005.

[60]   Chen, Y., Liang, S., Aung, K., Glezer, A., and J., J., Enhanced mixing in a simulated combustor using synthetic jet actuators,*37th Aerospace Sciences Meeting and Exhibit*, 1999.

[61]   Chen, Y., Scarborough, D., Liang, S., Aung, K., and J., J., Manipulating pattern factor using synthetic jet actuators, *38th Aerospace Sciences Meeting and Exhibit*, 2000.

[62]   Jumper, E. J. and Fitzgerald, E. J., Recent advances in aero-optics, *Progress in Aerospace Sciences*, Vol. 37, No. 3, Apr 2001, pp. 299–339.

[63]   Kranendonk, L. A. and Sanders, S. T., Optical design in beam steering environments with emphasis on laser transmission measurements, *Applied Optics*, Vol. 44, No. 31, 2005, pp. 6762–6772.

[64]   Forbes, A., Laser beam propagation in non-linearly absorbing media, *Proceedings of SPIE - The International Society for Optical Engineering*, Vol. 6290, International Society for Optical Engineering, Bellingham WA, WA 98227-0010, United States, San Diego, CA, United States, 2006, pp. 629003–.

[65]   Zubair, F. R., Garcia, P. J., and Catrakis, H. J., Aero-Optical Interactions Along Laser Beam Propagation Paths in Compressible Turbulence, *37th AIAA Plasmadynamics and Lasers Conference*, Jun 2006.

[66]   Hobbs, P. C. D., Shot noise limited optical measurements at baseband with noisy lasers, *Laser Noise, Proc. Soc. Photo-Opt. Instrum. Eng.*, Vol. 1376, 1990, pp. 216–221.

[67]   Allen, M. G., Carleton, K. L., Davis, S. J., Kessler, W. J., Otis, C. E., Palombo, D. A., and Sonnenfroh, D. M., Ultrasensitive dual-beam absorption and gain spectroscopy: applications for near-infrared and visible diode laser sensors, *Applied Optics*, Vol. 34, No. 18, 1995, pp. 3240–3249.

[68]   Song, K. and Jung, E., Recent Developments in Modulation Spectroscopy for Trace Gas Detection Using Tunable Diode Lasers, *Applied Spectroscopy Reviews*, Vol. 38, No. 4, 2003, pp. 395–432.

[69]   Sanders, S., Wavelength-agile lasers, *Optics & Photonics News*, Vol. 16, No. 5, May 2005, pp. 36–41.

[70]   Kranendonk, L. A., Walewski, J. W., Kim, T., and Sanders, S. T., Wavelength-agile sensor applied for HCCI engine measurements, *Proceedings of the Combustion Institute*, Vol. 30, No. 1, Jan 2005, pp. 1619–1627.

[71]   Wang, J., Sanders, S., Jeffries, J., and Hanson, R., Oxygen measurements at high pressures with vertical cavity surface-emitting lasers, *Applied Physics B: Lasers and Optics*, Vol. 72, No. 7, 2001, pp. 865–872.